93-79-7112
MOTC-IOT-92-H2BA06

仔波分析與時頻或時尺分析
在波浪研究之應用

交通部運輸研究所

中華民國九十三年五月

93-79-7112
MOTC-IOT-92-H2BA06

仔波分析與時頻或時尺分析在波浪研究之應用

著 者：李勇榮

交通部運輸研究所

中華民國九十三年五月

仔波分析與時頻或時尺分析在波浪研究之應用

著　　者：李勇榮
出版機關：交通部運輸研究所
地　　址：台北市敦化北路 240 號
網　　址：www.iot.gov.tw/chinese/lib/lib.htm
電　　話：(02)23496789
出版年月：中華民國九十三年五月
印 刷 者：
版(刷)次冊數：初版一刷 120 冊
本書同時登載於交通部運輸研究所網站
定　　價：　　元
展 售 處：
交通部運輸研究所運輸資訊組•電話：(02)23496880
三民書局重南店：台北市重慶南路一段 61 號 4 樓•電話：(02)23617511
三民書局復北店：台北市復興北路 386 號 4 樓•電話：(02)25006600
國家書坊台視總店：台北市八德路三段 10 號 B1•電話：(02)25787542
五南文化廣場：台中市中山路 6 號•電話：(04)22260330
新進圖書廣場：彰化市中正路二段 5 號•電話：(04)7252792
青年書局：高雄市青年一路 141 號 3 樓•電話：(07)3324910
GPN：1009301566

仔波分析與時頻或時尺分析在波浪研究之應用

交通部運輸研究所

GPN:1009301566
定價　100　元

交通部運輸研究所出版品摘要表

<table>
<tr><td colspan="4">出版品名稱：仔波分析與時頻或時尺分析在波浪研究之應用</td></tr>
<tr><td>國際標準書號（或叢刊號）</td><td>政府出版品統一編號
1009301566</td><td>運輸研究所出版品編號
93-79-7112</td><td>計畫編號
92-H2BA06</td></tr>
<tr><td colspan="3">主辦單位：港灣技術研究中心
主管：邱永芳
計劃主持人：李勇榮
研究人員：李勇榮
聯絡電話：04-26587183
傳真號碼：04-26587183, 04-26571329</td><td>研究期間
自 91 年 01 月
至 92 年 12 月</td></tr>
<tr><td colspan="4">關鍵詞：水波分析的三優化、各類屬離散仔波、熵值統計法、特性函數之相位分佈、最佳函基、半正交樞點順適仔波、最佳函基相應之連續仔波、水波物理之調適時頻窗。</td></tr>
<tr><td colspan="4">摘要：

本文首先以含蓋相當完整之各類屬離散仔波為研究對象，探討其基本解析與數值行為。我們開發完整而多功能之仔波分析程式，實際深入瞭解仔波之行為特性以作為其應用之區判。數值模擬之內涵包括各母仔波、父仔波、仔波相關函數之無限細部展開、以及其相關函數相位之線性濾波表現等。在可能的情況下並說明些這表現的一些實際物理義涵。而為了鑑取水波訊號分析之最佳離散仔波，我們以最小熵值統計法，應用各種規範明確取得最佳函基為半正交樞點順適仔波。此外，為了尋找與統計熵值表現相對應的數理解析因子，我們研究各仔波特性函數之相位分佈情形，從而認定不同函基於水波訊號之可應用性乃在於其特性函數相位分佈上線性之要求。再者，針對所鑑取得之最佳離散仔波，我們說明改進分析不定性之必要，從而引入連續仔波轉換之長處，並指出相應之連續仔波為何。在前述的雙重優化下，本文進一步探討如何增進仔波分析與水波物理之真確相似性，此處我們解說如何調適時頻窗以模擬不同尺度水波演化情形。整而言之，本研究從事了一個水波分析的三優化工程。最後作者謹表示：基於這些認知，我們深信任何函基，已知或待開發，其於水波訊號應用之適切性將不脫本文之區判與認定。</td></tr>
</table>

出版日期	頁數	定價	本 出 版 品 取 得 方 式
93 年 5 月	148		凡屬機密性出版品均不對外公開。普通性出版品，公營、公益機關團體及學校可函洽本所免費贈閱；私人及私營機關團體可按定價價購。

機密等級：

□限閱 □機密 □極機密 □絕對機密

（解密【限】條件：□ 年 月 日解密，□公布後解密，□附件抽存後解密，

□工作完成或會議終了時解密，□另行檢討後辦理解密）

■普通

備註：本研究之結論與建議不代表交通部之意見。

PUBLICATION ABSTRACTS OF RESEARCH PROJECTS
INSTITUTE OF TRANSPORTATION
MINISTRY OF TRANSPORTATION AND COMMUNICATIONS

<table>
<tr><td colspan="4">TITLE: Wavelet Time-Frequency Analysis and Its Applications to Water Waves – Wavelet Characterizations and the Optimum Basis</td></tr>
<tr><td>ISBN(OR ISSN)</td><td>GOVERNMENT PUBLICATIONS NUMBER
1009301566</td><td>IOT SERIAL NUMBER
93-79-7112</td><td>PROJECT NUMBER
92-H2BA06</td></tr>
<tr><td colspan="3">DIVISION: HARBOR & MARINE TECHNOLOGY CENTER
DIVISION DIRECTOR: Yung-Fang Chiu
PRINCIPAL INVESTIGATOR: Yueon-Ron Lee
PROJECT STAFF: Yueon-Ron Lee
PHONE: 886-4-26587183
FAX: 886-4-26587183, 886-4-26571329</td><td>PROJECT PERIOD
FROM Jan. 2003
TO Dec. 2003</td></tr>
<tr><td colspan="4">KEY WORDS: The three optimizations for water wave signal analyses, Discrete wavelet categories, Comprehensive programs, Entropy statistics, Phase distributions of the characteristic function, Optimal basis, Cardinal spline wavelet, The continuous wavelet transform corresponding to the optimum basis, Adaptation of the time-frequency windows</td></tr>
<tr><td colspan="4">ABSTRACT:

Comprehensive categories of discrete wavelets are studied first. The relevant characterizations and various intrinsic properties are extensively illustrated. Physical counterparts of analytical aspects are provided when possible. The entropy criteria are applied to the whole set of wavelets for signals obtained from wave-tank experiments, and the optimal wavelet basis is identified to be the semi-orthogonal cardinal spline dual wavelet. Besides, each individual wavelet's pertinency to the applications of water-wave-related signals is linked to the phase distribution of a wavelet characteristic function. That is to say, we identified the analytical essence of the statistical behaviors of the entropy results. Based on the identified discrete best basis, a second optimization is applied, and this is done through incorporating the advantages related to the continuous wavelet transform. And this in turn points to the counterpart continuous wavelet. Furthermore, for the better modeling of real physics, a third optimization is also implemented through the adaptation of wavelet time-frequency windows. With these results, the author firmly believes that if you ever find an individual wavelet you have great chance to assign it into one of the categories covered here; and if not, you have great reason to conceive that its properties must fall within (or between) the covered characterizations; and thus, in water wave applications, any wavelet's fate or possible usefulness is decreed accordingly - overall, it is really hard to beat the optimum basis and the methodology given in this study.</td></tr>
<tr><td>DATE OF PUBLICATION
May 2004</td><td>NUMBER OF PAGES
148</td><td>PRICE</td><td>CLASSIFICATION
☐SECRET
☐CONFIDENTIAL
■UNCLASSIFIED</td></tr>
<tr><td colspan="4">The views expressed in this publication are not necessarily those of the Ministry of Transportation and Communications.</td></tr>
</table>

Wavelet Time-Frequency Analysis
— An Optimum Basis and
Its Applications to Water Waves

Yueon-Ron Lee
Institute of Harbor and Marine Technology

Email: ronlee@ms4.hinet.net

Revision: 1.0, December 8, 2003, 02:43:06
Printed: July 8, 2004

LIST OF CONTENTS

LIST OF FIGURES

LIST OF TABLES

摘要

本研究首先以含蓋相當完整之各類屬離散仔波爲研究對象，探討其基本解析與數值行爲。我們開發一完整而多功能之仔波分析程式，實際深入瞭解仔波之行爲特性以作爲其應用之區判。數值模擬之內涵包括各母仔波、父仔波、仔波相關函數之無限細部展開、以及其相關函數相位之線性濾波表現等。在可能的情況下並說明些這表現的一些實際物理義涵。而爲了鑑取水波訊號分析之最佳離散仔波，我們以最小熵值統計法，應用各種規範明確取得最佳函基爲半正交樞點順適仔波。此外，爲了尋找與統計熵值表現相對應的數理解析因子，我們研究各仔波特性函數之相位分佈情形，從而認定不同函基於水波訊號之可應用性乃在於其特性函數相位分佈上線性之要求。再者，針對所鑑取得之最佳離散仔波，我們說明改進分析不定性之必要，從而引入連續仔波轉換之長處，並指出相應之連續仔波爲何。在前述的雙重優化下，本研究進一步探討如何增進仔波分析與水波物理之眞確相似性，此處我們解說如何調適時頻窗以模擬不同尺度水波演化情形。整而言之，本研究從事了一個水波分析的三優化工程。最後作者謹表示：基於這些認知，我們深信任何函基，已知或待開發，其於水波訊號應用之適切性將不脫本文之區判與認定。

ABSTRACT

Comprehensive categories of discrete wavelets are studied first. The relevant characterizations and various intrinsic properties are extensively illustrated. Physical counterparts of analytical aspects are provided when possible. The entropy criteria are applied to the whole set of wavelets for signals obtained from wave-tank experiments, and the optimal wavelet basis is identified to be the semi-orthogonal cardinal spline dual wavelet. Besides, each individual wavelet's pertinency to the applications of water-wave-related signals is linked to the phase distribution of a wavelet characteristic function. That is to say, we identified the analytical essence of the statistical behaviors of the entropy results. Based on the identified discrete best basis, a second optimization is applied, and this is done through incorporating the advantages related to the continuous wavelet transform. And this in turn points to the counterpart continuous wavelet. Furthermore, for the better modeling of real physics, a third optimization is also implemented through the adaptation of wavelet time-frequency windows. With these results, the author firmly believes that if you ever find an individual wavelet you have great chance to assign it into one of the categories covered here; and if not, you have great reason to conceive that its properties must fall within (or between) the covered characterizations; and thus, in water wave applications, any wavelet's fate or possible usefulness is decreed accordingly — overall, it is really hard to beat the optimum basis and the methodology given in this study.

Chapter 1

Introduction

1.1 Background

The usefulness of a particular data analysis methodology is highly case dependent; there simply exists neither a full-fledged analyzing function basis nor an all-purpose numerical scheme for all sorts of signals or applications.

Chronically, from the somewhat traditional and well established spectral perspective to the more recent wavelet viewpoints, we have:

- Fourier transform;
- Short time Fourier transform or windowed Fourier transform;
- The Gabor's analytical signal procedure and the relevant Hilbert transform;
- Various time-frequency transforms associated with individual distributions, such as Wigner Distribution, Page distribution, Choi-Williams distribution, and etc. [6];
- The discrete wavelet transform;
- The continuous wavelet transform or the integral wavelet transform.

We note here that, unlike discrete and continuous Fourier transforms, which are basically identical in both function bases and formulations, the discrete wavelet transform and continuous wavelet transform are essentially two different categories in that, first, they may use completely different function bases, second, they involve relatively quite independent formulations.

In the following discussions let assume the analytical target to be a one-dimensional time series signal; we therefore have the following general features for individual analysis methodologies.

The Fourier transform yields another one-dimensional data in frequency domain. The transform correspondence is one independent variable to another independent one.

For short time Fourier transform, it yields somewhat localized frequency contents; and, when the capping window is shifted along the time axis, it provides time-dependent spectral information. Through such multiple processes the transform correspondence is from the time variable to the time and frequency variables.

For Gabor's analytical signal procedure [13], it yields instantaneous frequency distribution and oscillation envelope curves along the time line. Here the frequency and the envelope cannot be regarded as independent variables. The independent variable in the two corresponding transform domains is bath time.

For various time-frequency transforms associated with individual distributions, they also provide time-varying frequency contents that are conceptually identical to the short time Fourier transform, except that the involved analyzing kernels are related to individual distributions rather than the Fourier kernel.

For the discrete wavelet transforms, the one-dimensional time series yields directly another one-dimensional coefficient series that contains the information that covers both time and scale (or representative frequency). The correspondence is one independent variable to two in one process.

As to the continuous wavelet transform, the one-dimensional time series yields a two-dimensional coefficient series that contains the information that is also varying both in time and in scale (or representative frequency). But here, every time point has a scale distribution components and every scale may play a role at a specific time. And the transform is a multi-process numerical scheme similar to the short time Fourier transform, except the core difference of the capping windows.

1.2 Non-stationary effects

It is well known that Fourier transform is suitable for characterizing stationary signals and not quite satisfactory for analyzing transient local phenomena. The reasons can be illustrated by the following properties of the transform.

- Any Function cannot be both time- and band-limited. If a function is limited (finitely supported) in one domain, then the independent variable of its corresponding function in the other domain stretches the entire real line (**R**). In real world situations, however, signals are almost always limited in time and space; meanwhile, hardware's capability is generally band-limited. This simply implies that there is not going to be a function basis that perfectly matches theory to practice. A slight variation of the Fourier transform is the short time Fourier transform, which is just the Fourier transform of the windowed signal, i.e., the original signal capped with or multiplied by a window function. In short time Fourier transform this property of mutual exclusivity in time and frequency localizations is indicated by the Balian-Low theorem, which basically states that if the window function $g(t)$ of a Gabor type frame

  $$g_{m,n}(t) = e^{-2\pi imt} g(t-n), \tag{1.1}$$

  in which $m, n \in \mathbf{Z}$, is well localized in time, then the associated Fourier transform window can not be well localized in frequency. The point here sounds a bit abstract, but, in reality, this is conceptually equivalent to the following points.

- The Gibbs phenomenon states that, if there is a jump in signal, then the overshoots, occurring at both sides of the discontinuity when the inverse Fourier transform is implemented, can never disappear and remain at constant. This amounts to say that it takes quite many a spectral components to make up a sharp transient feature and that a local variation affects a broad range of the spectrum just as the Fourier transform of the delta function (more precisely, delta distribution) covers the whole frequency axis.

- Fourier basis functions are periodic and extend bi-infinitely; signals thus studied are better to be periodic and sampled infinitely. The unavoidable side effects for not fulfilling these requirements are many: frequency leakages, smoothing errors, edge effects due to data truncations, aliasing due to under-sampling or non-periodicity (figure 1.1 is actually a case of under-sampling, where a linear chirp is sampled at a rate half of the Nyquist frequency), and, uncontrollable spectral variance due to the finite resolution or histogram processing.

Overall, the syndromes associated with the above listed items can be referred to the non-stationary effects.

1.3 Windowed transforms

Both short-time Fourier transform and wavelet transform try to remedy Fourier basis's deficiencies in characterizing transient phenomena by analyzing the set of localized signals. For the short time Fourier transform this can easily be executed by varying m and n in equation 1.1. For the wavelet transform this can be illustrated through the use of the Morlet wavelet by varying its translation and dilation variables.

Both transforms yield local spectral information – more precisely, local scale information, if the term ”frequency”, “Hz”, or “spectrum” is strictly reserved for sinusoidal functions. However, due to the Balian-Low theorem mentioned above, the waveform associated with short time Fourier transform can never be truly local in time since in reality the frequency domain of discrete Fourier transform is always band-limited by obeying the Nyquist law. In this regard, wavelets can be of exactly local; at least, they must have suitable or better decaying property such that they contain no zero-frequency component.

Let us further outline a few specific properties pertaining to individual transform:

- Both short time Fourier transform and wavelet transform are windowed transforms. In short time Fourier transform there exist two quite distinctive operations. The first operation is applying a suitable time-window to the signal; the second operation is performing the Fourier transform for the capped signal. The corresponding inverse transform (or reconstruction process) of the short time Fourier transform is naturally associated with a frequency-window and involves two similar distinctive operations too. However, in wavelet transform these two distinctive steps are not clearly observable — rather than using the very distinctive "window (either time- or frequency-window)" and "Fourier basis function (i.e., sine or cosine function)", the "window" and the "basis function" are synthesized in an inseparable specific form called "wavelet". In fact, one can clearly solidify this notion by comparing the Gabor type frame (equation 1.1) with the Morlet wavelet when the window function $g(t)$ of equation 1.1 is assumed to be a Gaussian bell. The intention for either the combined operation or synthesized operation is completely the same: to provide a mechanism (or kernel) for projecting a signal into modulated or oscillating wave constituents.

- The time-frequency windows in short time Fourier transform keep rigid for different scales since the window function $g(t)$ in Equation 1.1 does not depend on m, i.e., their widths (usually referring to time) and heights (usually referring to frequency) do not change for all frequencies. In wavelet transform, the windows are adjusted to different scales, but the sizes (or areas) of different windows are still fixed, i.e., each window's height and width are inversely proportional and the product remains constant (either for discrete wavelet transform or continuous wavelet transform). The concept of fixed size windows is illustrated by the fixed area of the gray blocks in the phase planes shown in Figures 1.1 and 1.2, where the discrete wavelet packet transforms are performed for a chirp signal using different bases originating from the same seeding mother wavelet. In the figures, since the bases are orthonormal, all time-frequency windows do not overlap. As for the continuous wavelet transform, various time-frequency windows severely tangle with each others. And we generally do not show the actual sizes and shapes of various windows — rather, each window is represented by a point (or a small area depicting the time-frequency resolution) having coordinates corresponding to its centroids in the time and frequency axes.

- The function basis of the short time Fourier transform is the unique orthonormal Fourier basis comprised of sine and cosine functions; whereas, for wavelet transform, apart from the very loose constrain that the basis function (or the mother wavelet) satisfies the admissibility condition (for continuous wavelet transform) or stability condition (for discrete wavelet transform), there is virtually no restriction on the choice of basis functions. The coefficients of short time Fourier transform, which represent local Fourier spectral information, still have the exact meaning of "frequency". In wavelet transform, wavelet coefficients refer to specific scales rather than "frequencies". Here, we generally suffer from their physical interpretability due to the following reasons: (1) No unique basis — the analyzing function or mother wavelet can be designed in a plenty of ways, and the basis functions related to the mother wavelet can be either dependent or independent (orthogonal or non-orthogonal); (2) Scale does not have unit — together with the first point, it severely hampers out ability to directly perceive the wavelet's size and physical shape; and, (3) No fixed algorithm to implement wavelet transform — many techniques and various adaptations exist, such as, the treatment using flexible time-frequency windows for continuous wavelet transform [12], multi-voice [9] or multi-wavelet [7, 8, 24] frames, and discrete wavelet transform using different dilation factors other than the most often seen value of 2 [1]. Generally speaking, these varieties may not be as disturbing in certain application fields (such as data transmission or signal decomposition and reconstruction) as they are for our studies focusing on the water wave physics.

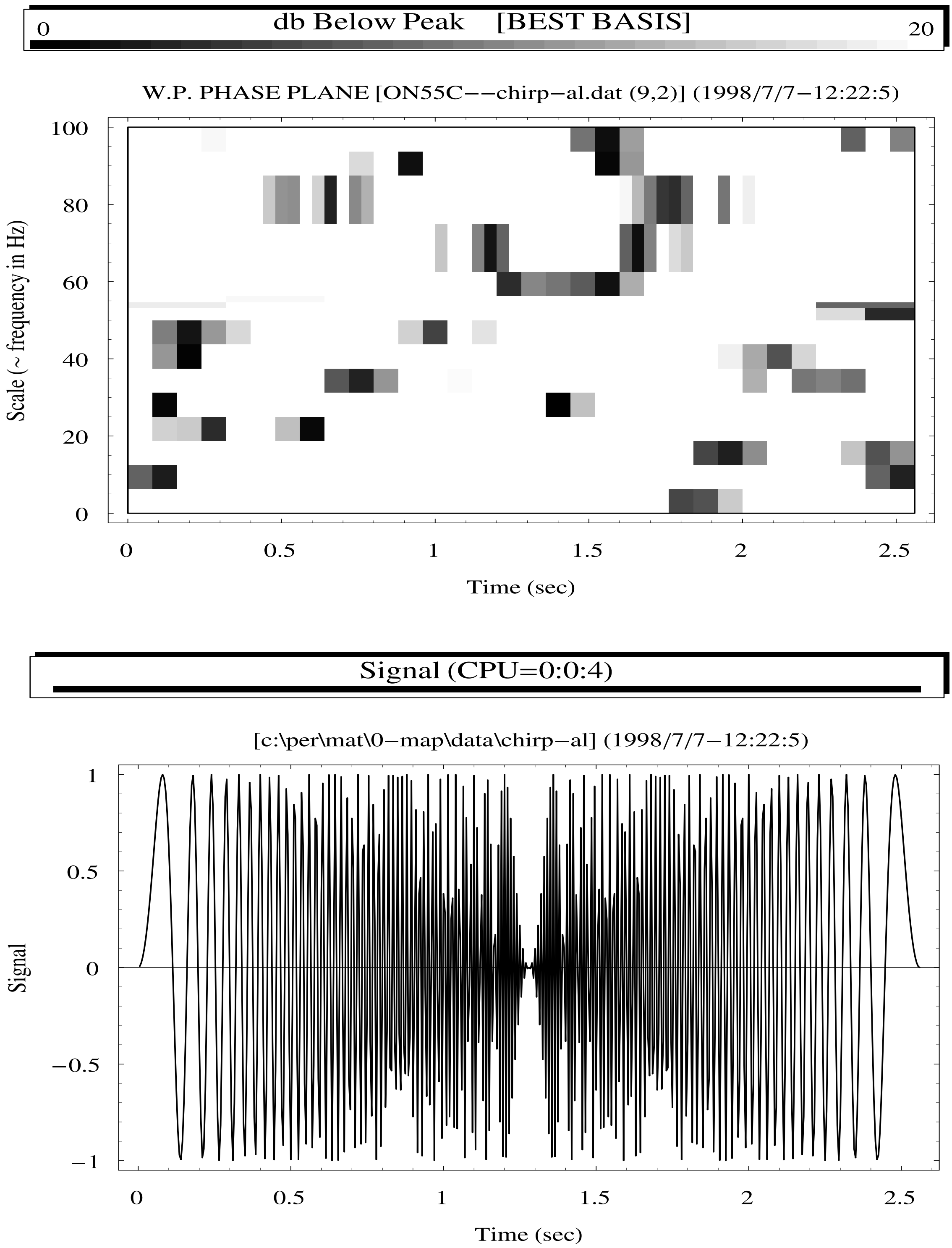

Figure 1.1: Phase plane of a wavelet packet's best basis time-frequency windows `(top)` for a linear chirp signal that is sampled under aliasing condition `(bottom)`. Here wavelet packets associated with coiflet of 30 convolution weights is used. The original signal, if not under-sampled, has linear instantaneous frequency distribution form 0 to 100 Hz. Note the non-symmetric effects and the scattering of windows due to the composite frequency bands that form the wavelet.

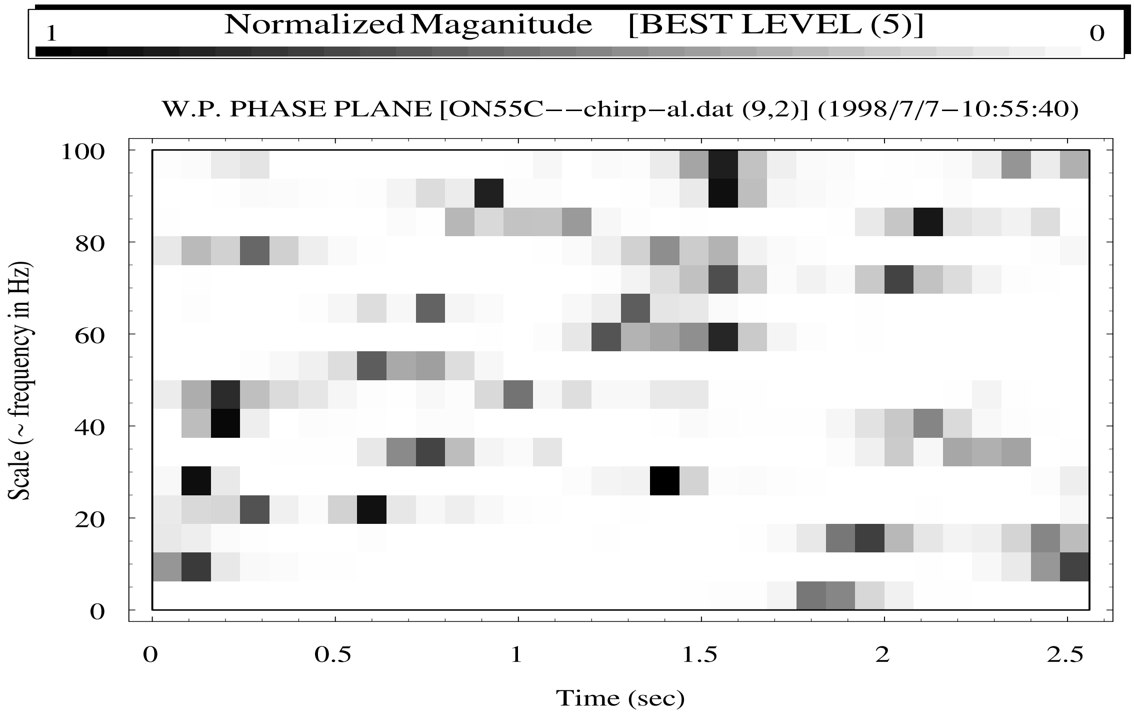

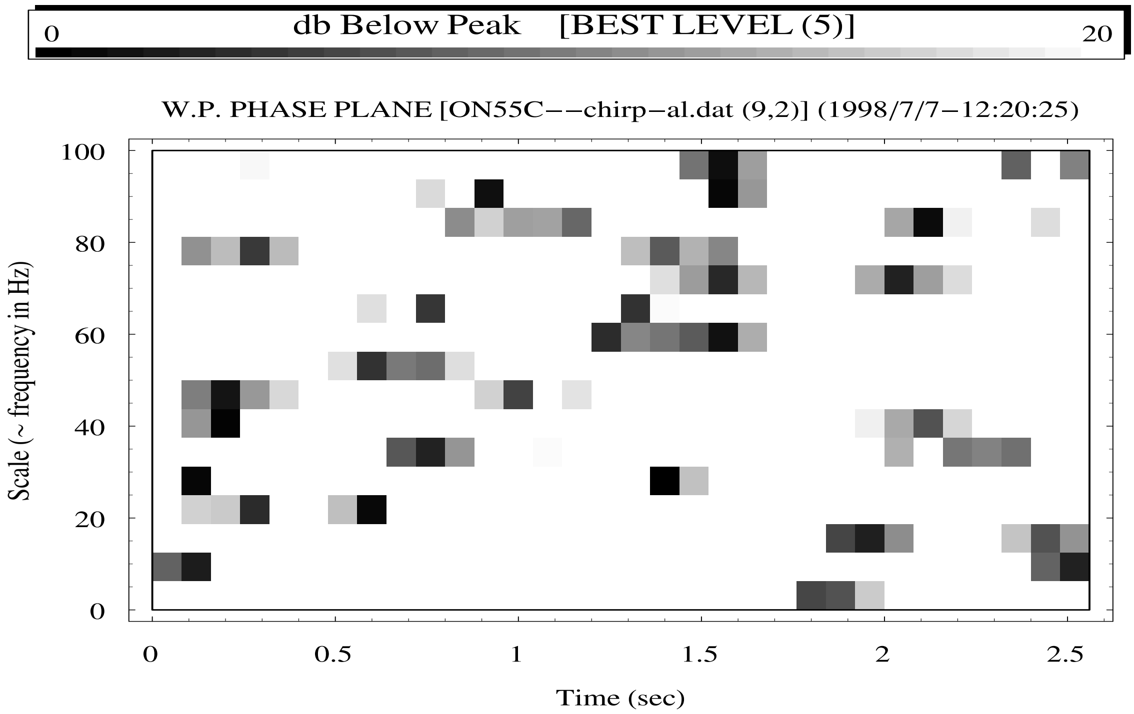

Figure 1.2: Phase planes (`top`: logarithmic measure; `bottom`: linear measure) of a wavelet packet's best level time-frequency windows using the same linear chirp and wavelet packets as in the previous figure. In view of the fact that a single orthonormal mother wavelet can yield many different wavelet packet representations, that there are basically infinitely many wavelet bases, and that we may use different graphic renderings, we are easily trapped in the dilemmas of choosing an appropriate basis.

- We note that the present scope focuses on the $L^2(\mathbf{R})$ Banach space, i.e., the Hilbert space, since some of the statements here may not apply to other function spaces or classes [9, 20]. Nevertheless, most of the intricacies that differentiate different spaces are only of analytic interest up until now (e.g., on the existence of multiresolution analysis (MRA), on the regularity and differentiability of wavelets and its associated scaling functions). From the practical point of view, it is far enough to restrict to the Hilbert space, i.e., a space of functions with finite energy contents.

1.4 The objectives

The foothold to use localized transforms in our water wave applications can be stated quite simply, as well as intuitively — if we perceive our signal as composed of waves which are limited in both life span and covering distance, i.e., constituent waves are evolving with time and in space, then it is natural to adopt wavelet as our analyzing function; furthermore, in addition to this modulation nature, if we also acknowledge that intrinsic instability due to nonliner effects or boundary conditions is everywhere to be found for even regular water waves, then it is still quite possible that wavelet decomposition can provide better descriptions of physics for stationary signals than what can be provided by Fourier decomposition. Besides, another advantage of using wavelets is the possible flexibility in adapting their wave forms to our desires; this is related to the modifications of time-frequency windows for better physical implications.

In this study the contents can basically be divided into five main subject matters.

In the first part we mainly focus on the characterizations of discrete wavelet categories. And the covered discrete wavelet categories should be quite comprehensive — in the sense that they have included all the extreme analytical properties in wavelet designs. And it is the author's belief that if you ever find an individual wavelet you have great chance to assign it into one of these categories, and if not, you have great reason to say that its properties fall within (or between) the covered characterizations and thus its possible usefulness (or destiny) trapped accordingly. The relevant characterizations and intrinsic properties for all the categories are extensively illustrated through the depictions of their mother and farther wavelets, the translations and dilations of wavelets, the zoom-ins or blowups of any kind of wavelets, the linear phase filtering features. Physical counterparts of analytical aspects are provided when possible.

In the second part, we work on the identification of optimum discrete wavelet basis specifically for the applications in studies of water wave related signals, here various entropy criteria are adopted for the whole comprehensive sets of wavelets (as well Fourier basis) using signals obtained from wind-wave-tank experiments.

In the third part we mainly focus on exploring the analytical essence of the behavior of any wavelet function basis concerning its performance or fitness in our water applications, in other words, what is the mathematical factor that leads to the different statistical performances based on the entropy. And this is related to the study of the phase distribution of a wavelet characterizing function (the $m_0(\xi)$ function) for each individual basis.

In the fourth part of the contents we mainly focus on the continuous counterpart wavelet of the identified basis, i.e., a continuous wavelet transform corresponding to the multiresolution analysis of the semi-orthogonal cardinal spline dual wavelet. In this part we first address why there is the need of a continuous transform, that is to say, the advantages and disadvantages of discrete and continuous wavelet transforms concerning their application to water wave studies.

In the fifth part, we address what can be done to improve the physical relevance between the basis functions and the wave constituents of our signals. Here the topics involve: the demand of better physics, the uncertainty relationship and the degrees of freedom for adaptivity, the physics of time-frequency windows of flexible size and shape, and finally the proof of the existence of admissability condition under such an adaptation.

Overall, it can be briefly summarized, to be used for water wave related signals, that the present research proposes a data analysis methodology that involves triple optimizations. ❖

Chapter 2

The Wavelet Bases Tested and Their Characterizations

2.1 Introduction

In almost all modeling experiments various modeling or scaling laws can at best be partially satisfied. The situation is further complicated for multi-scale and multi-dimensional phenomena. In the introduction chapter we noted the problems of proper scaling for the transient phenomenon that involves diversified scales. For water wave experiments it is acknowledgeable that there may be significant distortions concerning the coupling mechanisms targeted. For example, a limitation in space as well as the lack of scale diversification in the tank may hinder the development of certain mechanisms and impose restrictions upon the evolutions of certain interactions. With these understandings, as well as the cognizance regarding the inadequacy of the Fourier spectral approach in our applications as discussed in the first chapter, it is understandable that, if the modeling of the proposed physics is at all possible, the deployment of an optimized analyzing scheme using sensitive and appropriate basis functions is desired. Specifically speaking, we shall select among a broad array of functional bases the most appropriate one for our signals and describe the proper analyzing method. Akin to the interest of such an attempt, it warrants to give more systematical descriptions of different properties of various categories of wavelet function bases. Herein we cover a comprehensive set of discrete wavelet categories that has essentially included all the extreme and opposite analytical properties in wavelet designs.

2.2 The numerical programming

We develop the wavelet numerical analysis and all the relevant data processing from the ground up using the Asyst programming language. It is our desire that the program should provide full coverage of various wavelet bases and it should also capable of exploring any related characterizations of wavelet relevant functions. Besides, it should be quite flexible yet user-friendly. And it is our belief that any keyboard input of data or information should be minimized to none (cut and paste might in rare cases be unwillingly tolerated). To achieve such goal, several program add-ins and application auxiliaries are integrated; notably, these include:

- The Postfix language — This enables the generation of high quality Encapsulated Postscript figures directly form the core programming, and this much improves the overall code writing efficiency, as well as eliminates the painful task of plotting the numerous figures during testings. Besides, full annotations of parameters for all the figures are much possible and thus analyses are confidently error free.

- The on-screen real time display of PCX format figures — The Encapsulated Postscript figures is mainly for quality printing, but it forms in the background and dose not display in real time during the running process of the program; therefore, the on-screen real time display of figures should greatly enhance the debugging efficiency and make possible the writing of a huge and complex program that is also user-friendly, easy to maintain, as well as interactive and extremely flexible.

- The data spreadsheet interface — The input or output of data from and to Excel or Lotus-123 compatible worksheet is integrated. In cases that articulate figures are desired such a function is readily convenient.

- The data interface to Mathematica programming language — This eliminates human intervention for the transferring of results of Asyst analyses to the post generation of various two-dimensional phase plane figures.

- The WinEdt macro programming language — The language is specifically used to develop the shell environment or the development platform for the Asyst program code writing. With this all the code components are displayed in much a scientifically organized and eye-pleasant way. Missing such an integrated part the editing and the debugging of the programs must be quite painful and exhausting.

2.3 Wavelet bases tested and the relevant notations

The Riesz wavelet bases tested here can basically be divided into four categories: orthonormal (ON), semi-orthogonal (SO), bi-orthogonal (BO), and orthonormal wavelet packets bases. For the orthonormal category it is divided into several different subgroups: Daubechies wavelets (both the most and least asymmetric), Coiflets, Meyer wavelet, and Battle-Lemarié wavelets.

No detail accounts of these wavelets will be given; only the main criteria and core features of each categories will be briefed. Let first state the related notations and conventions needed for the context that follows. Let a function or a signal be denoted by $f(t)$; the two-scale scaling function of a Riesz basis be $\phi(t)$; the associate mother wavelet be $\psi(t)$ and its dyadic wavelets be $\psi_{j,k}(t) = \sqrt{2^j}\psi(2^j t - k)$, where $j, k \in \mathbf{Z}$ and k stands for translation and j for dilation. The concept of translations and dilations are illustrated in Figures 2.1 through 2.6.

The space V_j (formed by $\psi_{j,k}$, $k \in \mathbf{Z}$ for a given j) in the multiresolution ladder are nested in $\cdots \subset V_{-1} \subset V_0 \subset V_1 \cdots$, and the finest and the coarsest scale space, say, for a 1024-point signal, are V_{10} and V_0, respectively; the number of filter coefficients or the number of convolution weights be N if the associated wavelet is finitely supported (support length equals to $N - 1$); the dual wavelet and dual scaling function, if exist, be

$\widetilde{\psi}(t)$ and $\widetilde{\phi}(t)$; the inner product be $\langle \cdot, \cdot \rangle$; and the Kronecker delta be $\delta_{j,k}$, $j, k \in \mathbf{Z}$, which is equal to 0 for $j \neq k$ and 1 for $j = k$.

Up until now, all practical wavelets of discrete transform are associated with the theory of multiresolution analysis (MRA) [9, 17]. For Riesz wavelets there always exist dual wavelets except for orthonormal wavelets, which are self-dual. Any discrete wavelet transform involves two convolution operations: one yields detail information; another yields smooth information [22]. Convolutions can either be implemented in a direct way in the time domain for compactly supported wavelets or in an indirect way in the frequency domain. We list the basic properties (restricted to real-valued wavelets) and give the symbols of representation for various categories and subgroups as follows.

2.4 Orthonormal wavelets

The orthonormal wavelets covered here include the following categories: Daubechies most compactly supported wavelets (denoted as ONxxA); Daubechies least asymmetric wavelets (ONxxS); Coiflets (ONxxC); Meyer wavelet (Meyer); Battle and Lemarié wavelet (B&L). Here in all the subsequent annotation x is an integer related to support length (physically, the span of mother wavelet curve).

$$\psi = \widetilde{\psi}, \tag{2.1}$$

$$\phi = \widetilde{\phi}, \tag{2.2}$$

$$\langle \psi_{j,k}, \widetilde{\psi}_{l,m} \rangle = \delta_{j,l}\delta_{k,m}, \tag{2.3}$$

$$f(t) = \sum_{j,k} \langle f, \psi_{j,k} \rangle \psi_{j,k}, \tag{2.4}$$

One MRA ladder (single set of frame bounds),

One filter pair (one smooth and one detail).

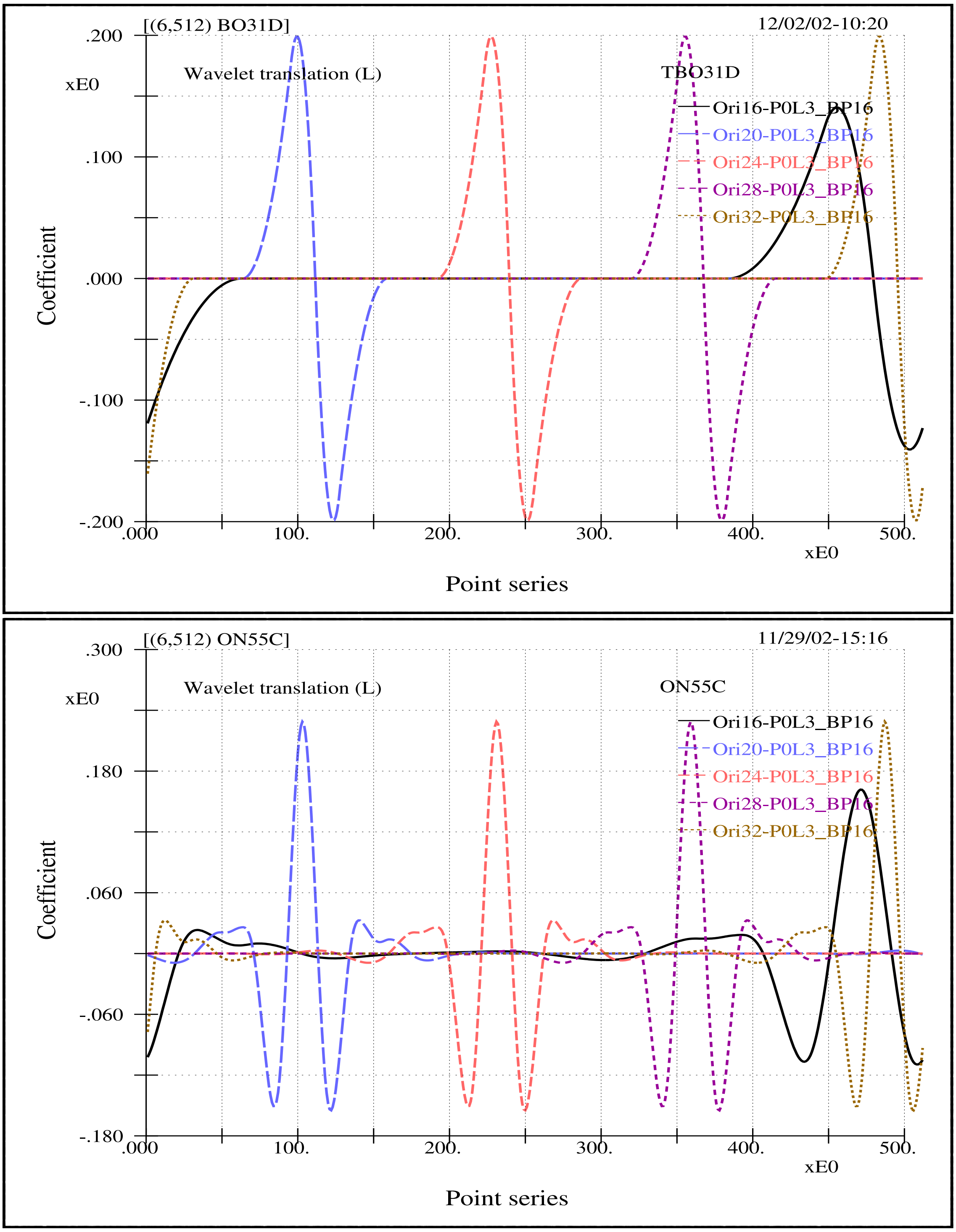

Figure 2.1: The wavelet translation concept within the scale range of level 3.

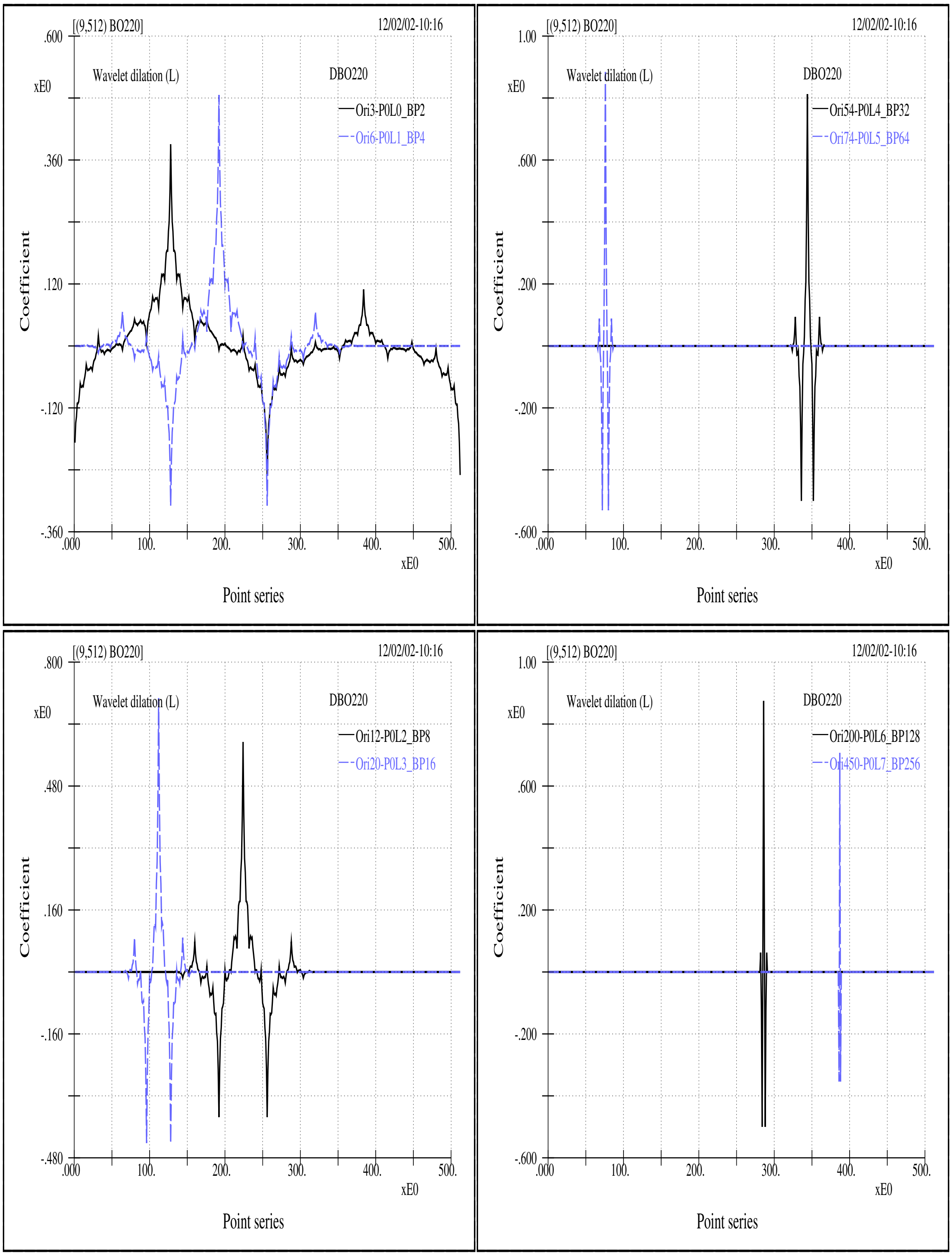

Figure 2.2: The wavelet dilation concept from scale level 0 to level 7 for the BO22O wavelet. Each wavelet curve corresponds to an individual translation location.

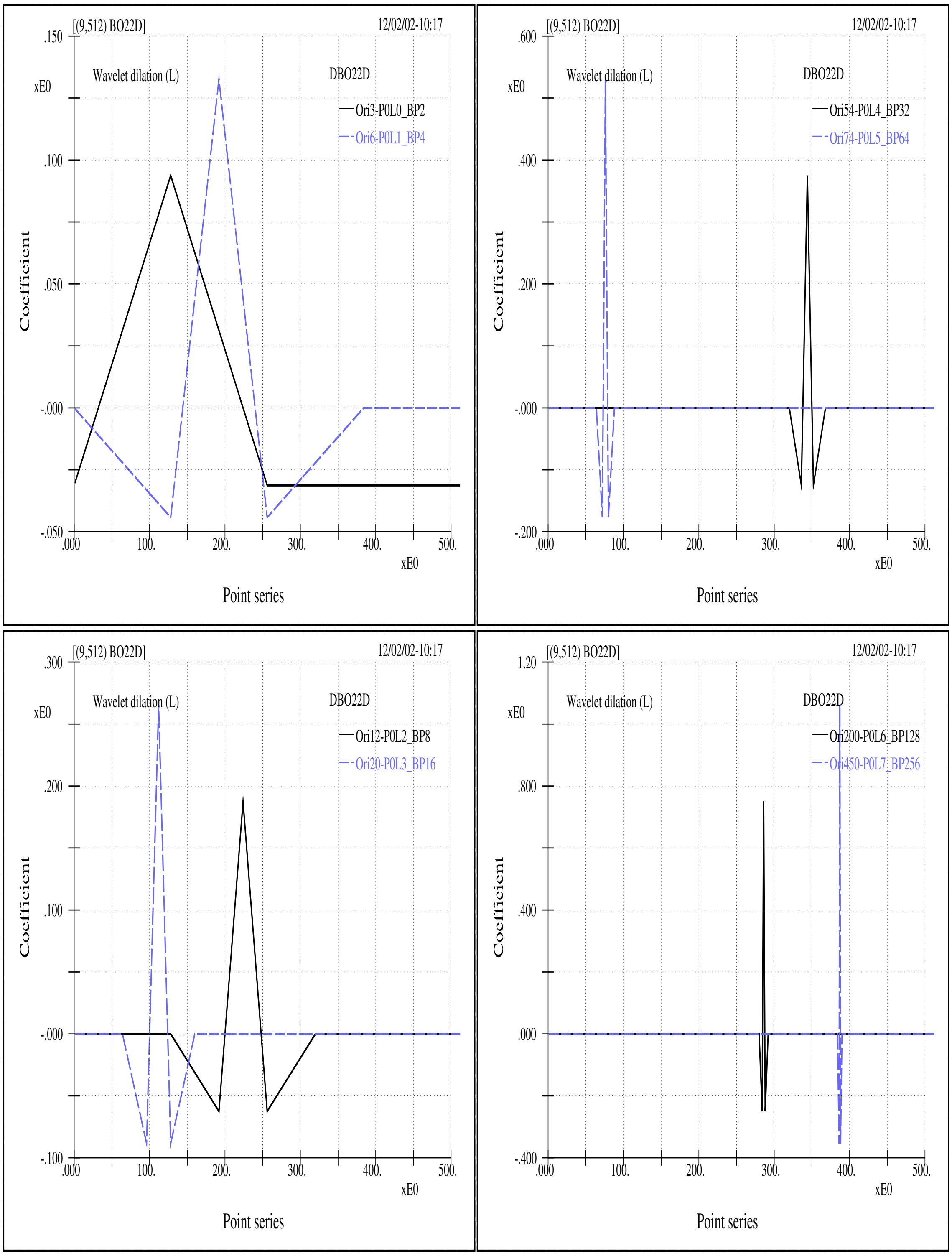

Figure 2.3: The wavelet dilation concept from scale level 0 to level 7 for the BO22D wavelet. Each wavelet curve corresponds to an individual translation location.

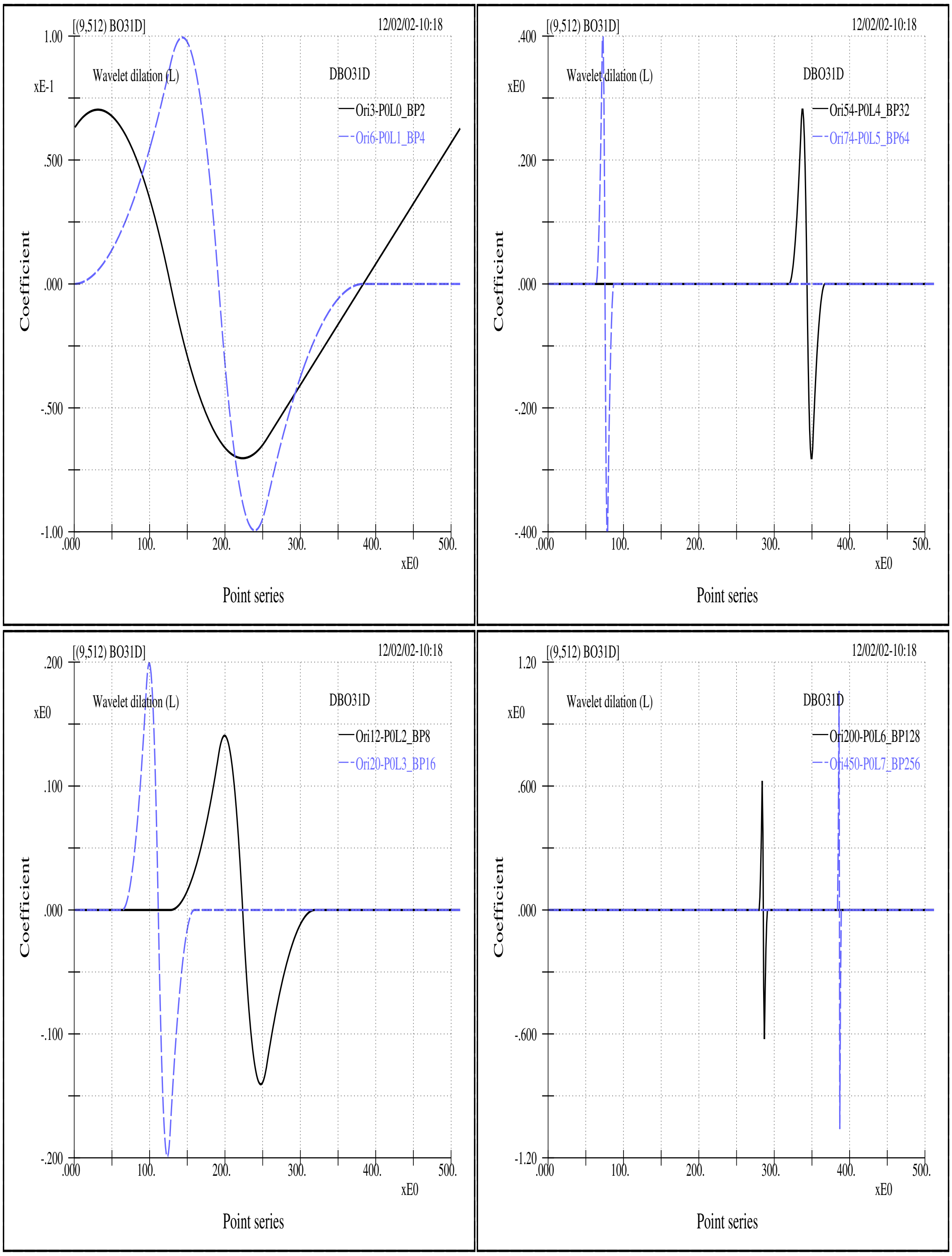

Figure 2.4: The wavelet dilation concept from scale level 0 to level 7 for the BO31D wavelet. Each wavelet curve corresponds to an individual translation location.

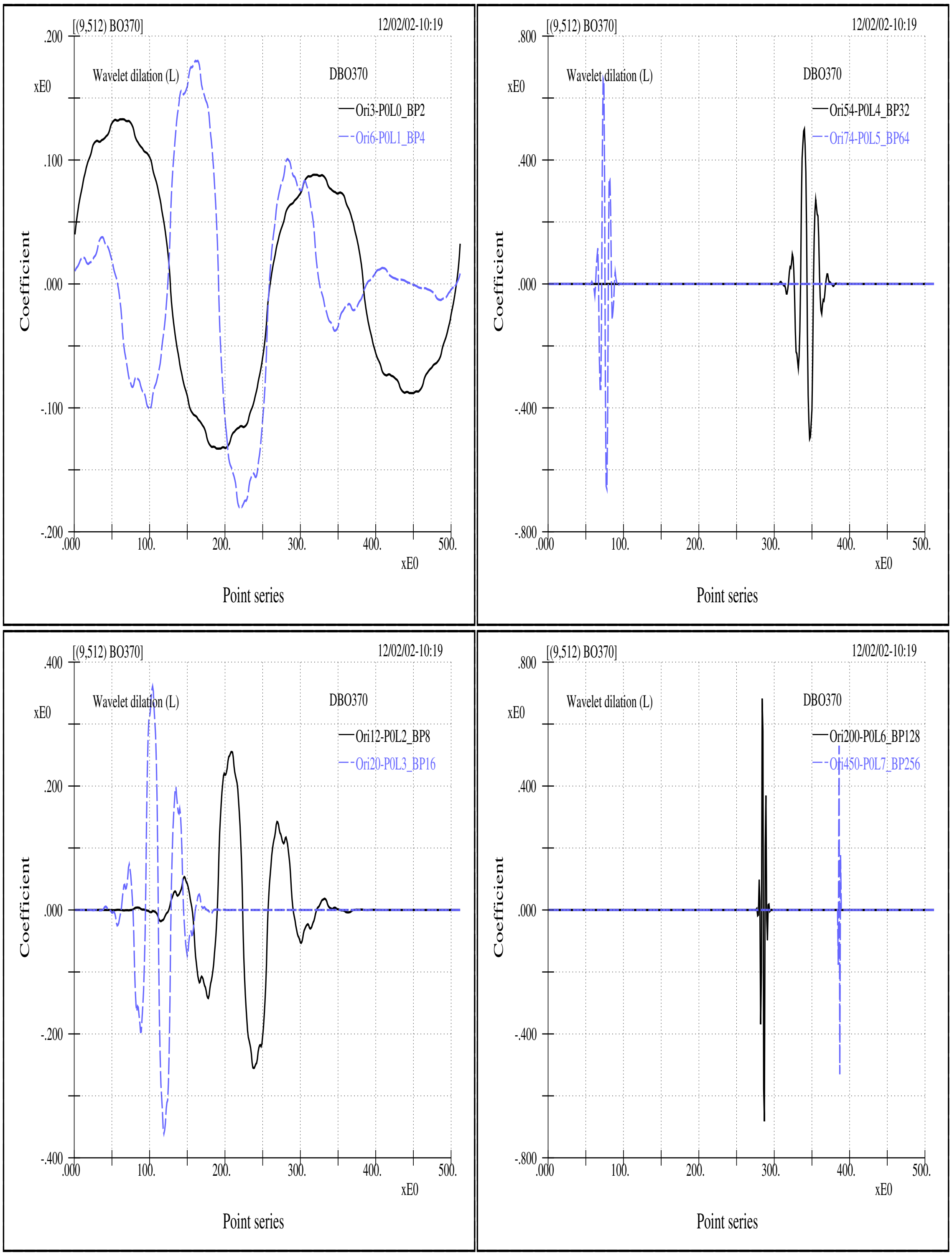

Figure 2.5: The wavelet dilation concept from scale level 0 to level 7 for the BO370 wavelet. Each wavelet curve corresponds to an individual translation location.

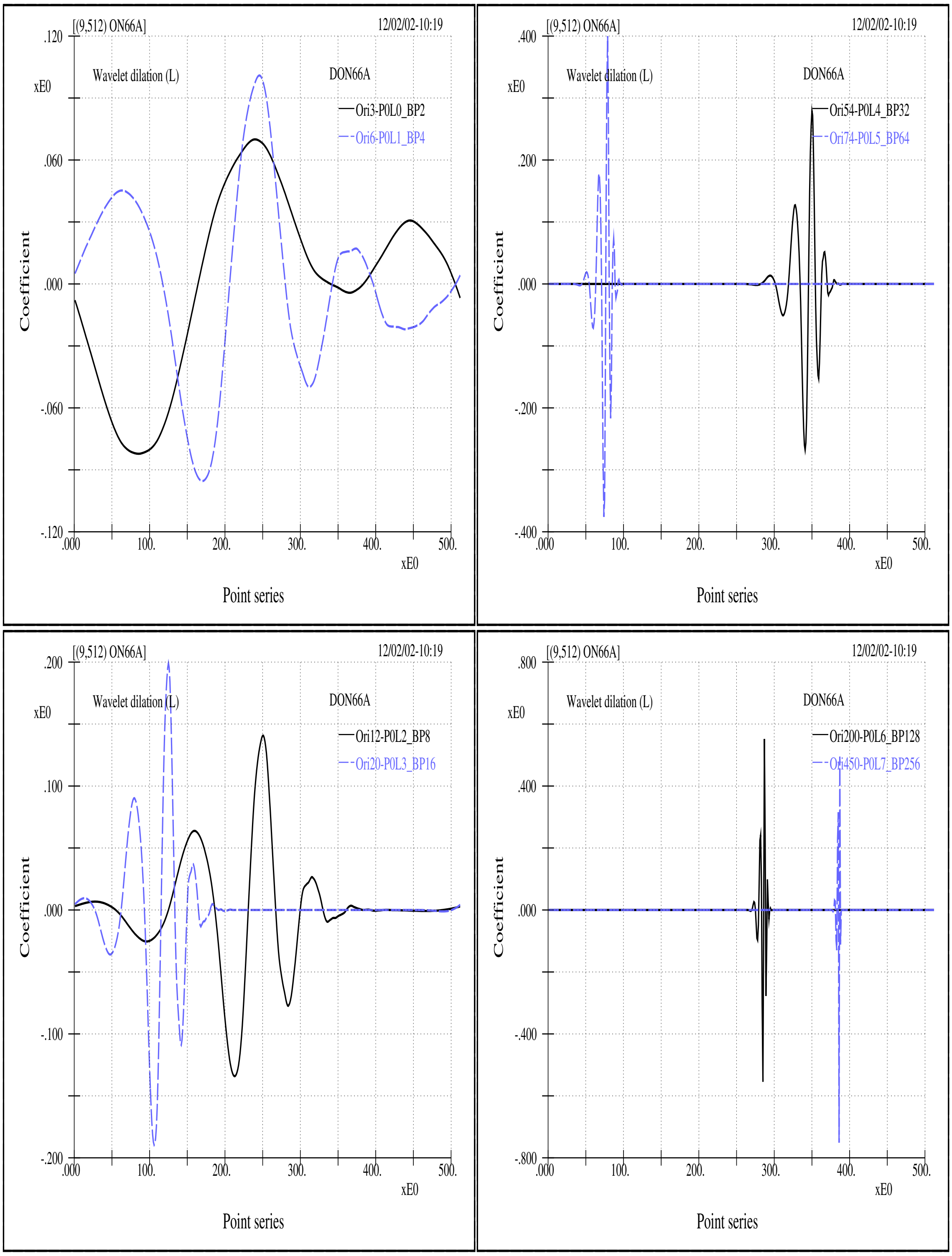

Figure 2.6: The wavelet dilation concept from scale level 0 to level 7 for the ON66A wavelet. Each wavelet curve corresponds to an individual translation location.

2.4.1 Daubechies most compactly supported wavelets (ONxxA)

The wavelets in this group have maximum number of vanishing moments for given compatible support width. Or stated otherwise, they are the most compactly supported wavelets for given compatible number of vanishing moments. The famous most compactly supported continuous wavelet belongs to this group and has only four filter coefficients. These wavelets are quite asymmetry (so, the "A" in ONxxA). The mother and farther wavelets for the group corresponding to the originating points of 12 (boundary point based on level 2) and 6 (boundary point based on level 3), respectively, for this group are shown in Figures 2.7 and 2.8. The vanishing moments and the number of filter coefficients are, respectively,

$$\int_{-\infty}^{\infty} t^l \psi(t) dt = 0, \qquad l = 0, 1, \cdots, x, \tag{2.5}$$

$$N = 2x, \tag{2.6}$$

where x is the integer number in ONxxA. The minimum number of x is 2.

2.4.2 Daubechies least asymmetric wavelets (ONxxS)

For a given support width, these wavelets, in contrast to those of the ONxxA subgroup, are the most symmetric ones (so, the "S" in ONxxS, but still not symmetric). They have the same representations of vanishing moments and number of filter coefficients as those of ONxxA. But the known minimum number of x is 4. The mother and farther wavelets for this group corresponding to the same originating points as the previous ones are shown in Figures 2.9 and 2.10.

2.4.3 Coiflets (ONxxC)

The Coiflets have vanishing moments for both ψ and ϕ; therefore, from Taylor expansion point of views [9], they have high compressibility for fine detail information (i.e., a great portion of the fine scale wavelet coefficients are relatively small); and henceforth, they have simple quadrature rule to calculate the fine smooth information (i.e., the calculation of the inner product of a function and the fine-scale scaling functions is more efficient). Since every discrete wavelet transform involves both smoothing and detailing operations, there may exist some advantages from these two properties for certain applications such as applications that do not stress lossless of signal contents or perfect reconstructions [7, 25]. Their vanishing moments and number of filter coefficients are

$$\int_{-\infty}^{\infty} t^l \psi(t) dt = 0, \quad l = 0, 1, \cdots, x, \tag{2.7}$$

$$\int_{-\infty}^{\infty} \phi(t) dt = 1, \tag{2.8}$$

$$\int_{-\infty}^{\infty} t^l \phi(t) dt = 0, \quad l = 1, \cdots, x, \tag{2.9}$$

$$N = 6x. \tag{2.10}$$

For this group the mother and farther wavelets are shown in Figures 2.11 and 2.12.

2.4.4 Meyer wavelet (Meyer)

The Meyer wavelet (denoted as Meyer or ME in figures) is the wavelet with most compact support in frequency domain (here, if without any specific assignment, "finitely supported" refers to time domain). Therefore, due to contrast properties between the two Fourier domains, the wavelet is infinitely differentiable in time domain, i.e., has an infinite Lipschitz regularity C^∞ and does not have exponential decay. And the support length $N \to \infty$. The associated mother and farther wavelets corresponding to the same originating points are shown in Figure 2.13.

2.4.5 Battle and Lemarié wavelet (B&L)

The Battle and Lemarié wavelet (denoted as B&L or LE in figures) of m^{th} order is constructed from the orthonormal scaling function derived by applying the standard orthonormalization trick to the m^{th} order cardinal B-spline N_m [2, 4]. For $m = 1$, it is exactly the Haar wavelet. The latter is the only finitely supported wavelet in this group (also the case of BO11O=BO11D to be mentioned below) and is also a discontinuous wavelet with the most compact support. All other wavelets in this group are infinitely supported. These wavelets have an exponential decay and possess C^{m-2} regularity. The mother and farther wavelets for the Battle-Lemarié wavelet are shown in Figure 2.14. Compared to the curves of Meyer wavelet (Figure 2.13), they look quite identical even though their constructions, or derivations, or formula involved (including Lipschitz regularity and decay property) are completely different.

2.5 Semi-orthogonal wavelets (SO*x*O and SO*x*D)

The semi-orthogonal wavelets are inter-scale, but not inner-scale, orthogonal. Their scaling functions are cardinal B-spline N_m and have finite two-scale relations. Although there are two distinctive (independent) filter pairs (one for the decomposition and the other for the reconstruction), there is only one MRA V_j-ladder. It was shown by Chui [4, 5] that the cardinal B-spline wavelet of an order higher than $m = 3$ is almost a modulated Gaussian (but a modulated Gaussian is not a wavelet). Therefore only the fourth order Cubic B-spline wavelet ($m = 4$) is tested. It has the following characterizations.

$$\psi \neq \widetilde{\psi}, \tag{2.11}$$

$$\phi = \widetilde{\phi}, \tag{2.12}$$

$$\langle \psi_{j,k}, \psi_{l,m} \rangle = \langle \widetilde{\psi}_{j,k}, \widetilde{\psi}_{l,m} \rangle = \delta_{j,l}, \tag{2.13}$$

$$f(t) = \sum_{j,k} \langle f, \psi_{j,k} \rangle \widetilde{\psi}_{j,k} = \sum_{j,k} \langle f, \widetilde{\psi}_{j,k} \rangle \psi_{j,k}, \tag{2.14}$$

$$N = 3x - 1 \quad \text{for SO}x\text{D}, \tag{2.15}$$

$$N \to \infty \quad \text{for SO}x\text{O}. \tag{2.16}$$

One MRA ladder ,

Two filter pairs ,

The mother and farther wavelets of the fourth order and the associated dual wavelets are shown in Figure 2.15.

2.6 Bi-orthogonal wavelets (BOxyO and BOxyD)

The wavelets in this category are constructed also by Daubechies, and are sometimes called non-orthogonal wavelets. As is well known all real-valued orthonormal compactly supported wavelets, except the Haar wavelet, are not symmetrical. However, from the point of view of reconstructing a signal from its partially truncated wavelet coefficients, the symmetry is a desired property of the filter when a more natural perception or smoother variations is important. There is a very practical implication here: if non-symmetrical function bases are used, then a small change in the wave form causes significant variations of scale information. In other words, to have minor impacts to the data analysis, it is desirable to have bases as symmetrical as possible. Moreover, when considering that random errors, or noise, or uncontrolled factors are present, we should be able to comprehend the significance of this property. In fact many of the figures given in this study indicate such a feature. The symmetry can be achieved by sacrificing orthogonality; if this is the case one has dual pairs for both wavelets and scaling functions. It is obvious that conditions for semi-orthogonal cases are more general than those of orthogonal ones, and the bi-orthogonal cases are even more general. This situation is clearly indicated by the additional freedom of dual scaling function, as is reflected by the two parameters x and y in the notations of BOxyO and BOxyD. Nevertheless, the wavelets in this category involve only one pair of independent filters for both decomposition and reconstruction even though there involve two different MRA ladders that are associated with their own individual sets of Riesz bounds. This is quite opposite to the case of semi-orthogonal wavelets where they involve one MRA ladder but with two filter pairs.

$$\psi \neq \widetilde{\psi}, \tag{2.17}$$

$$\phi \neq \widetilde{\phi}, \tag{2.18}$$

$$\langle \psi_{j,k}, \widetilde{\psi}_{l,m} \rangle = \langle \phi_{j,k}, \widetilde{\phi}_{l,m} \rangle = \delta_{j,l}\delta_{k,m}, \tag{2.19}$$

$$f(t) = \sum_{j,k} \langle f, \psi_{j,k} \rangle \widetilde{\psi}_{j,k} = \sum_{j,k} \langle f, \widetilde{\psi}_{j,k} \rangle \psi_{j,k}, \tag{2.20}$$

$$N = 2y + x - 1 \quad \text{for BO}xy\text{O and } x \text{ odd}, \tag{2.21}$$

$$N = 2y + x - 2 \quad \text{for BO}xy\text{O and } x \text{ even}, \tag{2.22}$$

$$N = 2y + x - 1 \quad \text{for BO}xy\text{D and } y \text{ odd}, \tag{2.23}$$

$$N = 2y + x - 2 \quad \text{for BO}xy\text{D and } y \text{ even}. \tag{2.24}$$

Two MRA ladders,

One filter pair,

The mother and farther wavelets for this group and the associated dual wavelets are shown in Figures 2.16 through 2.19.

2.7 Wavelet packets

The wavelet coefficients derived from an orthonormal wavelet decomposition can be further decomposed by using either the set of filter coefficients (called two-scale sequence in Chui [4]) associated with the original wavelet, or different sets of filter coefficients associated with other orthonormal wavelets. Therefore, basically there can be infinitely many wavelet packet decompositions. These further decompositions are of a tree-like refinement process and are called the wavelet packet transform. The wavelet packet coefficients give better frequency resolutions with longer time supports. There are no simple formulas to describe the tree-like decompositions, but a schematic plot help elucidate the mechanism shown in Figure 2.20. The branch patterns and the number of branches can be chosen in any way so long as there is no repeat occurrences within any column under the stretch of the coefficients. That is to say, any column, wide or narrow, must have one and only one contribution from all levels (rows). Due to the tree-like process the computational works are dramatically increased.

For this category we have two criteria for selecting our best basis. One is still called the "best basis"; another "best level basis". Take for example, for a 1024-point signal, the finest level occurs at $j = \log_2 1024 = 10$ and there are 2^{10} different choices of bases. And within these 2^{10} choices the one which yields the minimum entropy is called the "best basis". And if we enforce the restriction that all wavelet packets be at the same level j, then we have 10 levels (0 to 9) to choose from; the level that yields minimum entropy is called best level basis. The indexes of a wavelet packet coefficient, i.e., the subscript and superscript of U labeled in the figure determine the time of occurrence of that coefficient and also indicate the associated support length and frequency resolution, i.e., the shape and location of the coefficient's time-frequency window within the phase plane. Concepts regarding the wavelet packet transform can be seen in Figure 1.1. Again we also see the effects of non-symmetrical filtering. One specific feature is that the areas of all individual windows are all equal.

2.8 Wavelet blowups

Wavelets are fractal in nature, that is to say, no matter how detail we zoom into the wavelet curve its blowups all show similar characterization, and this is related to the wavelet differentiability, regularity, support length, and decaying property.

The Asyst program is written to be able to blow any wavelet constructions, such as mother and father wavelets, wavelet bases and wavelet packet bases at any point on any level. A few examples are shown in Figures 2.21 to 2.28.

Her we note that wavelets with fancy analytical properties are often of bizarre wave forms and not of our choice for studying water wave related physics — either judging from they entropy values to be given in the next chapter or form their stability conditions.

Moreover, this blowup exercise hints the behaviors of several numerical and theoretical aspects of wavelet analysis, such as the edge effects, the possible differences of function curves due to finite resolution, and the convergent or error propagation property.

Figures 2.27 and 2.28 show the blow-ups of bi-orthogonal wavelet BO31O and BO35O, respectively. Relevant data for BO31O is: Origin of wavelet curve: level 2, position 12 (i.e., element U_2^{12} in figure 2.20); Blow-up point: 150; data length: 512. Each sub-figure shows successive blow-up scale of 2^6. Here the blow-ups diverge rapidly, i.e., the wavelet fails to identify itself numerically in the refinement cascade. Relevant data for BO35O is: Origin of wavelet curve: level 2, position 12 (i.e., element U_2^{12} in figure 2.20); Blow-up point: 225; data length: 512. Each sub-figure shows successive blow-up scale of 2^6. Here the blow-ups converge but go with peculiar inclinations.

Figure 2.26 also exhibits the grouping tendency of wavelet packets. ❖

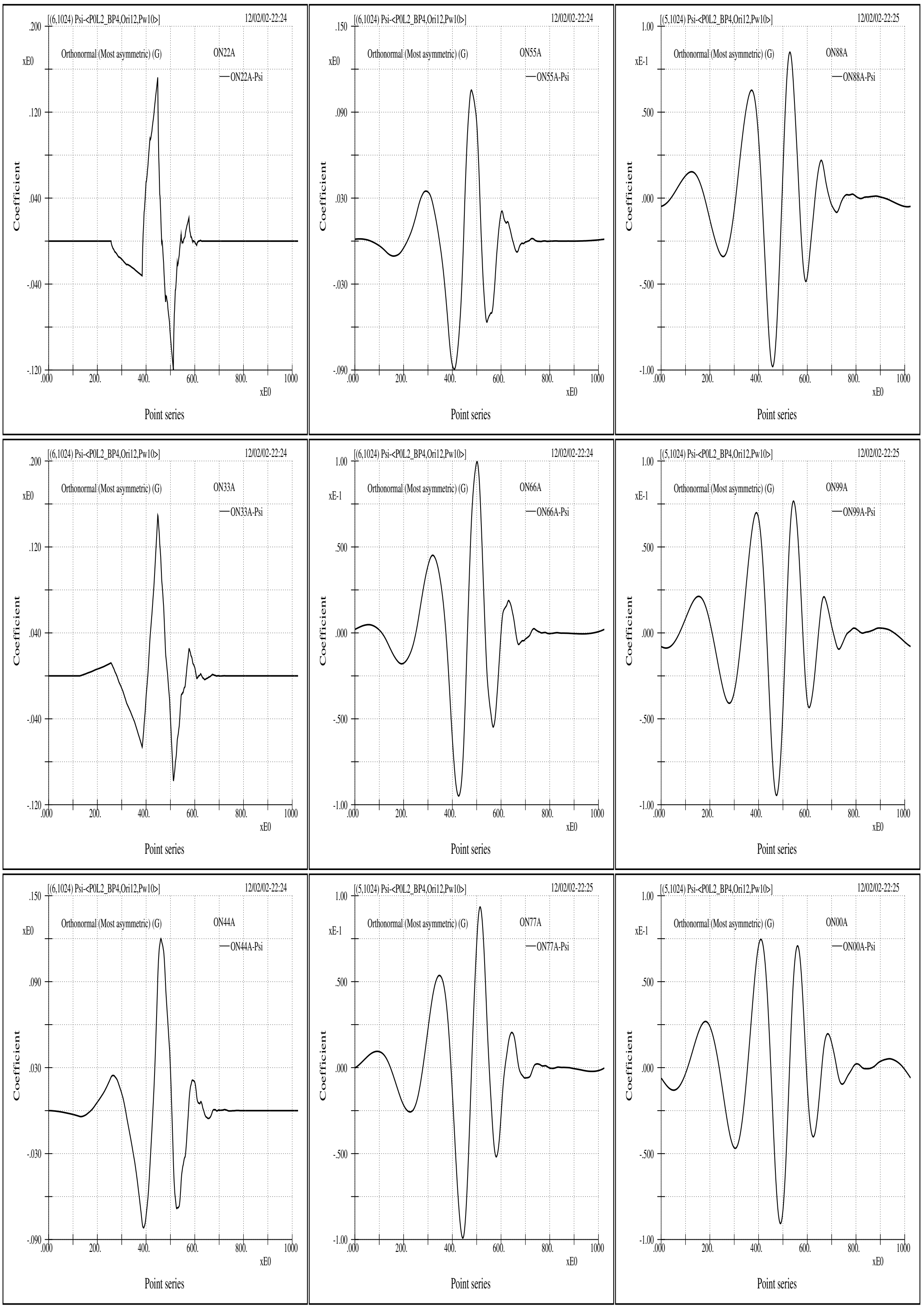

Figure 2.7: The mother wavelets of the ONxxA group originating from the point location of 12. Here the boundary point should be based on a level less or equal to 3.

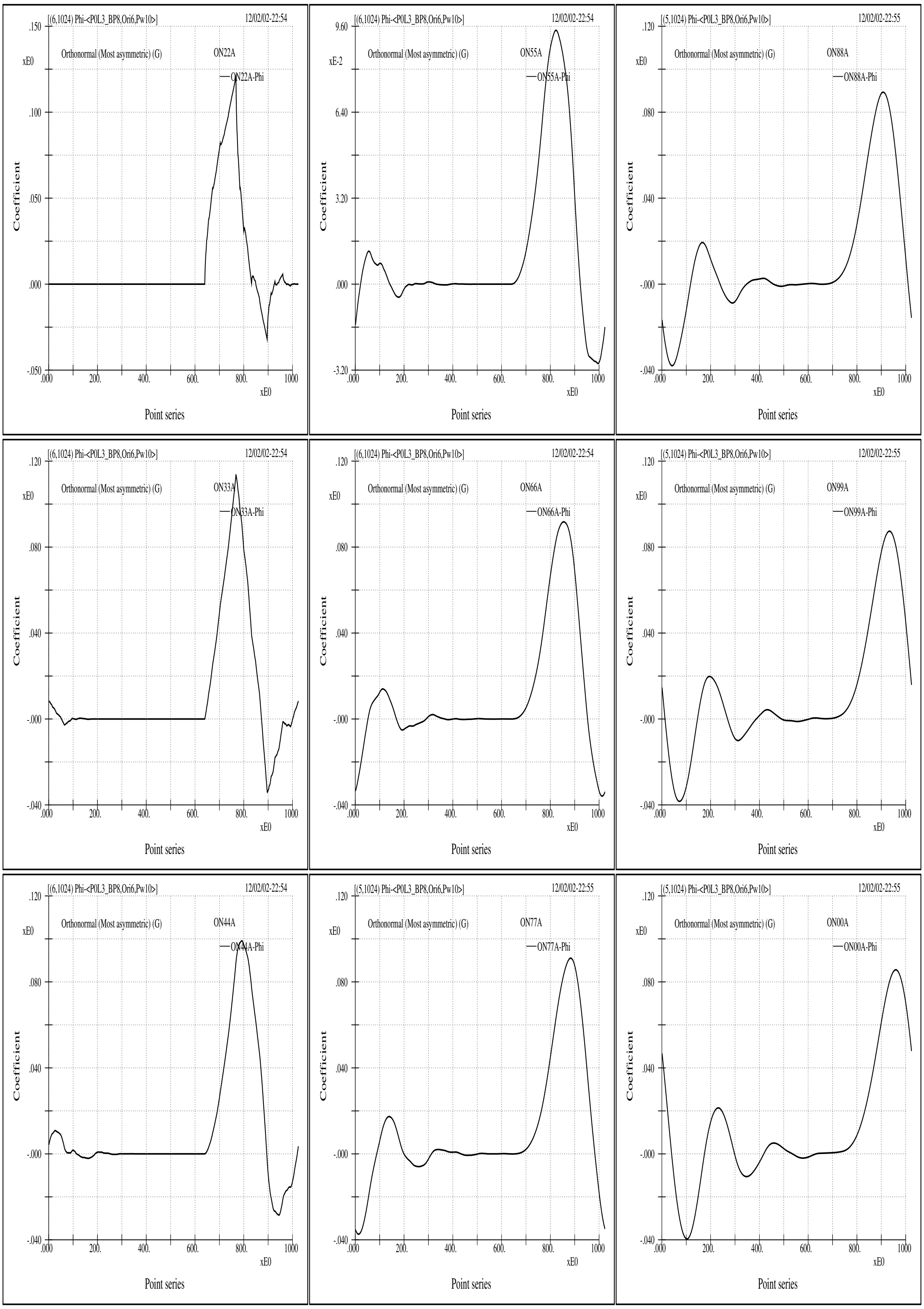

Figure 2.8: The farther wavelets of the ONxxA group originating from the point location of 6. Here the boundary point should be based on a level higher or equal to 3.

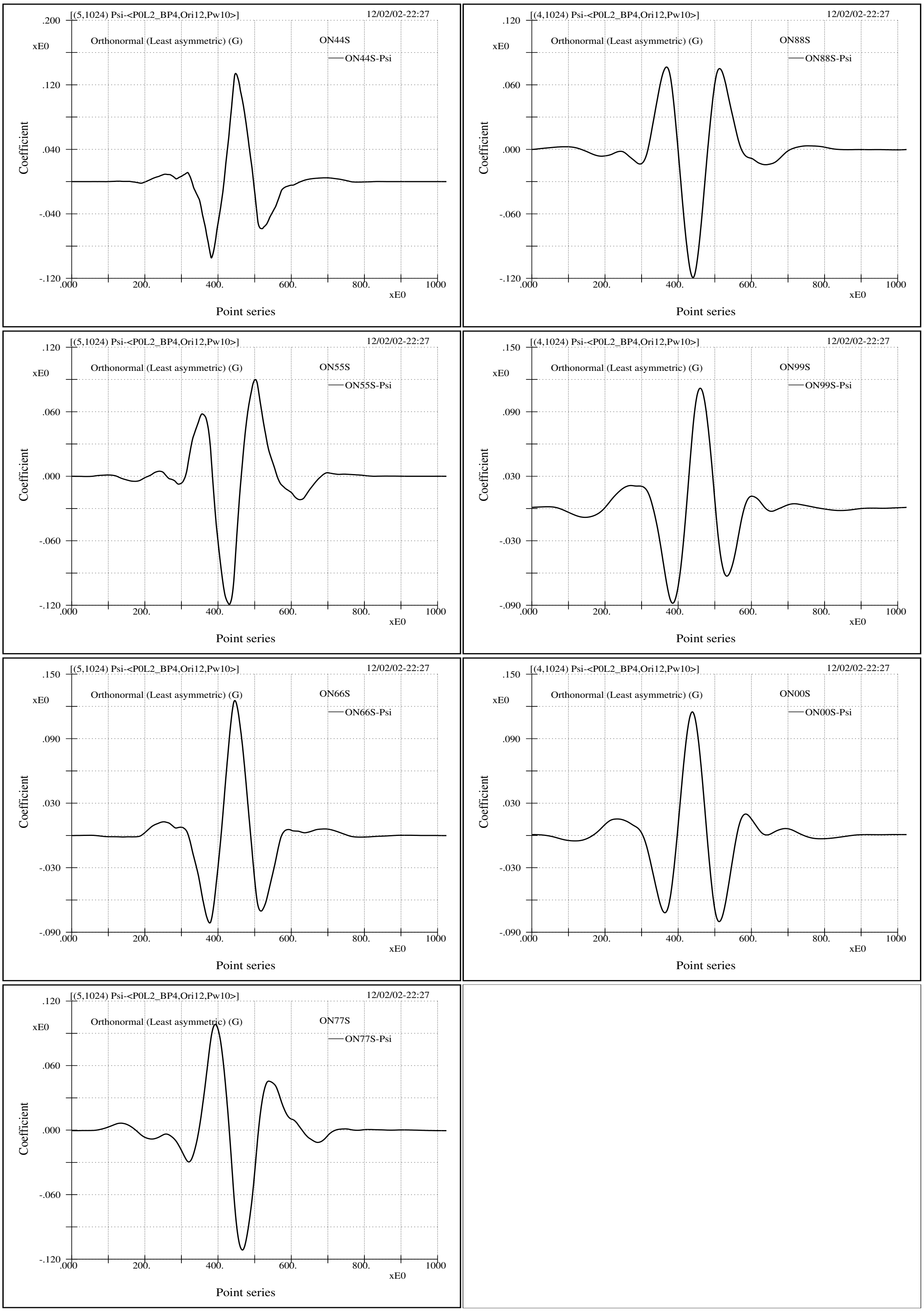

Figure 2.9: The mother wavelets of the ONxxS group originating from the point location of 12. Here the boundary point should be based on a level less or equal to 3.

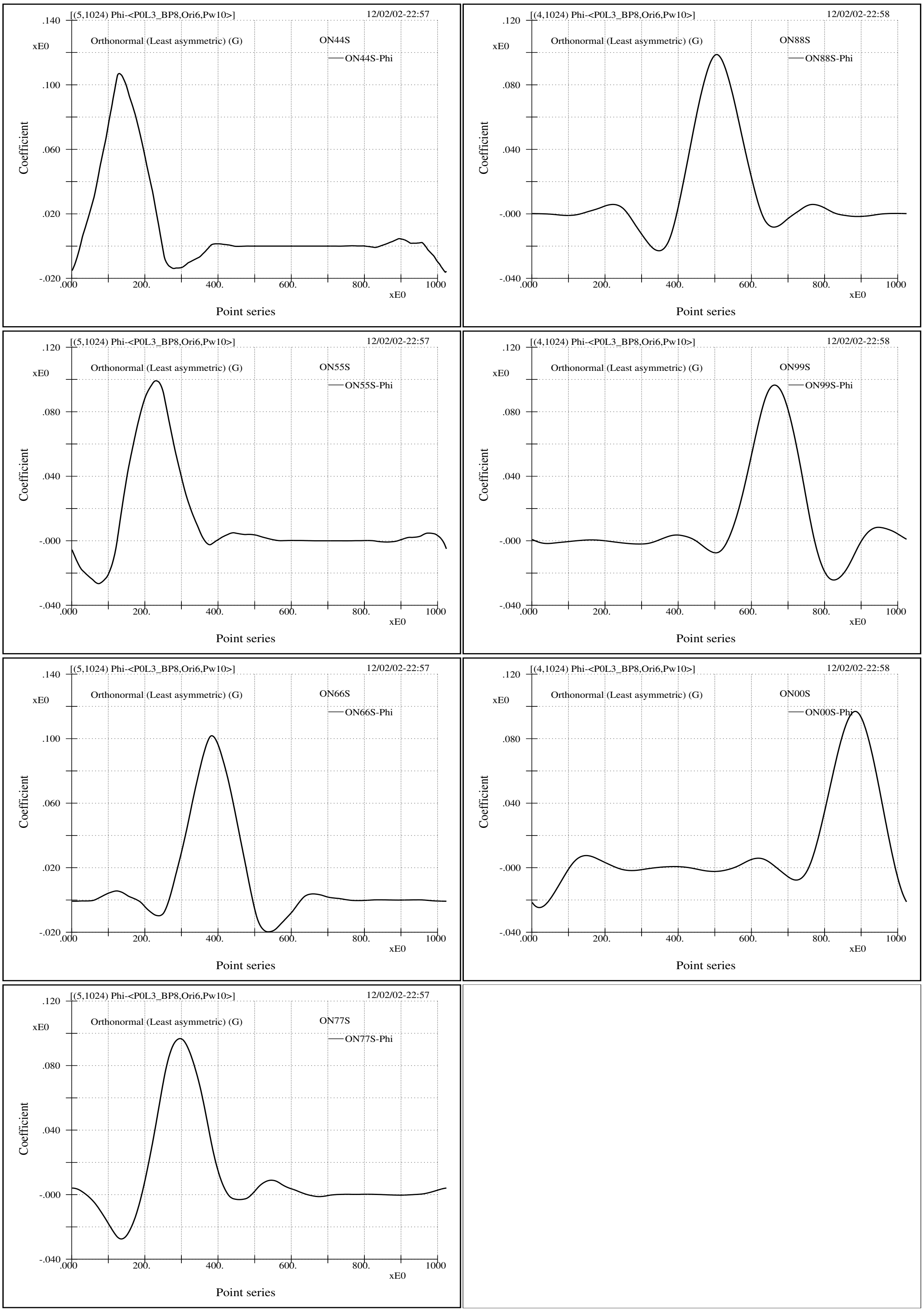

Figure 2.10: The farther wavelets of the ONxxS group originating from the point location of 6. Here the boundary point should be based on a level higher or equal to 3.

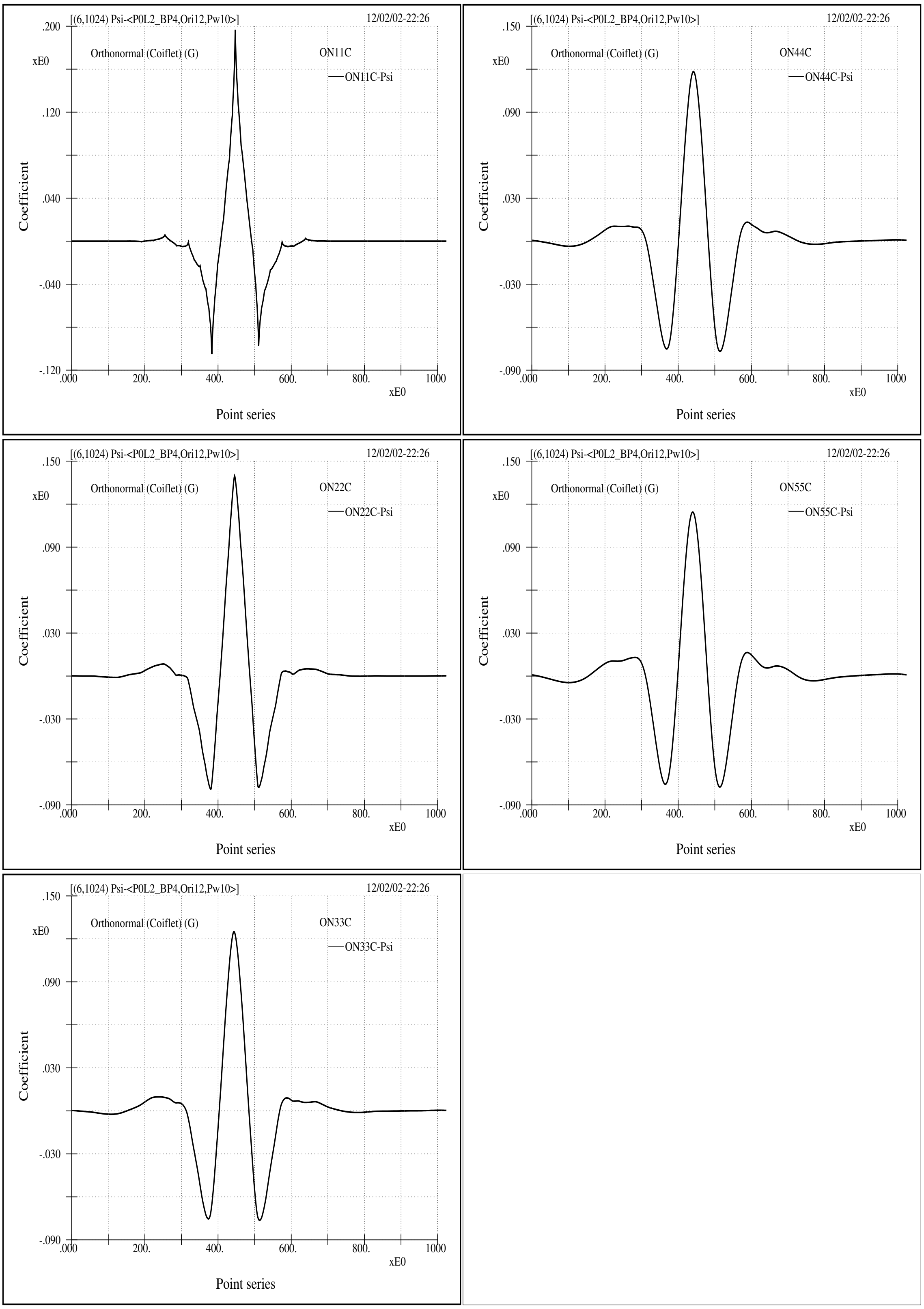

Figure 2.11: The mother wavelets of the ONxxC group originating from the point location of 12. Here the boundary point should be based on a level less or equal to 3.

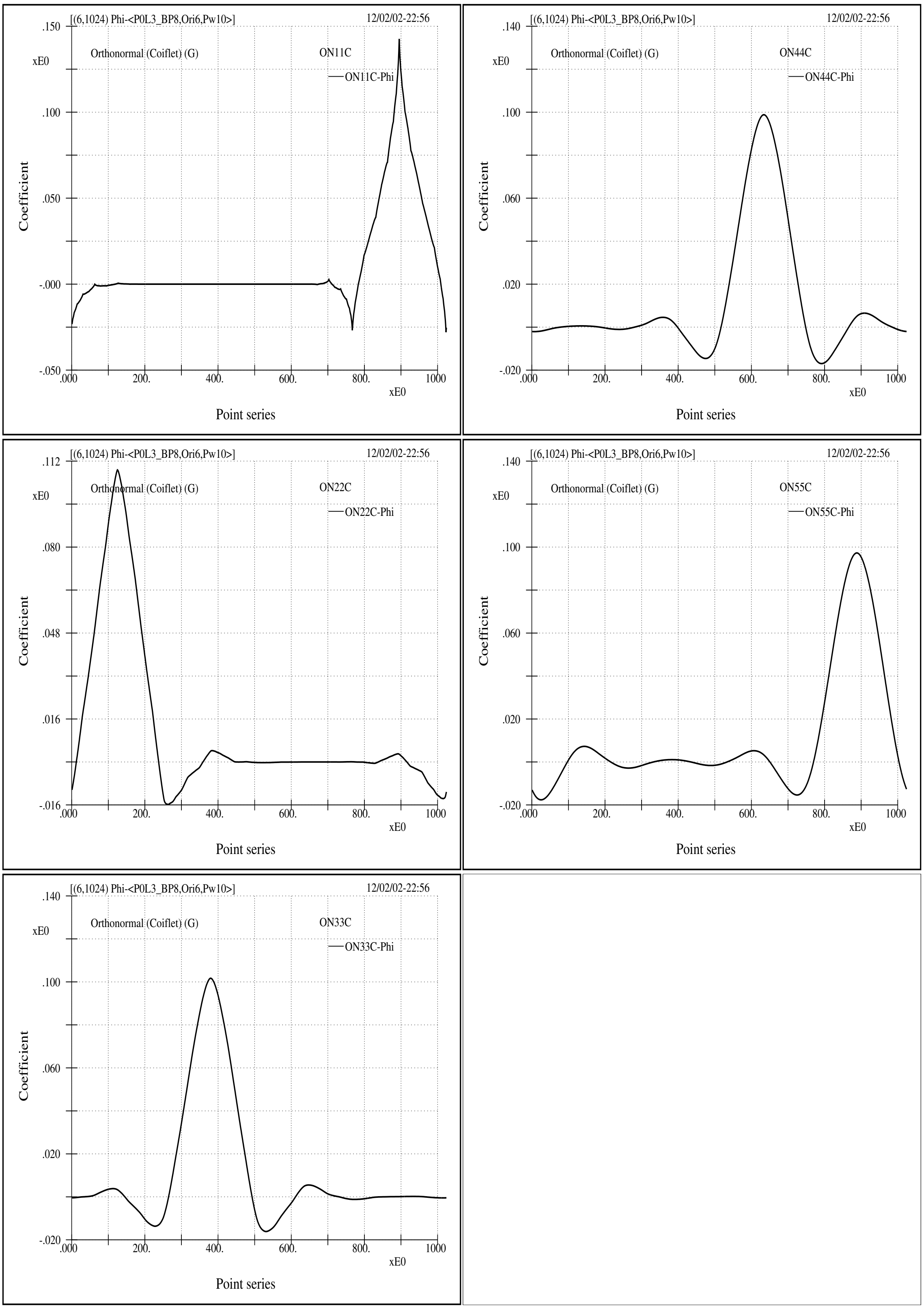

Figure 2.12: The farther wavelets of the ONxxC group originating from the point location of 6. Here the boundary point should be based on a level higher or equal to 3.

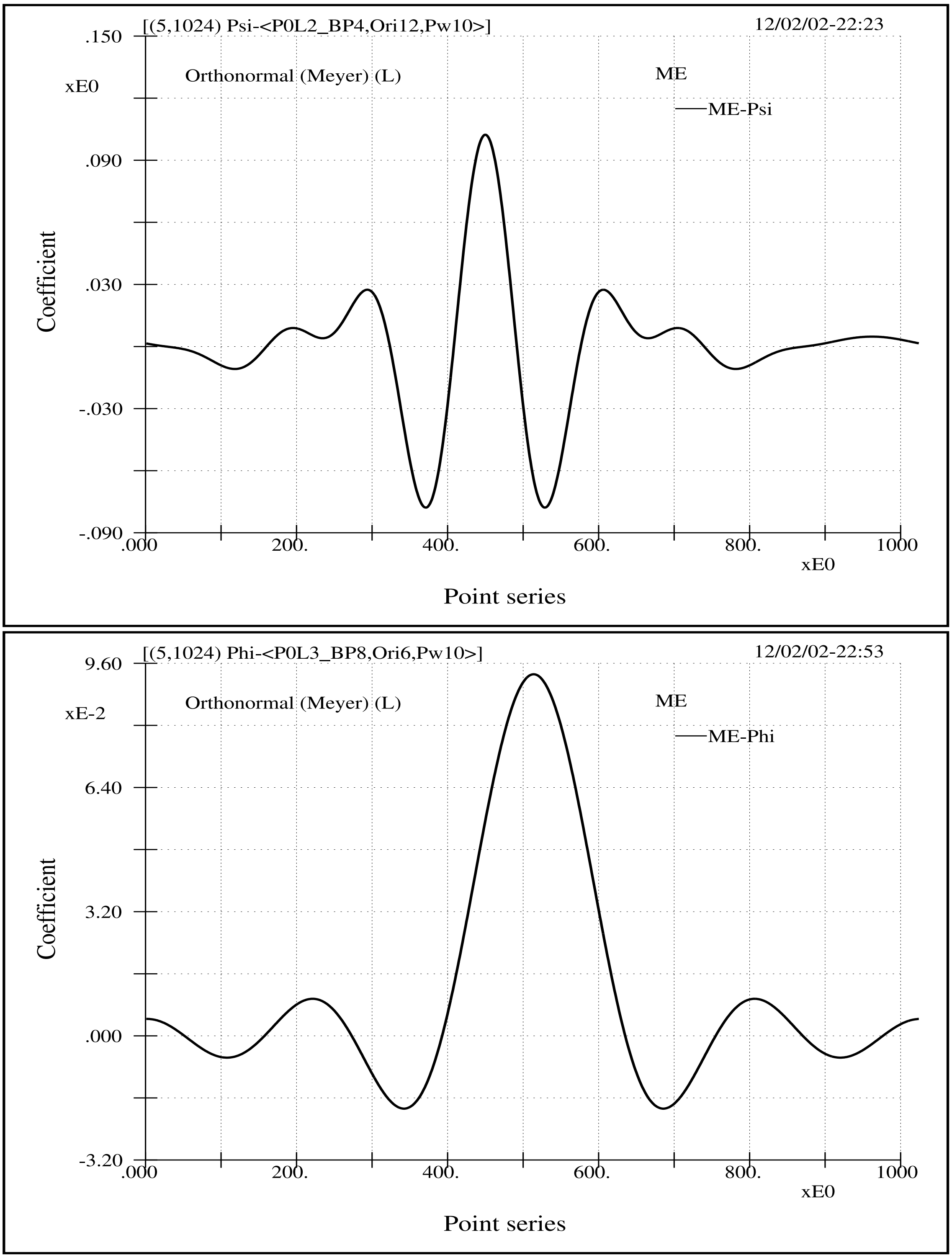

Figure 2.13: The mother `(top)` and farther `(bottom)` wavelets of the Meyer wavelet originating from the point location of 12 and 6, respectively, for the boundary point based on level 3. This figure is to be compared to the next one.

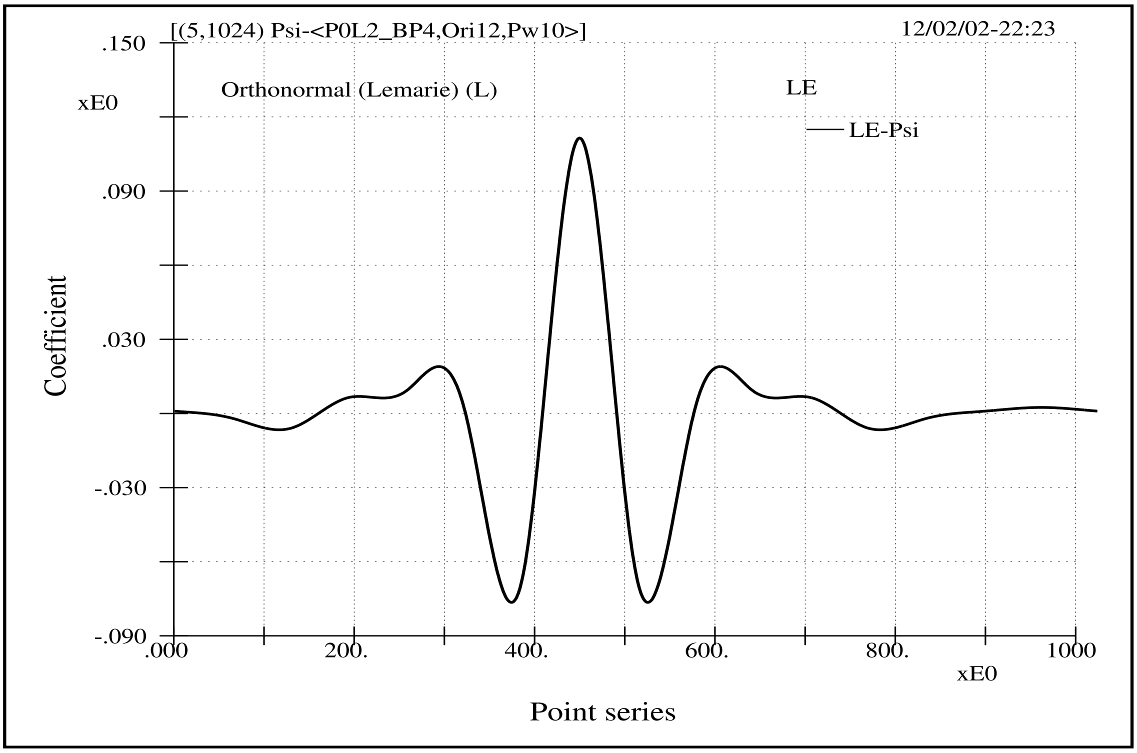

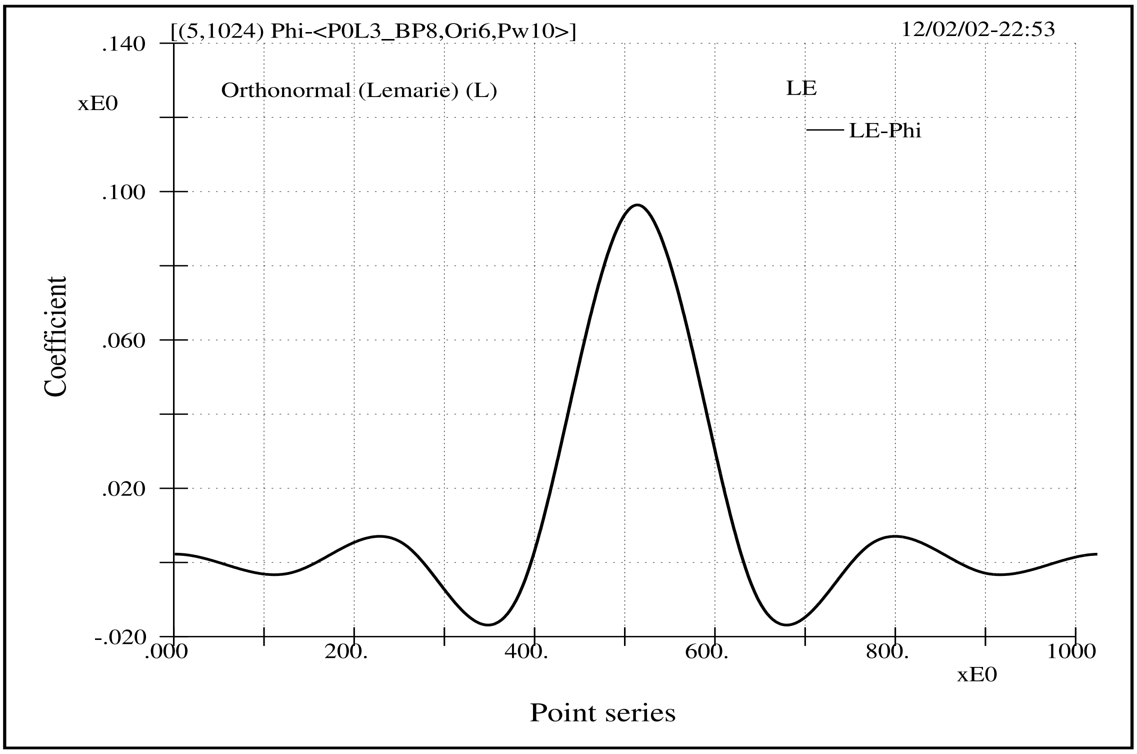

Figure 2.14: The mother `(top)` and farther `(bottom)` wavelets of the Battle and Lemarié wavelet originating from the point location of 12 and 6, respectively, for the boundary point based on level 3. Comparing the wavelet functions shown here with those shown in last figure (Figure 2.13), we see that two wavelets of similar looks but with quite distinctive constructions and analytic properties (such as regularity, differentiability, rate of decay, support length, etc.) It therefore gives rise the concerns that many complicated aspects of discrete Riesz wavelet seem not to reflect their associations with practical concerns.

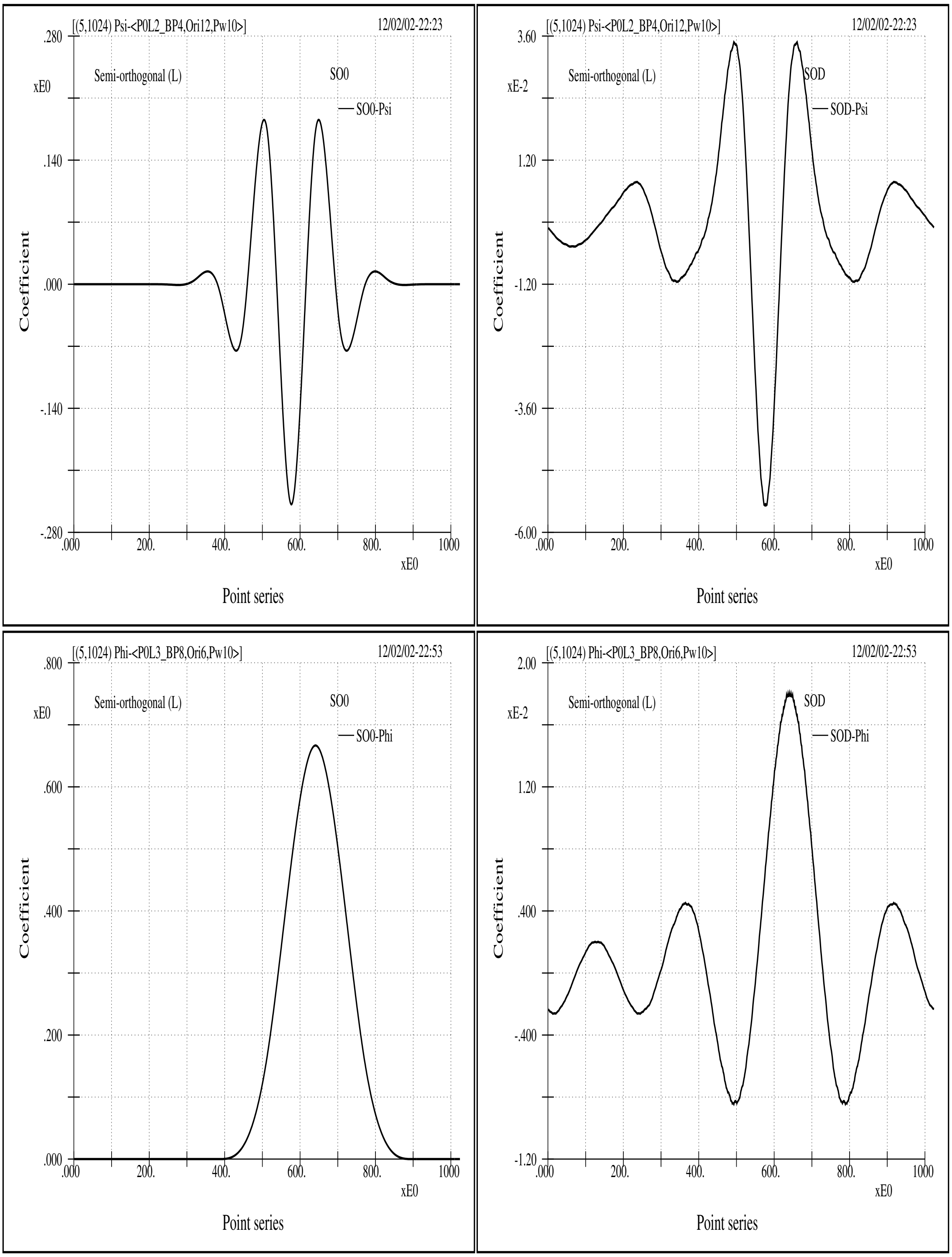

Figure 2.15: The mother `(top left)` and farther `(bottom left)` wavelets, as well as their duals `(right)`, of Chui's semi-orthogonal wavelet [4, 5] originating from the point location of 12 and 6, respectively, for the boundary point based on level 3.

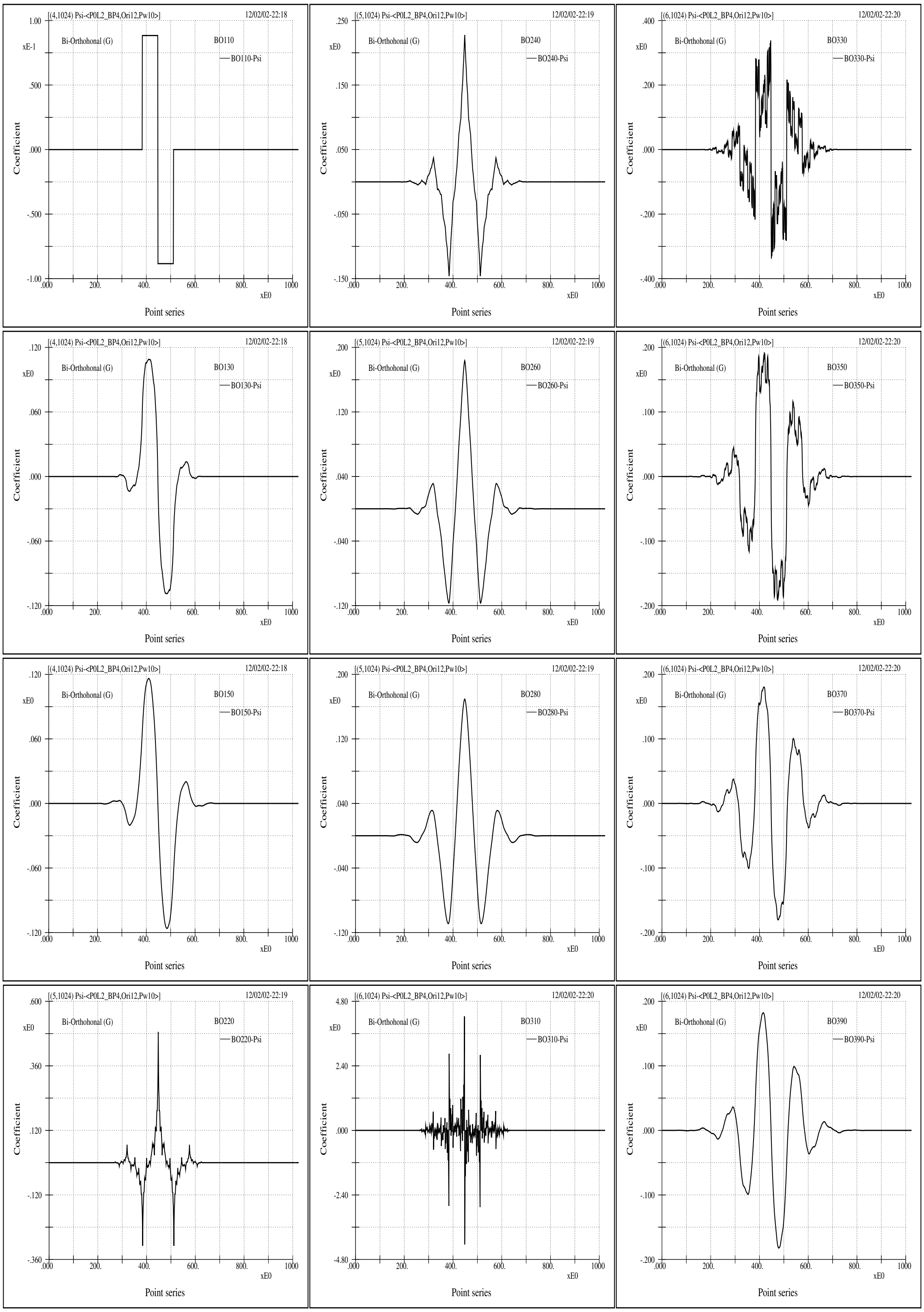

Figure 2.16: The mother wavelets of the BOxxO group originating from the point location of 12. Here the boundary point should be based on a level less or equal to 3.

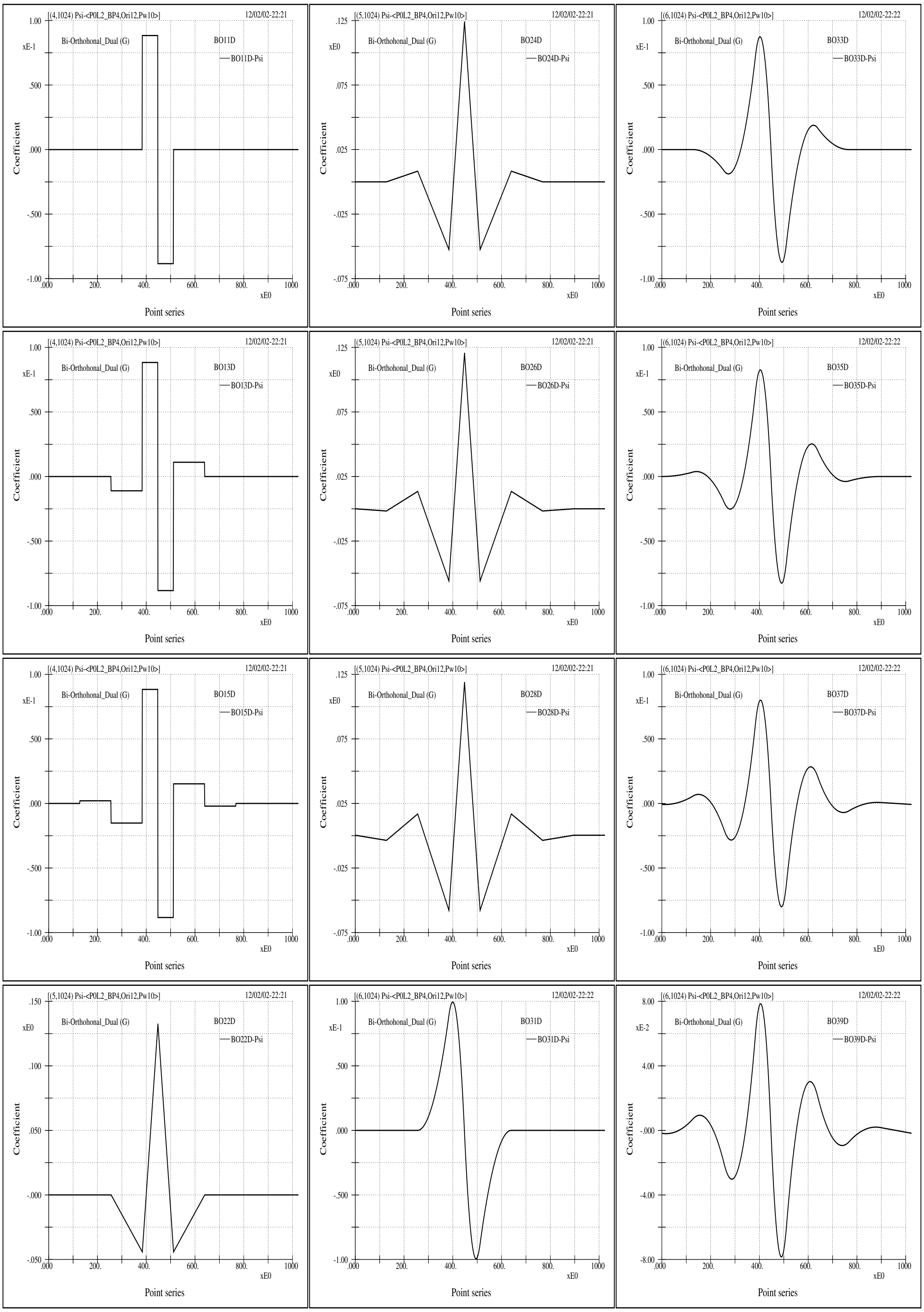

Figure 2.17: The mother wavelets of the BOxxD group originating from the point location of 12. Here the boundary point should be based on a level less or equal to 3.

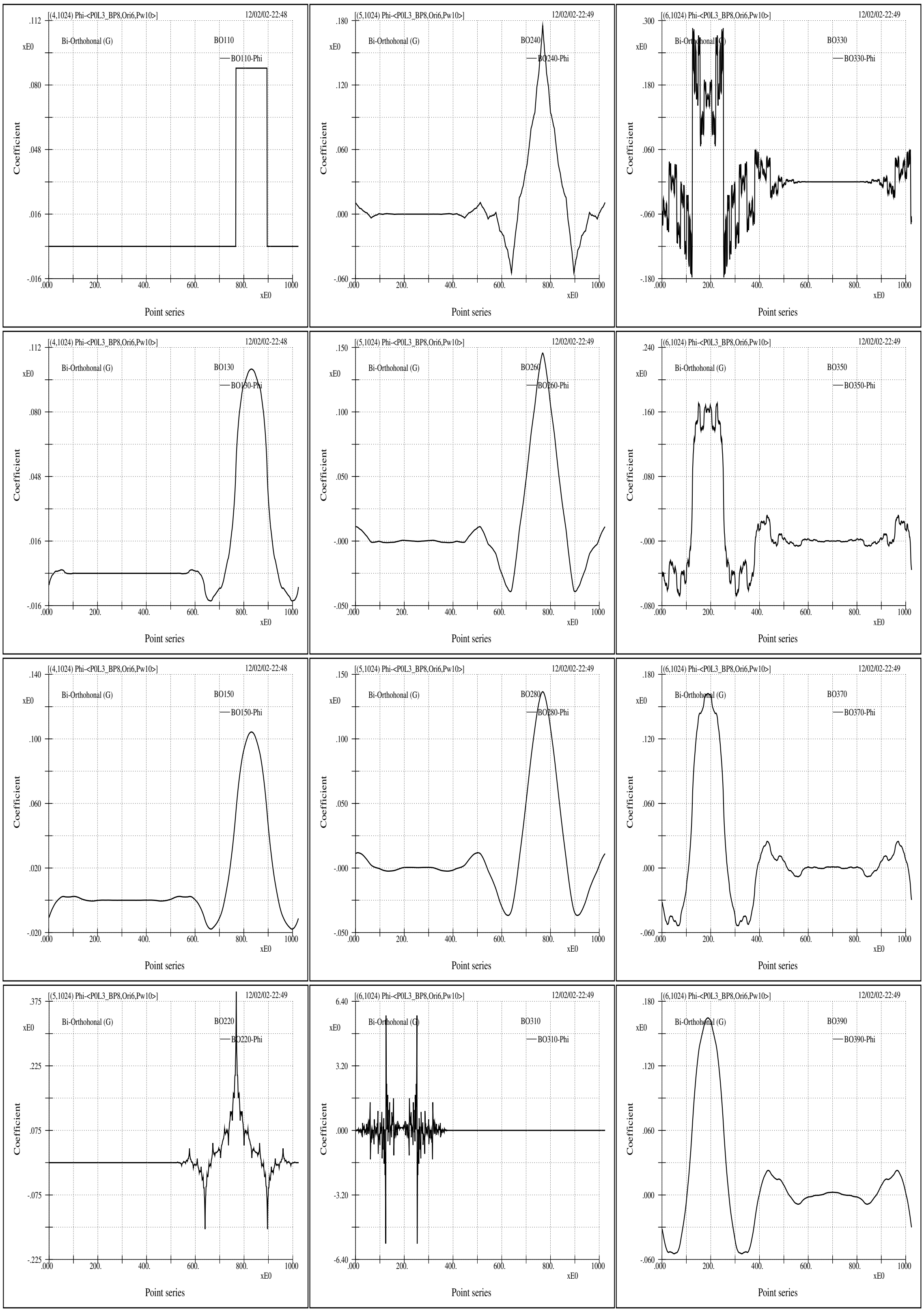

Figure 2.18: The farther wavelets of the BOxxO group originating from the point location of 6. Here the boundary point should be based on a level higher or equal to 3.

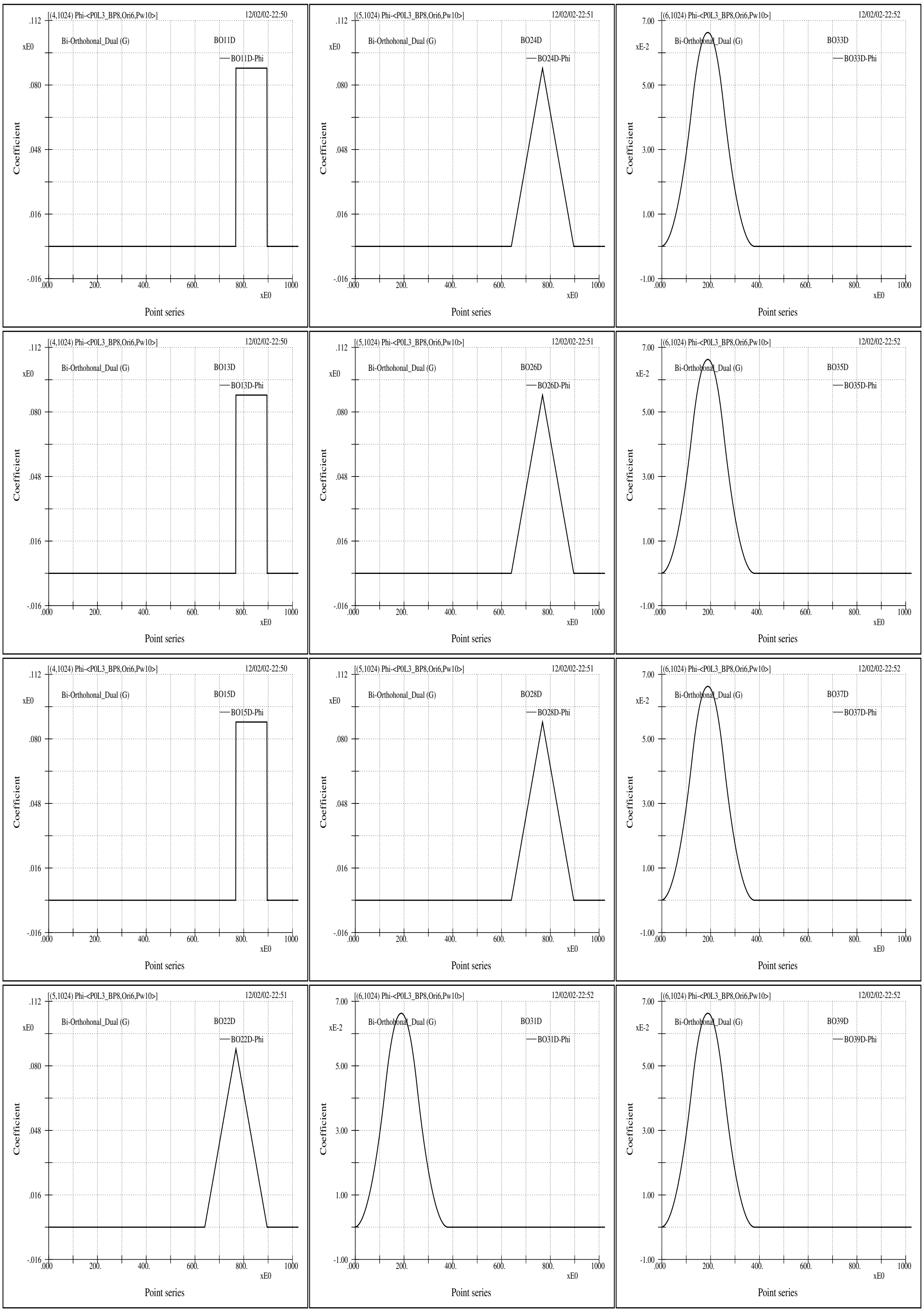

Figure 2.19: The farther wavelets of the BOxxD group originating from the point location of 6. Here the boundary point should be based on a level higher or equal to 3.

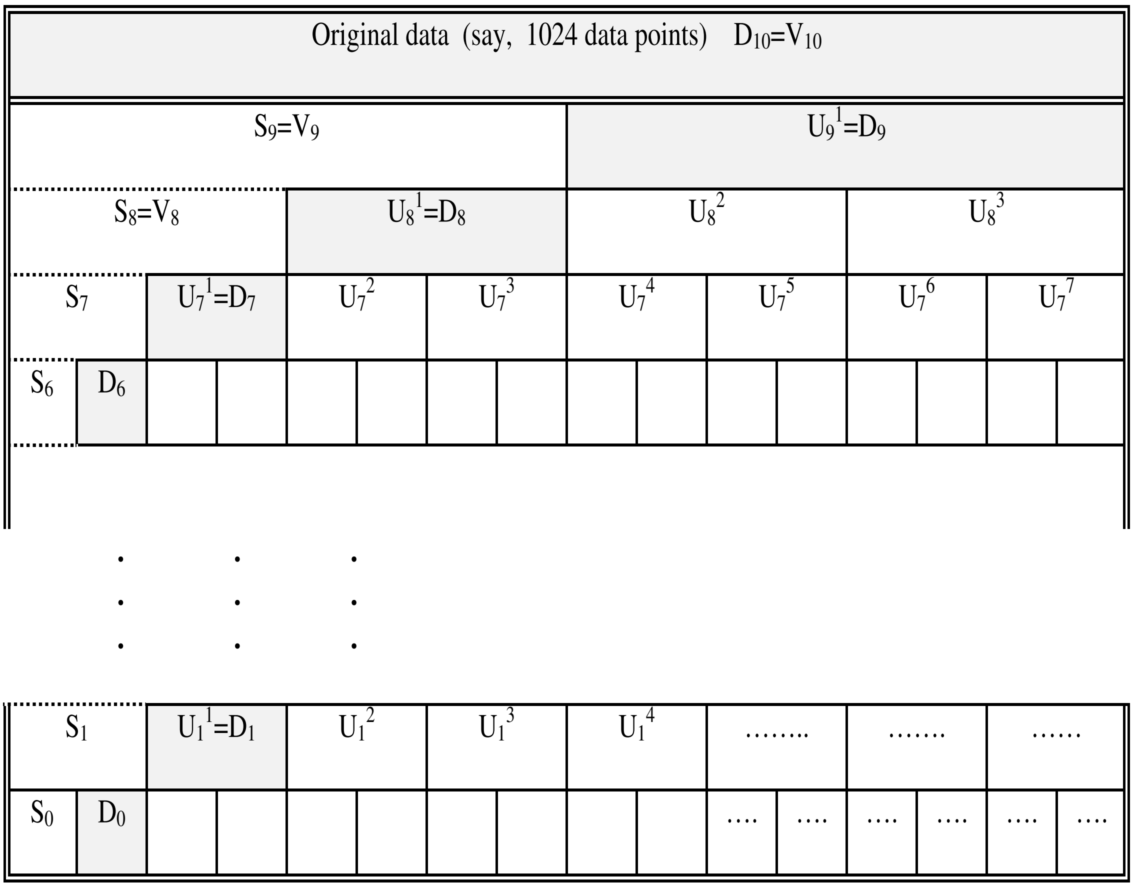

Figure 2.20: Schematic representation of the tree-like structure of the wavelet packet decomposition. S(=V in the text) and D stand for smooth and detail information, respectively. U with superscript larger than 1 stands for further decomposition of D by wavelet packets. All subscripts mean scale levels. All superscripts mean relative locations of the frequency bands for compatible subscripts.

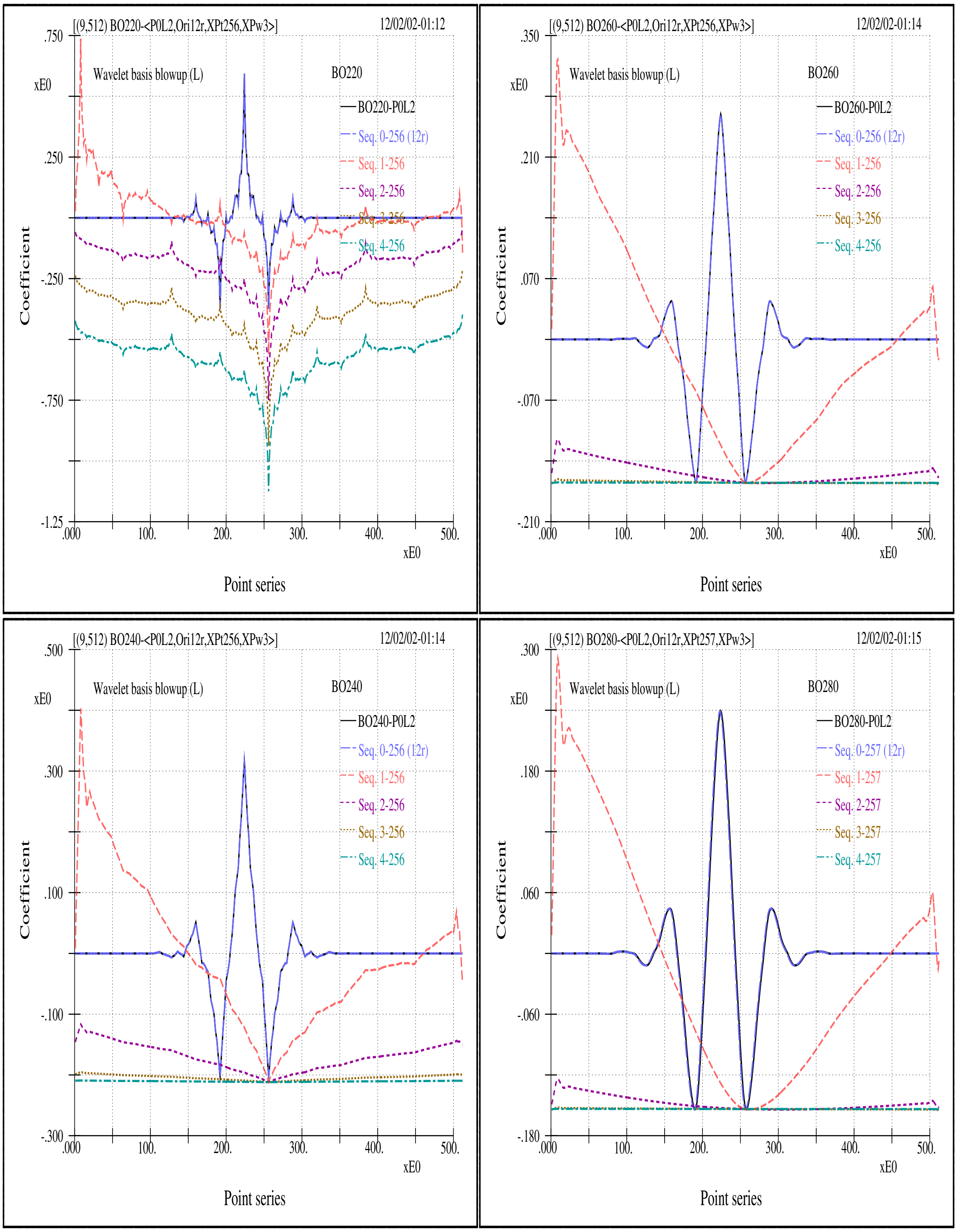

Figure 2.21: The blowups of a few wavelets of the BO2xO group. Each successive blowup scale is 2^3. The originating point of the wavelet function and the blowup location point are labeled in individual sub-figure.

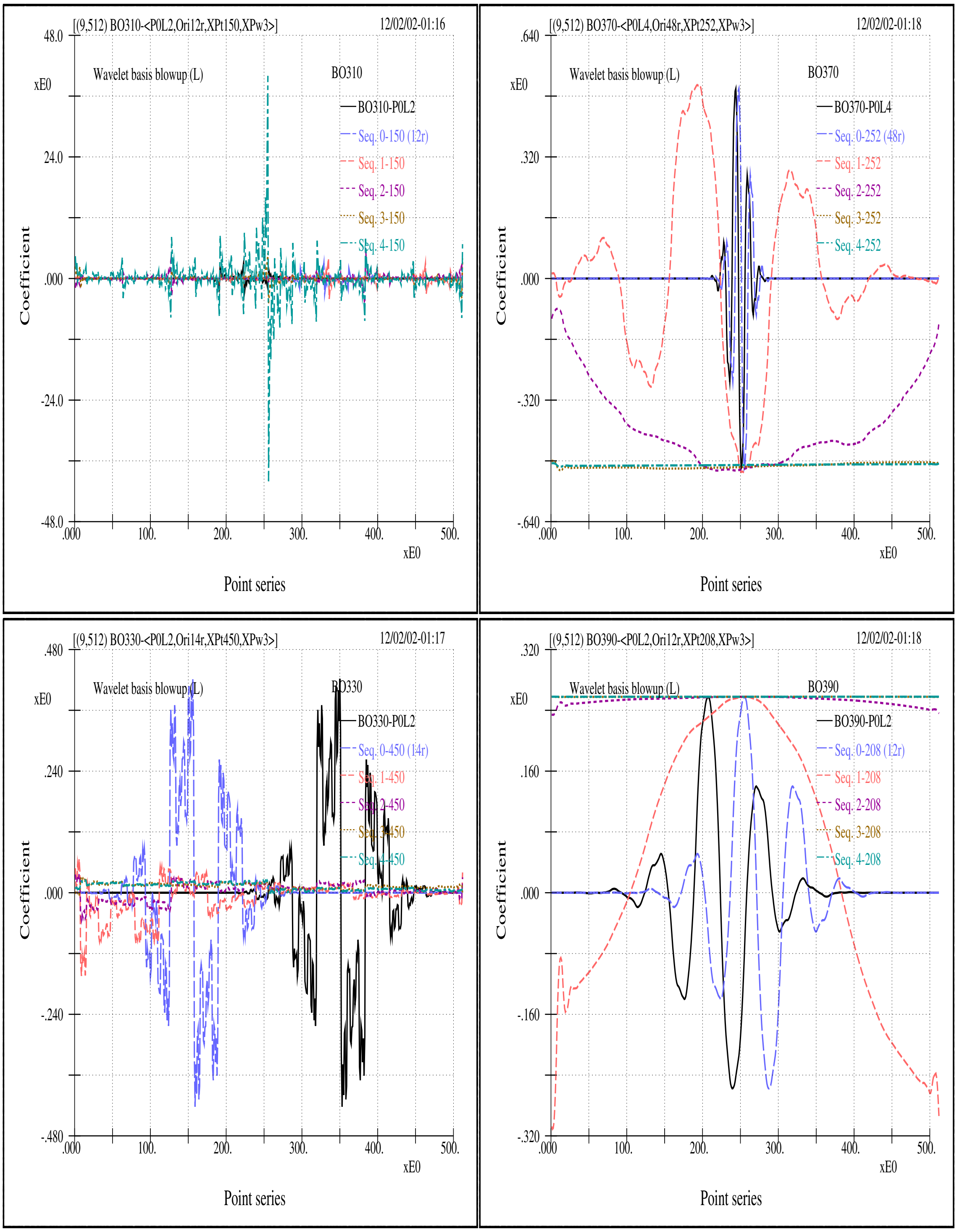

Figure 2.22: The blowups of a few wavelets of the BO3xO group.

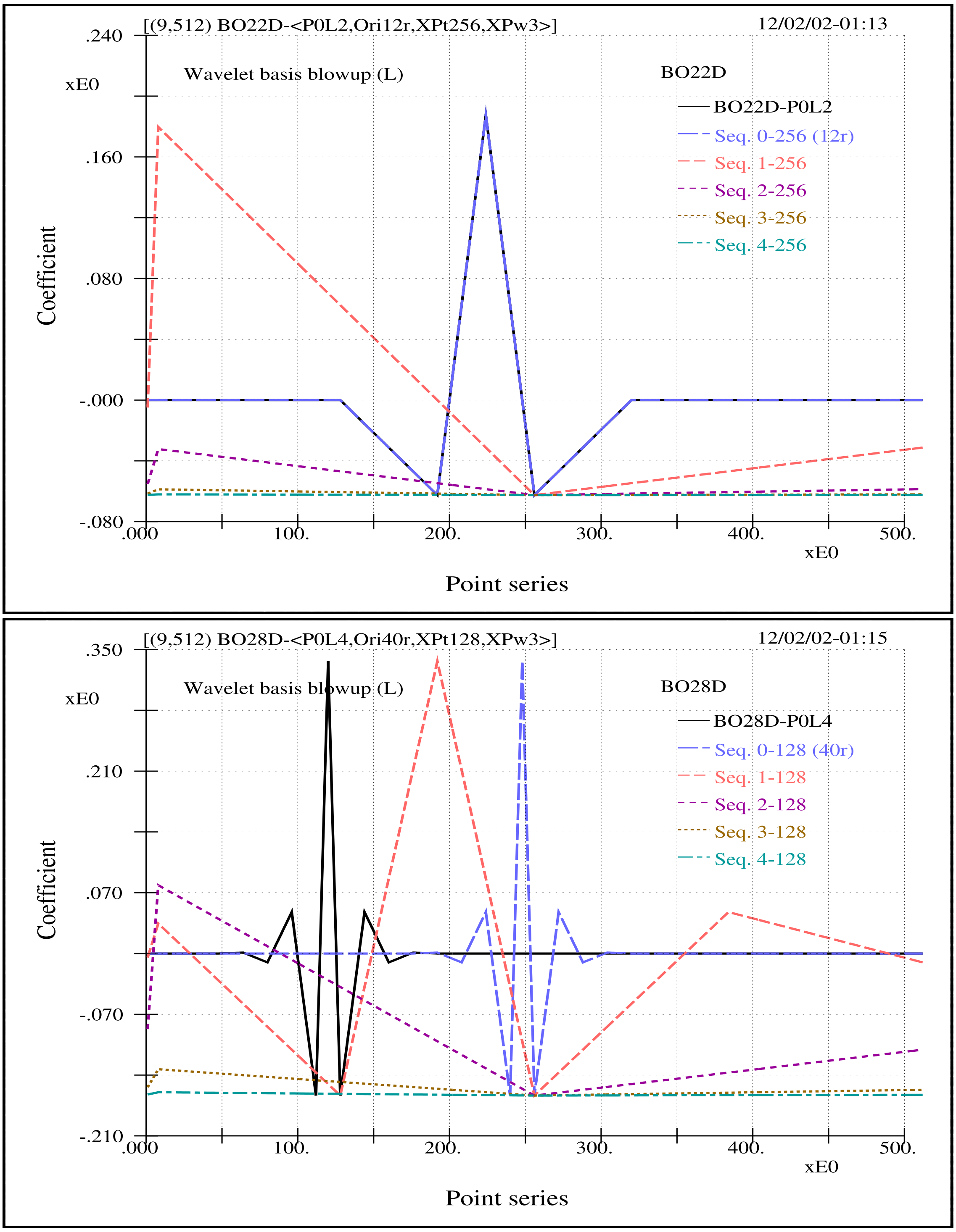

Figure 2.23: The blowups of a few wavelets of the BO2xD group.

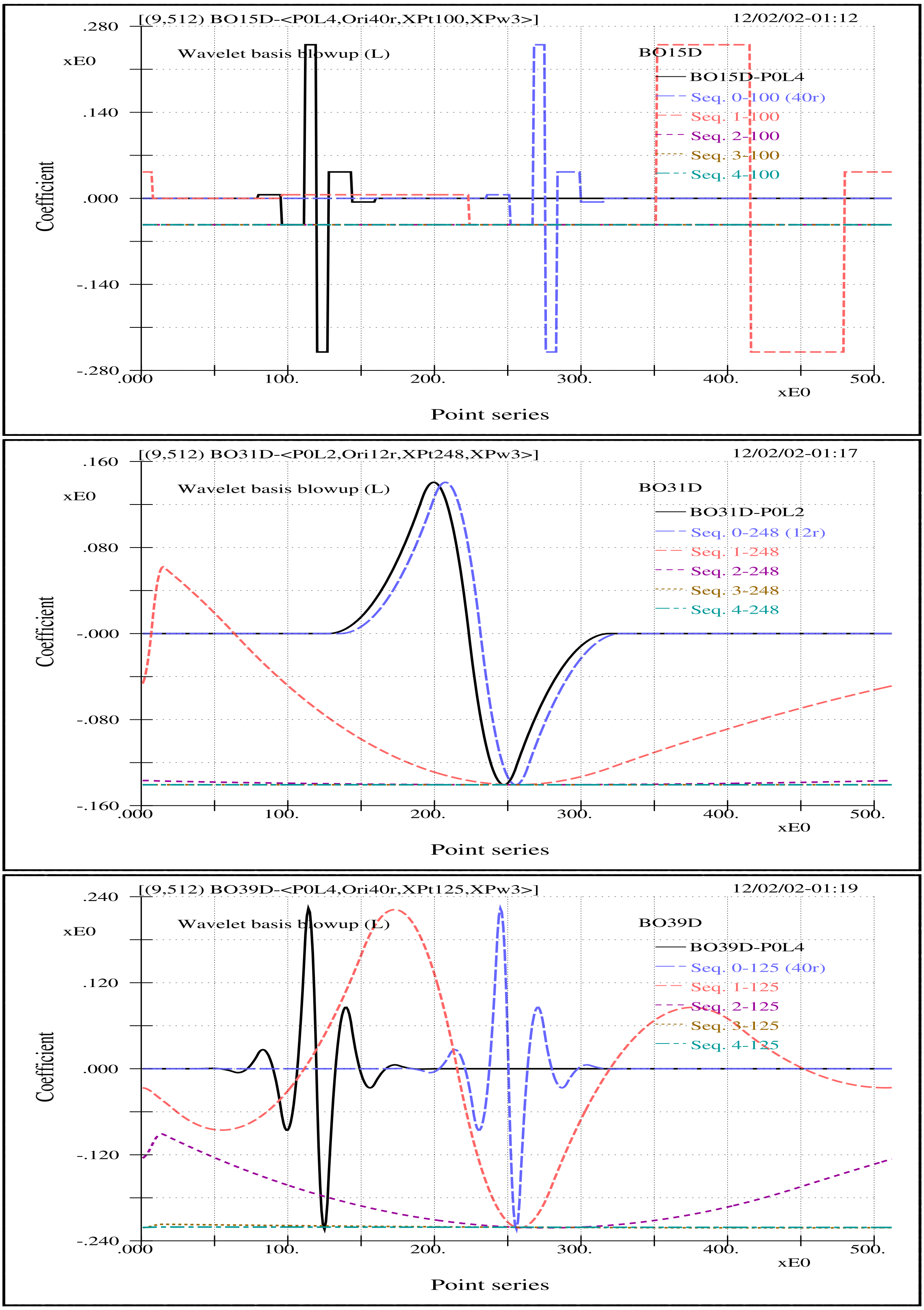

Figure 2.24: The blowups of a few wavelets of the BOxyD group.

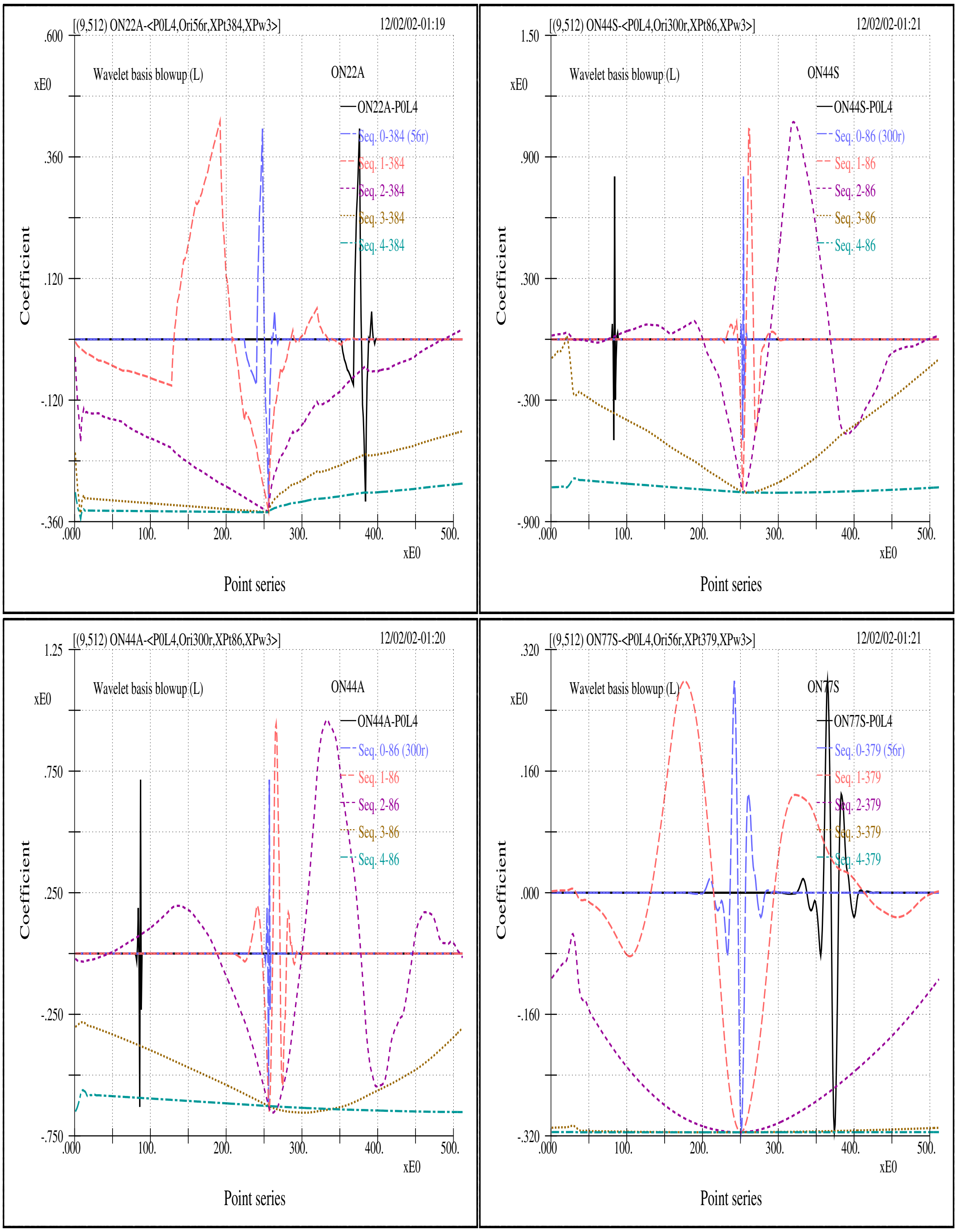

Figure 2.25: The blowups of a few wavelets of the ONxxA and ONxxS groups.

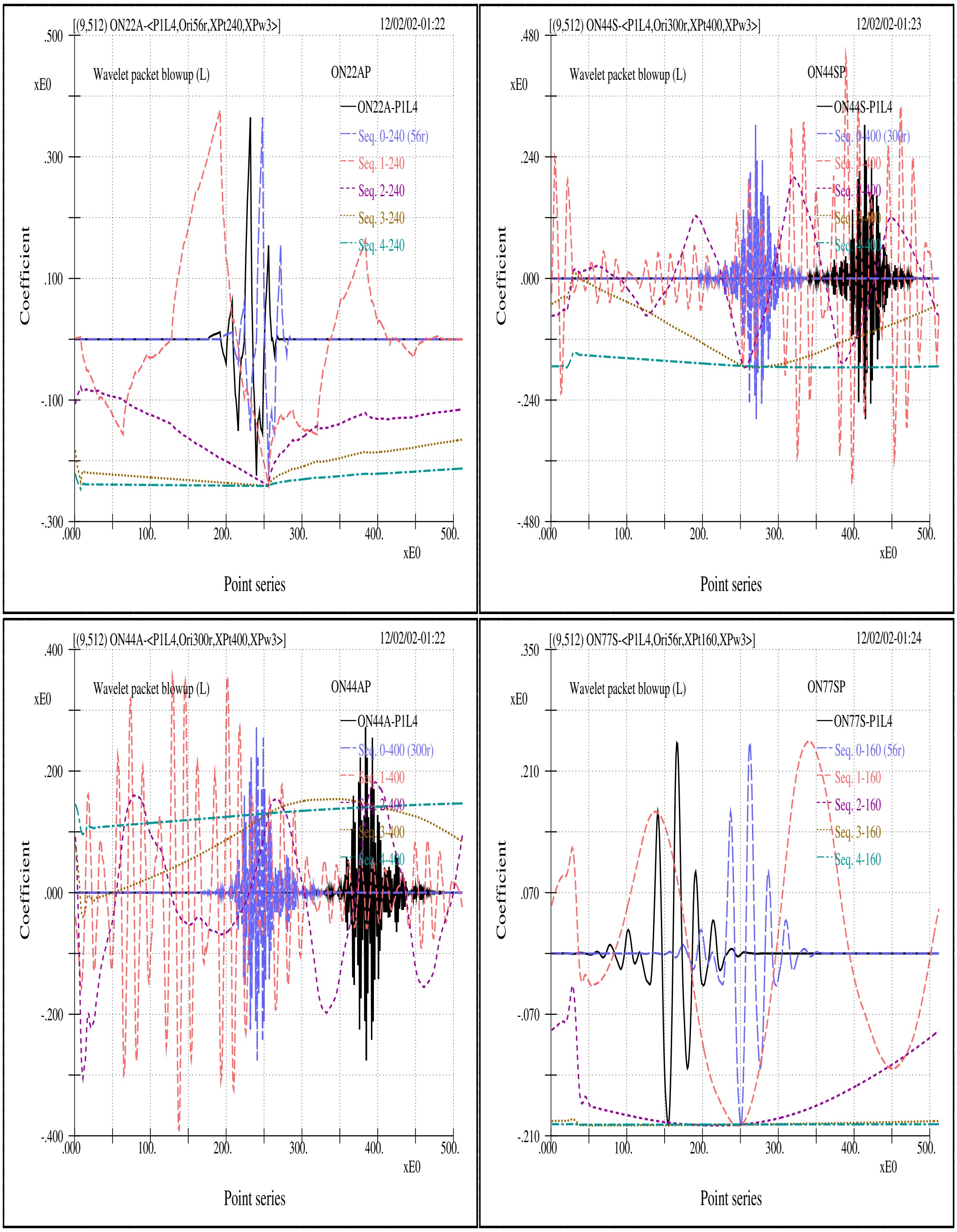

Figure 2.26: The blowups of a few wavelet packets of the ONxxA and ONxxS groups. Note the grouping tendency of the wavelet packets.

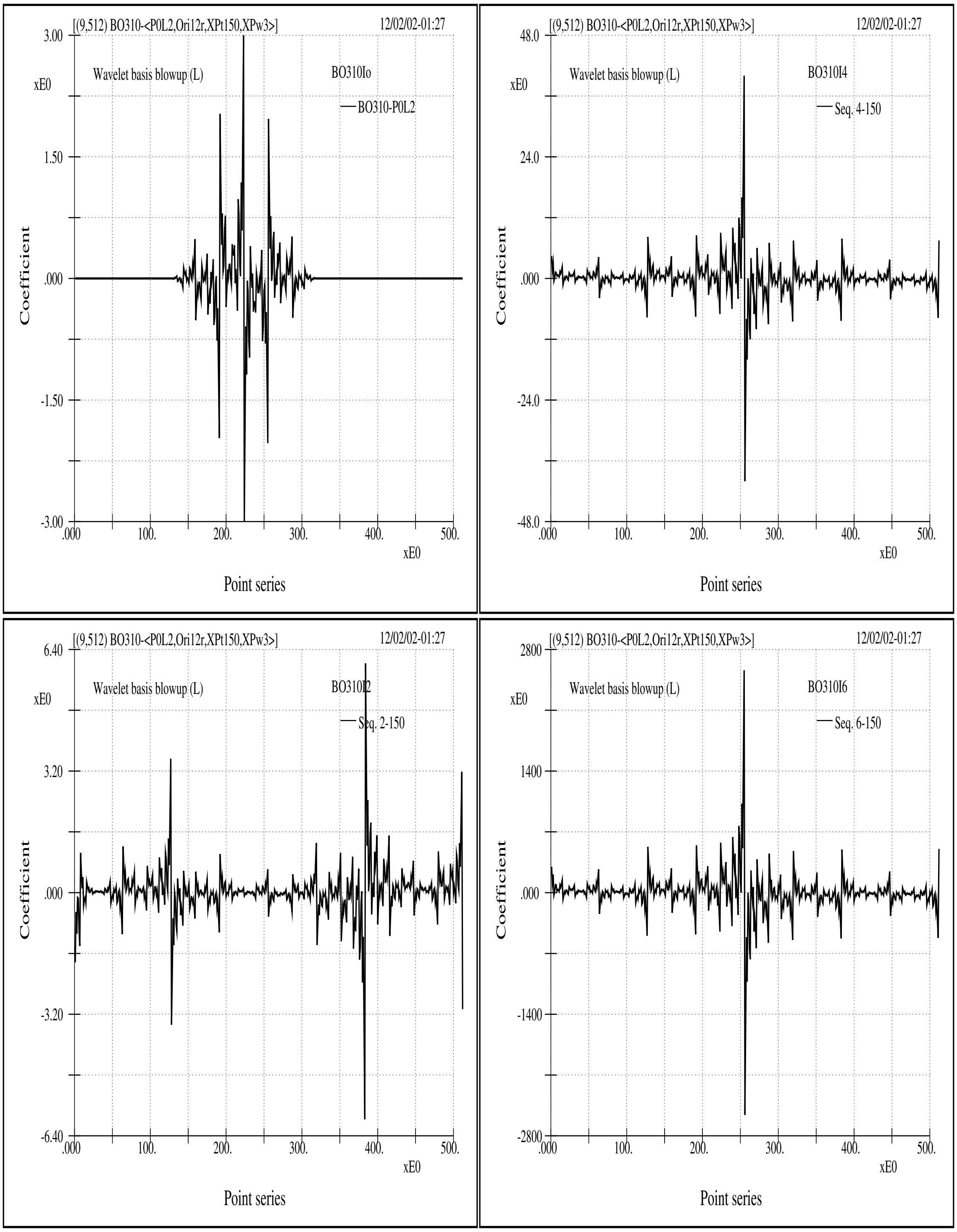

Figure 2.27: The blowups of the BO31O wavelet, noting the vast difference in the ordinate. Here successive blowup scale is 2^6.

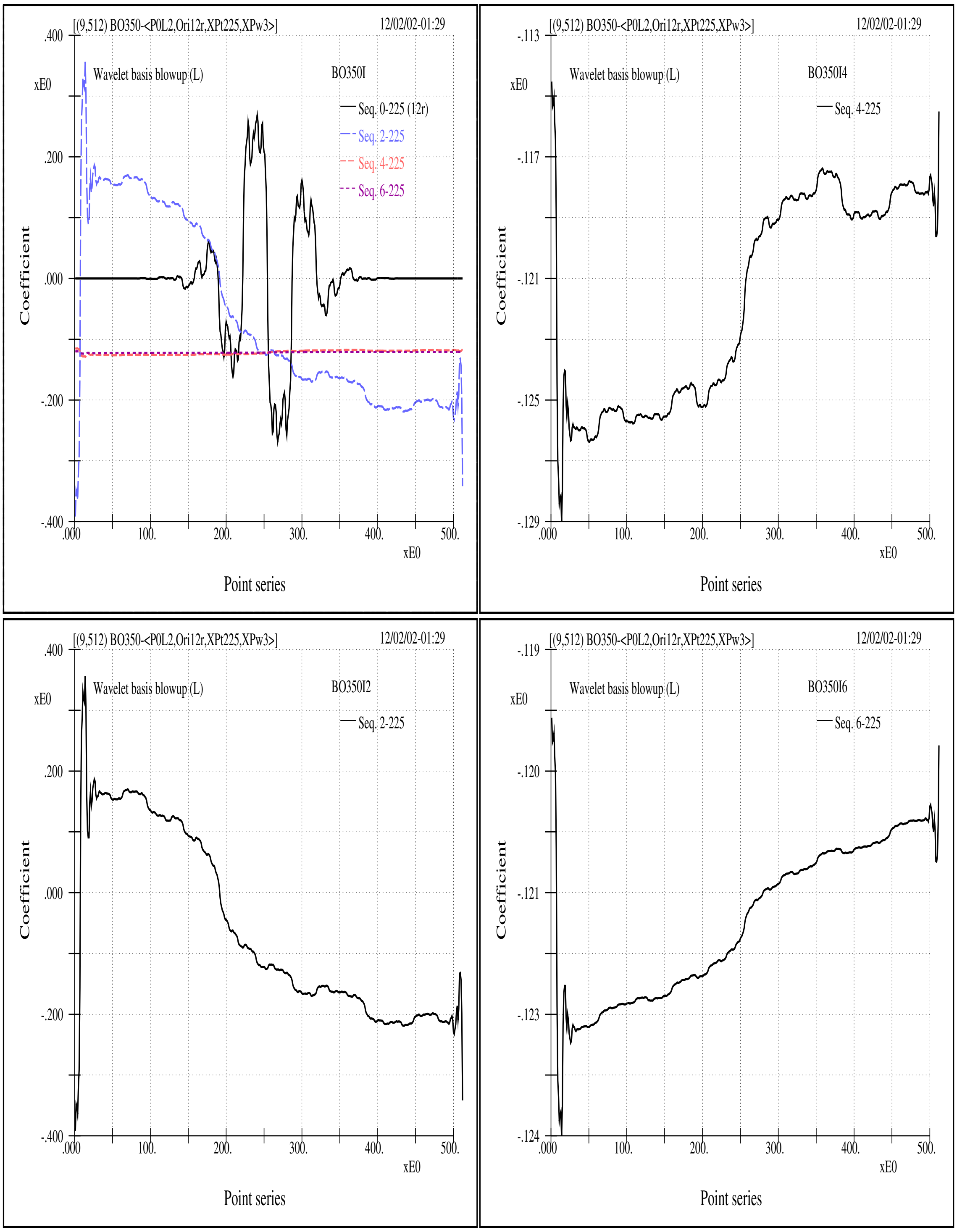

Figure 2.28: The blowups of the BO35O wavelet, noting the difference of the inclinations of the zoom-in curves. Here successive blowup scale is 2^6.

Chapter 3

The Entropies and the Best Wavelet Basis

3.1 Entropy's physical pertinence

In studying the physics of certain phenomena using wavelets one of the most intriguing questions is how to choose the analyzing wavelet(s). The concern here is quite in contrast to those studies where they are mainly numerically or analytically oriented. For example, in coding of images or acoustic signals the goals are straightforward: the maximum compression with minimum handling and the highest effectiveness with least distortion; under such circumstances mathematical relevance between signal and wavelet can be materialized much more explicitly than physical pertinence needs to be unfolded for our applications.

From this point of view, for our interests in characterizing the physics of water-wave related phenomena, it seems, at first, that the aspiration is not on "efficiency" or "compactness". However, with the understanding that the compactness of a coding means the closeness between signal component(s) and analyzing function(s) along with the conception that wave forms which do not look like our signals (or signal components) are obscured from intuitive perceptions of physics, it is justified to find the wavelets that provide the most efficient or most economical representations for out signals. And this viewpoint is related to the concept of entropy — seeming to converge to the same objective for what are emphasized in different disciplines.

The works in this chapter are mainly numerical experiments on measuring the "distances" between our signals and various Riesz wavelet bases given in several wavelet treatises [4, 9, 20, 22]. No attempt to make new constructions of bases or to extend the existing constructions is made. Nevertheless, we have tried to include various categories of Riesz wavelets. We will come to realize that there is really no need to extend the existing constructions if the associated two-scale scaling function or father wavelet is not changed, and that a few sparse fractal-oriented wavelets [19] are just as impractical as they may be in our applications.

The wavelets tested are dyadic wavelets with "mathematical sampling rate" 1 (no unit). They are of most practical interests in applications for discretely sampled signals. Furthermore, we restrict our scope to laboratory water waves. The criteria used are the entropy statistics of discrete transform coefficients, including Fourier coefficients.

3.2 The entropy criteria

Entropy is a terminology in the statistical physics, thus it gives indication without assurance. The entropy can be viewed as a measure of the "distance" between a signal and its reconstructed signal using partially truncated transform coefficients. To avoid the somewhat mystified notions as one might get from some of the readings, it may be better to give straightforward descriptions by going through the actual numerical process first and returning to its statistical implication later. Let suppose that we have a 1024-point sampled data, then there is a set of 1024 wavelet coefficients (C=$\{c_i\}$). Take the absolute or squared value of these coefficients, sort them, and then divide the sequence into M (say, 100 or 200 or 300) divisions which are equally spaced from 0 to the maximum value of the coefficients. Then we have the statistics of occurrence for each division, and the distribution of these normalized occurrences is the probability density distribution or probability density function (denoted by pdf), say $\{p_1, p_2, \cdots, p_{M-1}, p_M\}$. The entropy is

$$H(p) = -\sum_i p_i \log p_i . \tag{3.1}$$

Where, when $p_i = 0$, it is assumed that $0 \log 0 = 0$, since in reality one can assumed that there exists an almost zero probability in that interval without affecting the total sum of probability, after all it is only a statistics and the modification virtually has no influence on the norm value. If absolute values of c_i are taken, $H(p)$ is the L^1-norm entropy; if squared values are taken, it is squared L^2-norm entropy. Of course another power can be used, but the squared L^2-norm, being the energy, is physically the most significant. The practical aspect of this definition of entropy is: let suppose two probability distribution functions sorted in a decreasing order are p and q, if p decreases faster than q, then $H(p) \leq H(q)$ [25]. The above inequality of entropy is only one-way correct and the reverse is not always true, but smaller entropy implies that more energy is concentrated within a smaller number of wavelet coefficients. Therefore, if only a fixed percentage of coefficients is kept, the truncated error, i.e., the distance from the total sum, is likely to be smaller for set of coefficients with smaller entropy

There is another notion, sometimes referred as the geometric notion [25], for calculating the entropy. Again, the procedures is given first and the simple physical interpretation next. By setting the number of divisions to be the same as the number of coefficients and by defining probability density to be the normalized (with respect to the total power) value of the squared wavelet coefficient, that is to say, the total energy is $\|C\|^2 = \sum_i |c_i|^2$ and the probability density is $p_i = |c_i|^2/\|C\|^2$, we get the alternative form of entropy by substituting P_i into Equation 3.1:

$$H(p) = \log \|C\|^2 - \frac{\sum_i |c_i|^2 \log |c_i|^2}{\|C\|^2}. \tag{3.2}$$

The notion here is simple: if one just put more weight on coefficients of small energy and less weight on coefficients of large energy (all coefficients being normalized), then the weighted energy is an indication of entropy. And since taking the log of a value is sort of a weighting operation and since the total energy is finite, small entropy therefore means that the number of significant coefficients is small, or stated otherwise, more energy is concentrated in fewer coefficients.

One equivalent indicator of entropy of a pdf is the theoretical dimension $D(p)$ and is defined as [25]

$$D(p) = e^{H(p)} = \prod_i \left(p_i^{-p_i} \right). \tag{3.3}$$

As was stated, entropy does not tell how conclusive the result is. But our numerical results yield little ambiguity regarding the judgement that we can make.

3.3 Results and discussions

To increase the definiteness of the comparisons, we calculate entropy based on several setups: direct coefficient entropy related to L^2-norm based on Equation 3.3 (column 1 in Tables 3.1 and 3.2), pdf entropy related to L^2-norm with 300 (column 2) and 200 (column 4) divisions, and pdf entropy related to L^1-norm based on Equation 3.1 (column 3). Theoretical dimension for one of the setups is also given (column 5). The tables show the results using a wind-wave signal from a wave tank experiment. It is noted that if the peak frequency (or the primary scale) of other signal is significantly different, then, to be consistent in comparison, the analyzed signal lengths and the sampling rates should be properly adjusted according to its peak frequency. This is because in the discrete wavelet transform we need to keep track of the actual physical size of translation so as to have physical perception of the wave forms. Table 3.1 give results from all orthonormal wavelets (including B&L, Meyer, ONxxA, ONxxS, and ONxxC), semi-orthogonal wavelets (Cubic B-spline, SO3O and SO3D), as well as from Fourier spectrum. Table 3.2 give results from bi-orthogonal wavelets. Many distinctive features can be derived from the tables.

- The dual wavelet always gives much smaller entropy than as given by their counterpart wavelet. This certainly verifies that, for our water-wave signals, using

$$f(t) = \sum_{j,k} \langle f, \widetilde{\psi}_{j,k} \rangle \psi_{j,k} \tag{3.4}$$

provides a much better efficiency in decomposition and reconstruction than using

$$f(t) = \sum_{j,k} \langle f, \psi_{j,k} \rangle \widetilde{\psi}_{j,k}. \tag{3.5}$$

This also points out that dual wavelets rather than their counterpart wavelets should always be used as the decomposing basis for either better physical implications or improved computational efficiency. It may also worth noting that the practical shapes of all the listed bi-orthogonal wavelets, especially those with small x and y values, are visually quite unrealistical (such as those shown in Figures 2.27 and 2.28). Furthermore, for these bi-orthogonal wavelets, it can be concluded that there is going to be very little improvement by further extending the support width related to y without extending the support width related to x; since increasing the width (y) from some point on gives no effect on the shape of dual wavelets (such as $y = 7$ or 9 for $x = 3$) and since it is the dual, rather than the counterpart, wavelet that matters for better approximation.

- Entropy values of all orthonormal subgroups do not fall to the level of non-orthogonal ones. Besides, difference in entropy values of long and short supports can barely be differentiated, even though there seems to be a very slight indication that entropy values related to longer support are somewhat smaller. Here the property reflects the role of linear phase filtering as mentioned earlier.

- Among all the orthonormal wavelets none distinguishes itself from the others. And we see no clear tendency within any subgroup. However, from the analytical point of view, the Meyer wavelet is infinitely differentiable or smooth, the B&L is second order differentiable, and the others have various degrees of differentiability or regularity [9]. It is therefore understandable that at the present stage many analytical properties of orthonormal wavelets are of little practical interests for our signals.

- The most striking result is that the dual Cubic B-spline wavelet yields a far smaller entropy value, even lower than that of the spectral coefficients. Figure 3.1 shows the comparisons of the cumulative probability distribution curves for several wavelet bases as well as for Fourier basis. This striking feature is reflected by the extreme flatness of the SO3D curve, nearly horizontal up until 90 percent of energy ratio. At about 96 percent of the energy ratio there is a crossing between spectral curve and the SO3D curve. These features practically imply that semi-orthogonal wavelet coefficients are better than Fourier coefficients in describing the details of the signals. Figure 3.2 shows the reconstructions of a section of a signal from its spectral and SO3D wavelet coefficients of which 35 percent are kept. It is seen that the wavelet basis yields truer details than does Fourier basis. Again, the reasons for the SO3D's strong performance can be attributed to the following characters: total positivity of the scaling function and complete oscillation of the wavelet. That is to say, the scaling function has no oscillation or zero-crossing; the corresponding wavelet has no unnecessary oscillation, or no oscillation that is without zero-crossing. Physically, the two characteristics hint that our laboratory water waves are far less transient when compared with orthonormal or bi-orthogonal wavelets, and also imply that the description of waves based on suitable support length or life span is more likely to adhere to the physics.

- For the wavelet packet category we have the best basis and best level criteria. It may not be difficult to gain a prior idea that the chance is slim for getting better results using either of the bases. The obvious reason is due to the inherent limitation of wavelet packet transform — wavelet packet transforms are associated only with orthonormal bases. Since the primitive analyzing functions are orthonormal and since orthonormal wavelets perform poorly as just given above, it is therefore hard to anticipate the same strong performance as that of semi-orthogonal wavelets. Nevertheless, both wavelet packet criteria do show improvements when compared with the original orthonormal basis, and the performance of the best basis is certainly better than that of the best level. Figure 3.1–(b) gives the wavelet packet best bases and best level curves for B&L and Meyer's wavelets; they do show improvements when compared with the corresponding curves in Figure 3.1–(a) using regular wavelet transforms. It is quite certain that the improvement is not to the degree of semi-orthogonal wavelet or that of the Fourier spectrum.

- Figure 3.3 shows cumulative distribution curves of the best level, best basis, and a few different levels bases wavelet packet coefficients, as well as the curve for the corresponding regular wavelet transform coefficients; here, all the curves are associated with ON77S. The curve for the best level comes close to that for the best basis. Again, wavelet packet best basis and best level yield lower entropy values than other relevant wavelet bases, but still their curves are far away from that of SO3D.

- Among orthonormal wavelets, we do not see clear differences arising from different degrees of symmetry (least asymmetric ONxxS or most asymmetric ONxxA); however, semi-orthogonal and bi-orthogonal wavelets are symmetric or antisymmetric, and their entropy values (concerning dual wavelets) are comparatively lower. It therefore indicates that the linear phase filtering is desired since symmetry or anti-symmetry implies linear phase of the two-scale sequence [4, 9]. Without the linear phase filtering visual impairment may occur. The non-symmetric distribution of time-frequency windows shown in Figures 1.1 illustrates such a significant impact. Though symmetry is desired, it is hard to describe its influence since there are other factors that need to be considered (such as the support length and regularity, e.g., Meyer and B&L wavelets are also symmetric but their entropy values are not comparable to that of the ideal one).

Table 3.1: Entropy of orthonormal and semi-orthogonal wavelet coefficients as well as spectral coefficients under various statistic criteria.

Wavelet	L**2 coefficient entropy (0 division)	L**2 probability entropy (300 divisions)	L**1 probability entropy (300 divisions)	L**2 probability entropy (200 divisions)	Theotetical dimension (L**2 300 divisions)
B&L	4.691	1.330	3.417	1.179	3.782
Meyer	4.647	1.294	3.365	1.132	3.646
SO3O	4.833	1.669	3.756	1.488	5.307
SO3D	1.823	0.219	1.306	0.172	1.245
Spectrum	2.809	0.270	3.044	0.244	1.310
ON22A	4.993	1.761	3.891	1.516	5.815
ON33A	4.773	1.384	3.499	1.225	3.975
ON44A	4.790	1.517	3.596	1.363	4.559
ON55A	4.819	1.553	3.631	1.367	4.727
ON66A	4.790	1.373	3.456	1.203	3.946
ON77A	4.675	1.355	3.461	1.203	3.877
ON88A	4.645	1.229	3.283	1.082	3.418
ON99A	4.719	1.412	3.501	1.252	4.106
ON00A	4.787	1.423	3.511	1.244	4.149
ON44S	4.835	1.461	3.557	1.281	4.311
ON55S	4.758	1.492	3.576	1.298	4.426
ON66S	4.754	1.402	3.501	1.225	4.065
ON77S	4.751	1.336	3.331	1.188	3.804
ON88S	4.714	1.366	3.481	1.224	3.918
ON99S	4.755	1.469	3.570	1.288	4.345
ON00S	4.635	1.278	3.378	1.134	3.591
ON11C	4.938	1.696	3.832	1.457	5.452
ON22C	4.827	1.468	3.520	1.284	4.342
ON33C	4.756	1.488	3.573	1.333	4.427
ON44C	4.690	1.297	3.337	1.157	3.658
ON55C	4.644	1.309	3.405	1.154	3.703

Table 3.2: Entropy of bi-orthogonal wavelet coefficients under various statistic criteria.

Wavelet	L**2 coefficient entropy (0 division)	L**2 probability entropy (300 divisions)	L**1 probability entropy (300 divisions)	L**2 probability entropy (200 divisions)	Theoretical dimension (L**2 300 divisions)
BO11O	5.395	2.623	4.502	2.299	13.777
BO11D	5.395	2.623	4.502	2.299	13.777
BO13O	4.943	1.806	3.883	1.627	6.084
BO13D	5.266	2.371	4.373	2.053	10.708
BO15O	4.866	1.678	3.755	1.495	5.357
BO15D	5.227	2.291	4.327	1.987	9.882
BO22O	5.282	2.362	4.363	2.083	10.609
BO22D	4.434	1.181	3.284	1.034	3.257
BO24O	4.963	1.862	3.985	1.634	6.438
BO24D	4.359	1.090	3.220	0.962	2.975
BO26O	4.881	1.703	3.835	1.492	5.490
BO26D	4.332	1.064	3.174	0.940	2.899
BO28O	4.857	1.624	3.782	1.452	5.073
BO28D	4.318	1.069	3.157	0.941	2.914
BO31O	5.824	3.174	4.741	2.835	23.894
BO31D	4.377	1.058	2.655	0.936	2.880
BO33O	5.084	2.001	4.062	1.756	7.393
BO33D	4.205	1.102	2.827	0.965	3.011
BO35O	4.850	1.697	3.847	1.506	5.457
BO35D	4.125	1.026	2.776	0.908	2.789
BO37O	4.790	1.658	3.821	1.442	5.247
BO37D	4.106	0.986	2.737	0.873	2.679
BO39O	4.776	1.660	3.835	1.432	5.258
BO39D	4.098	0.967	2.713	0.866	2.629

3.4 Summary

Using various criteria of entropy statistics of transform coefficients we identify among a vast array of Riesz bases the best basis for our signals. It is found that, except the B-spline semi-orthogonal wavelets, no wavelet basis tested here can reach the level of approximation given by Fourier spectra. Still, many of the properties of the wavelets studied here are more of analytical interests and hard to be physically significant. The strong performance of the semi-orthogonal wavelet indicates the usefulness of modulated Gaussian wavelets (or the Morlet wavelets) for our applications. Coupling with a few additional features that are specific to continuous wavelet transforms – such as its redundancy nature, the flexible time-frequency resolutions, and the desirable conciliatory segment of interest – promising uses in future applications might be anticipated. ❖

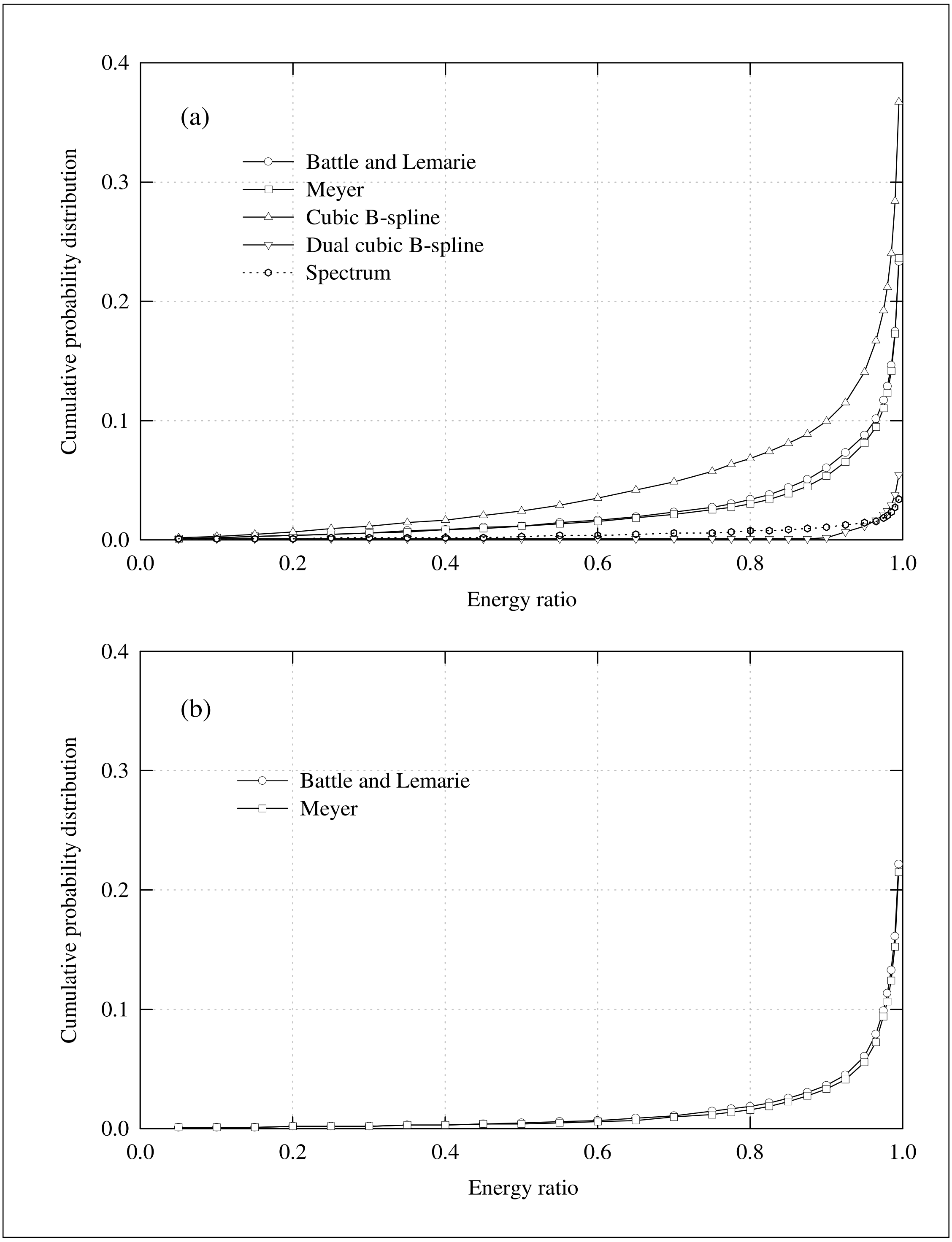

Figure 3.1: The cumulative probability distribution curves of the transform coefficients using different bases associated with three different transform categories: wavelet, wavelet packet, and Fourier transforms. Individual function bases are labeled in the figure. The top figure shows those of the wavelet group as well as a curve for spectral coefficients; the bottom figure shows those of wavelet packets best bases based on two orthonormal bases used in the top figure.

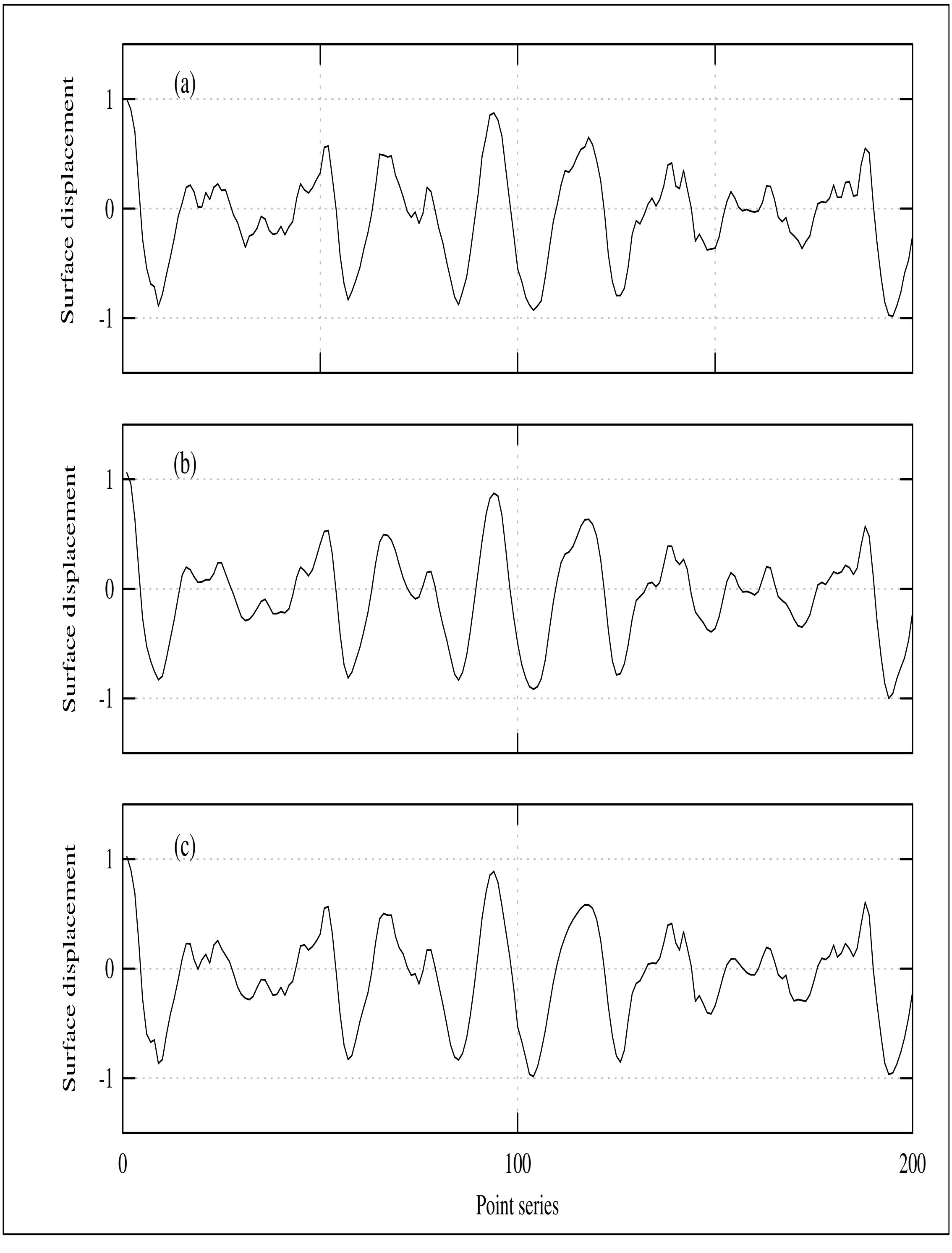

Figure 3.2: Comparison of reconstructed signals using truncated spectral coefficients and semi-orthogonal wavelet coefficients. Here 35% of the coefficients are kept. The original signal is shown in (a), signal reconstructed from spectral coefficients in (b), and that from SO3D wavelet coefficients in (c). The semi-orthogonal wavelet is seen to better portrait the original signal, especially the small scale transient features.

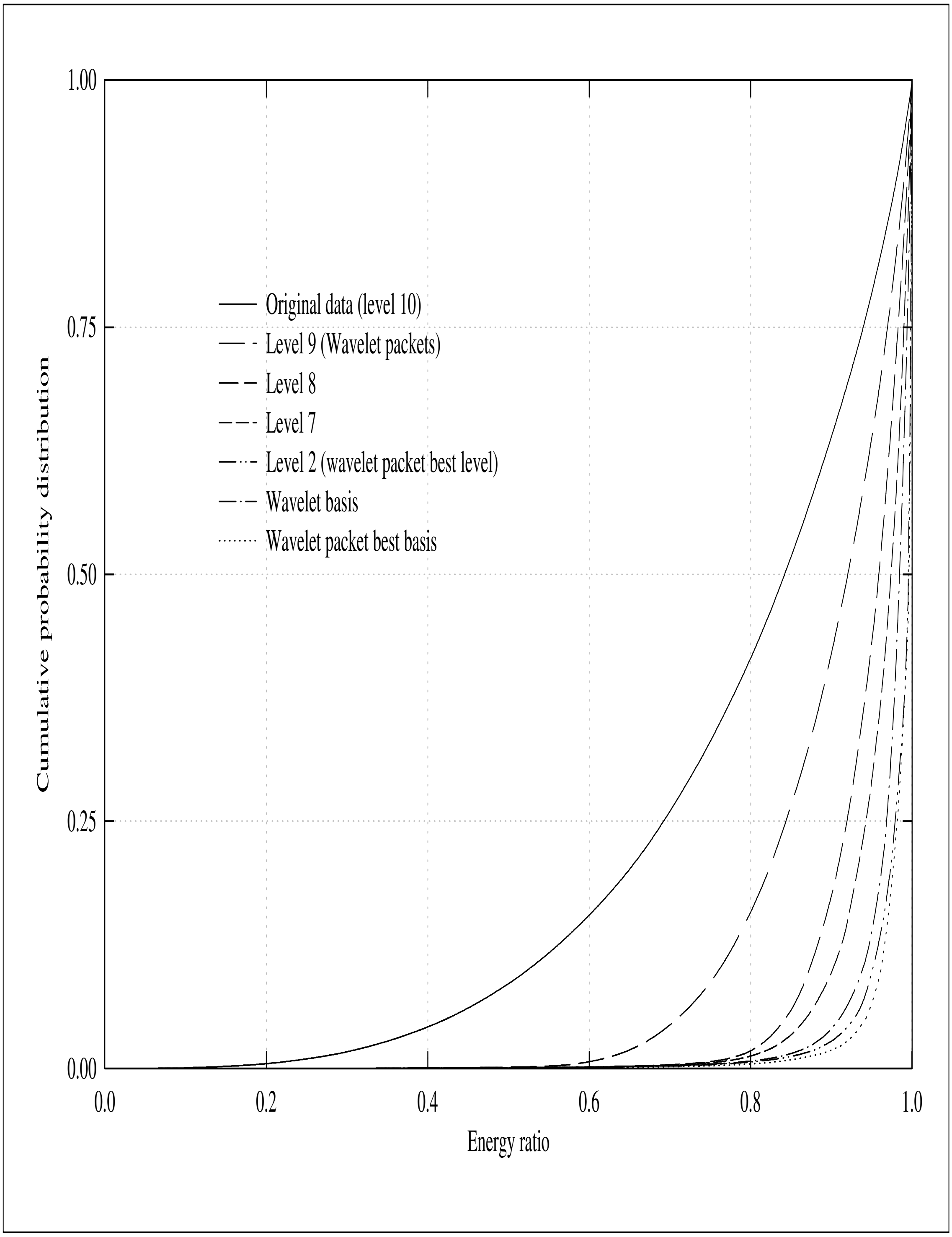

Figure 3.3: The cumulative probability distribution curves of the sorted wavelet and wavelet packet coefficients (L^2-norm squared, i.e., energy content) for various bases which all originate from a single mother wavelet. These bases include those of various wavelet packet levels, wavelet packet best basis, as well as the seeding wavelet basis ON77S; as are indicated in the legend.

Chapter 4

The Phase Distributions of the Wavelet Characteristic Function

4.1 The wavelet Characteristic function m_0

In the last chapter, by providing the entropy values of the transform coefficients for comprehensive bases of discrete wavelet category as well as the Fourier basis, the optimal basis for the simulation of water wave signals is identified to be the semi-orthogonal cubic spline wavelet; The entropy results are of statistical approach, and they by no means touches any mathematical insight of the various function bases. Herein this chapter, by studying the phase distribution of a wavelet characterizing function for each basis, the analytical essence that gives rise the practical usefulness of a function basis is shown to be the requirement of a linear phase of the characterizing function.

Following the convention used by Daubechies [9], the wavelet characterizing function is termed as the $m_0(\xi)$ function, which is the kernel of individual wavelet and has the following mathematical content:

A multiresolution analysis consists of a sequence of the closed subspaces V_j of the nested ladder,

$$\cdots V_2 \subset V_1 \subset V_0 \subset V_{-1} \subset V_{-2} \subset \cdots, \tag{4.1}$$

and satisfies the requirement

$$f \in V_j \iff f(2^j \cdot) \in V_0. \tag{4.2}$$

The invariance of V_0 under integer translations states that

$$f \in V_0 \Longrightarrow f(\cdot - n) \in V_0 \text{ for all } n \in \mathbb{Z}. \tag{4.3}$$

Now comes the main statement that there exists $\phi \in V_0$ so that

$$\{\phi_{0,n};\, n \in \mathbb{Z}\} \text{ is an orthonormal or Riesz basis in } V_0, \tag{4.4}$$

where, for all $j, n \in \mathbb{Z}$, $\phi_{j,n}(x) = \sqrt{2^{-j}}\phi(2^{-j}x - n)$. Here the ϕ is often called the scaling function of the multiresolution analysis. Furthermore, for the $\{\phi_{j,n};\, j, n \in \mathbb{Z}\}$ there exists its counterpart wavelet basis $\{\psi_{j,k};\, j, k \in \mathbb{Z}\}$, $\psi_{j,k}(x) = \sqrt{2^{-j}}\psi(2^{-j}x - k)$, such that

$$P_{j-1} f = P_j f + \sum_{k \in \mathbb{Z}} \langle f, \psi_{j,k} \rangle \psi_{j,k}. \tag{4.5}$$

Since $\phi \in V_0 \subset V_{-1}$ and $\phi_{-1,n}$ are basis in V_{-1}, we have

$$\phi = \sum_n h_n \phi_{-1,n}, \tag{4.6}$$

with

$$h_n = \langle \phi, \phi_{-1,n} \rangle. \tag{4.7}$$

We therefore have

$$\phi(x) = \sqrt{2} \sum_n h_n \phi(2x - n) \tag{4.8}$$

or

$$\widehat{\phi}(\xi) = \frac{1}{\sqrt{2}} \sum_n h_n e^{-in\xi/2} \widehat{\phi}(\xi/2). \tag{4.9}$$

In an alternative form

$$\widehat{\phi}(\xi) = m_0(\xi/2)\widehat{\phi}(\xi/2), \tag{4.10}$$

where

$$m_0(\xi) = \frac{1}{\sqrt{2}} \sum_n h_n e^{-in\xi}. \tag{4.11}$$

Suffice it to say that the $m_0(\xi)$ function is comprised of the summation of the wavelet construction convolution coefficients (or weights corresponding to the support length of the wavelet) multiplied by the complex exponential functions of their individual scales, and the function is intrinsic to the transcendental formulations of the mother wavelet and the two-scale equation.

4.2 Phase distribution of the m_0 function

Figures 4.1 to 4.8 show the phase distributions of all the covered wavelet categories. A few notable points are summarized below.

- Wavelets with similar visual appearance may show extremal phase difference, such as those shown in Figures 4.1 and 4.2.

- In view of the entropy results given in the next chapter, as well as the phase distributions of all the wavelet considered, we see that linear phase distribution is not sufficient to guarantee a best performer for the water wave signals – and it seems that a constant phase is required. The semi-orthogonal wavelet (Figure 2.15) is the one with such a property (Figure 4.3).

- Most of the phase distribution curves for the bi-orthogonal wavelets and their duals are the same not only within their subgroups but also crossing the subgroups. This proves that lengthening the support length of the wavelet of this category provides no benefit.

- The lengthening of support length of the orthonormal wavelets may still yield more irregular phase distribution curves. Again this disproves any possible benefit that may arise from further expanding the construction of these orthonormal wavelets.

- Judging from the last point, since two extremal categories of orthonormal wavelet have been covered, we therefore don't see any possibility that there exists other orthonormal wavelet that may provide suitable and better characterization for water wave physics. ❖

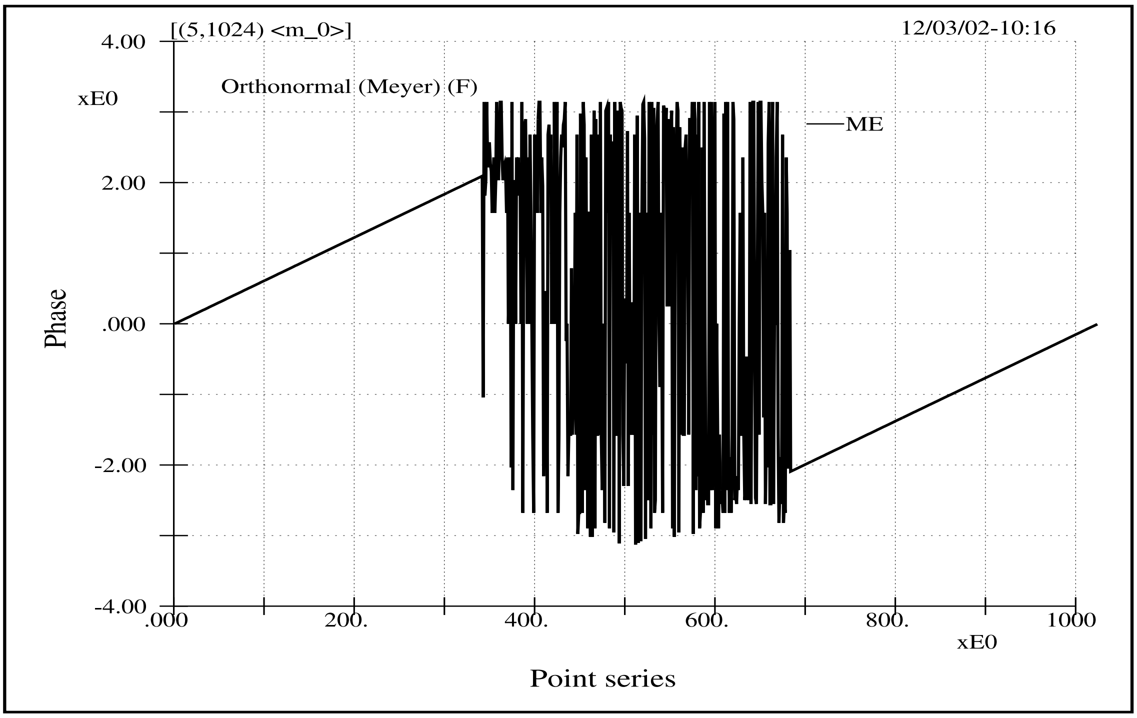

Figure 4.1: The phase distribution of the m_0 function of the Meyer wavelet.

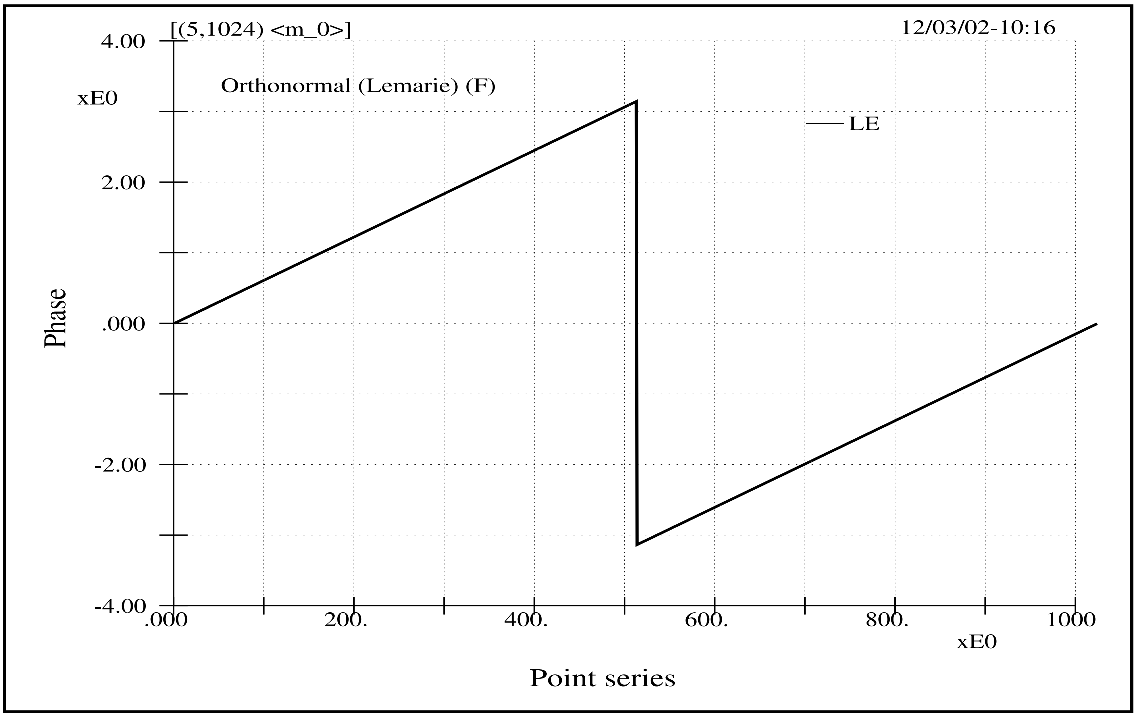

Figure 4.2: The phase distribution of the m_0 function of the Battle and Lemarié wavelet, noting the difference from that of Meyer wavelet.

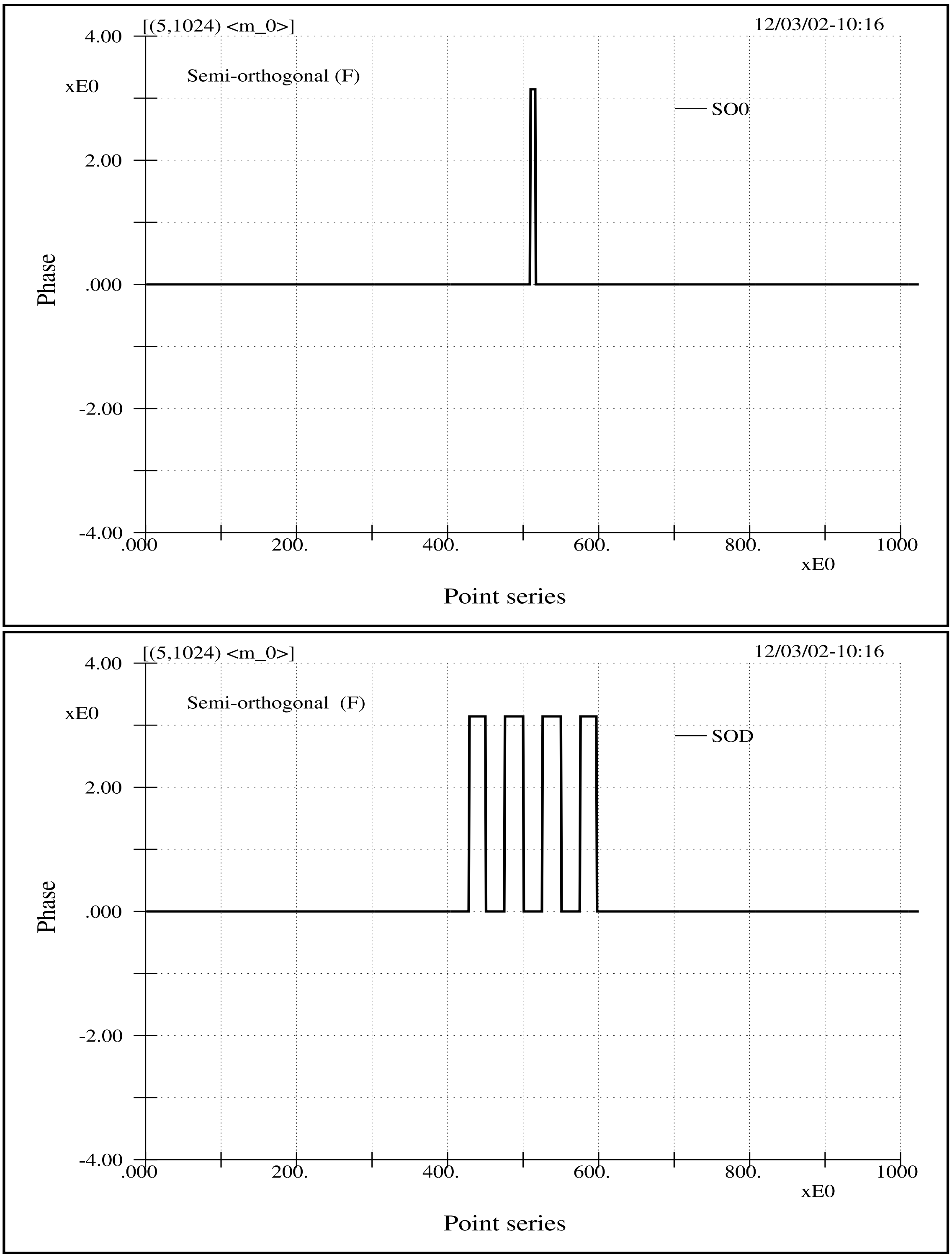

Figure 4.3: The phase distributions of the m_0 functions of the semi-orthogonal wavelet and its dual.

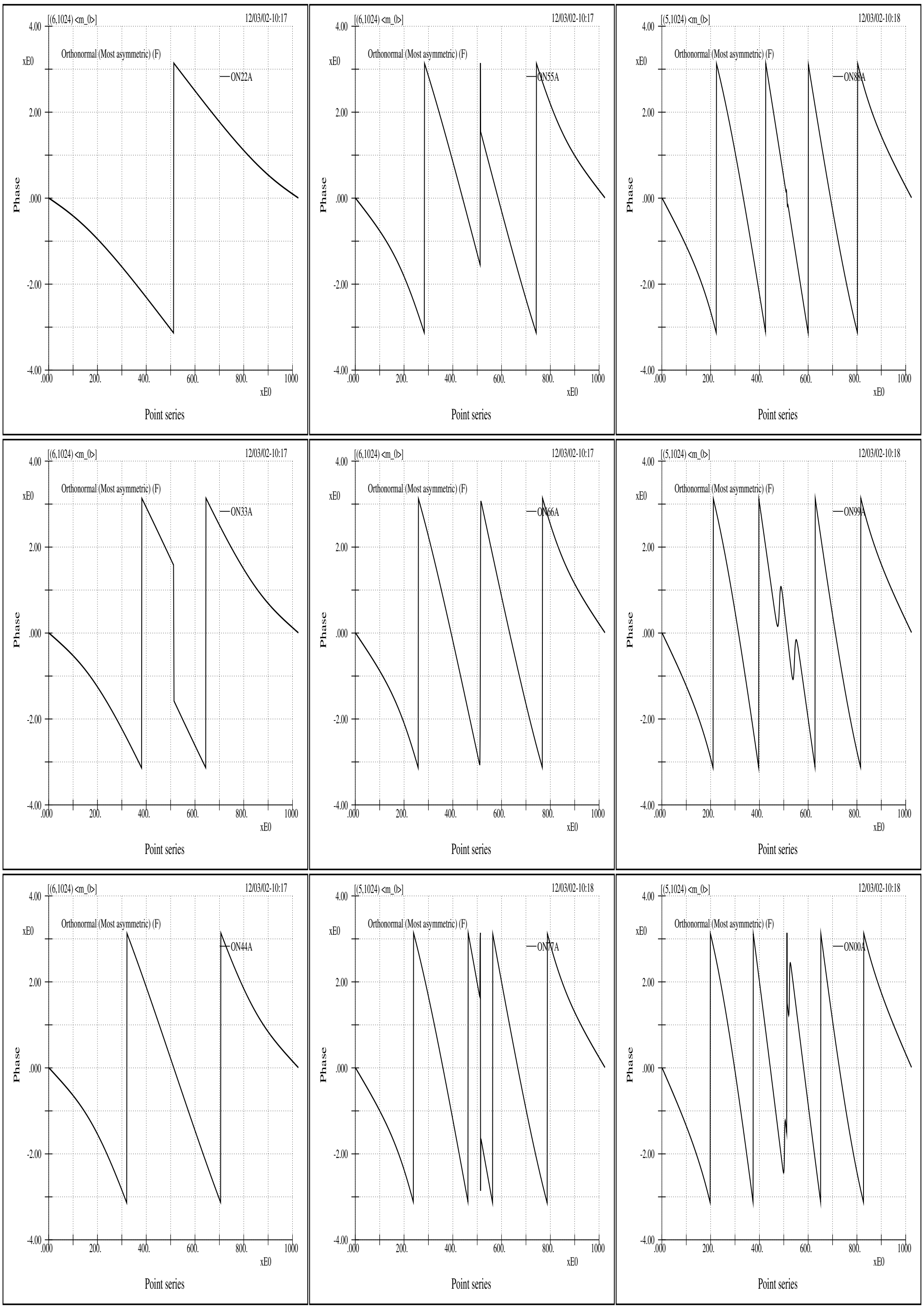

Figure 4.4: The phase distributions of the m_0 functions of the wavelets of the most asymmetric group.

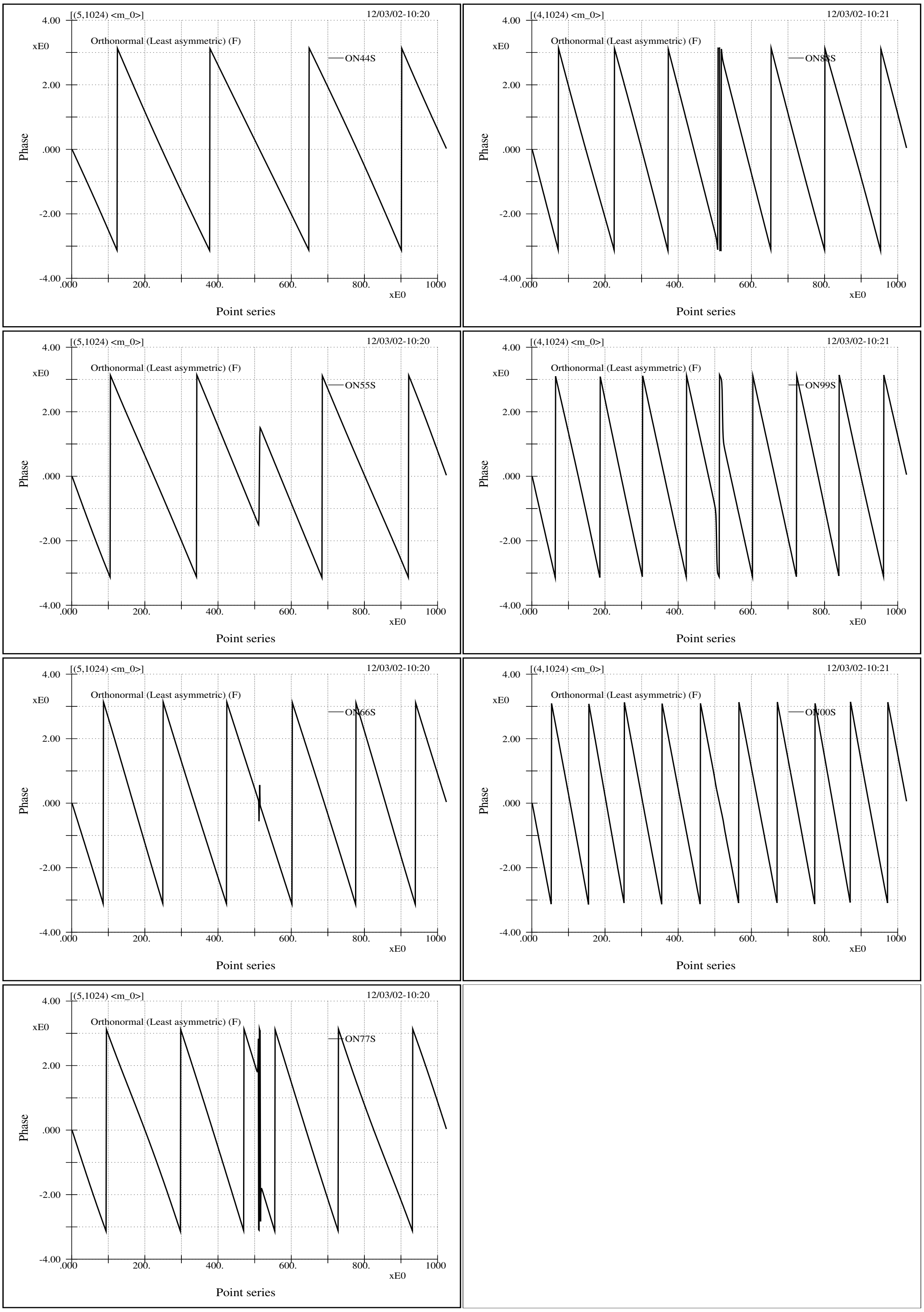

Figure 4.5: The phase distributions of the m_0 functions of the wavelets of the least asymmetric group.

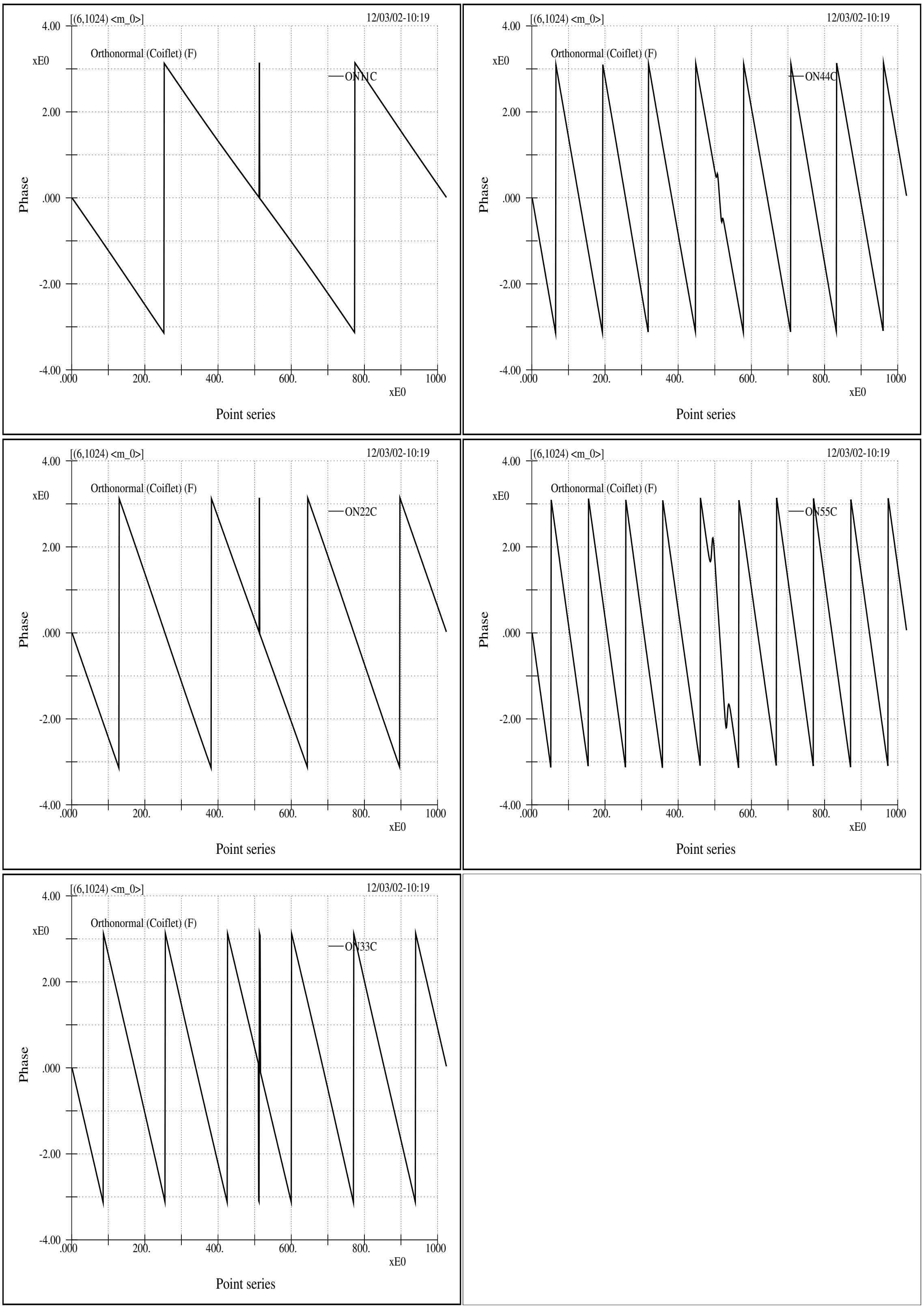

Figure 4.6: The phase distributions of the m_0 functions of the coiflets.

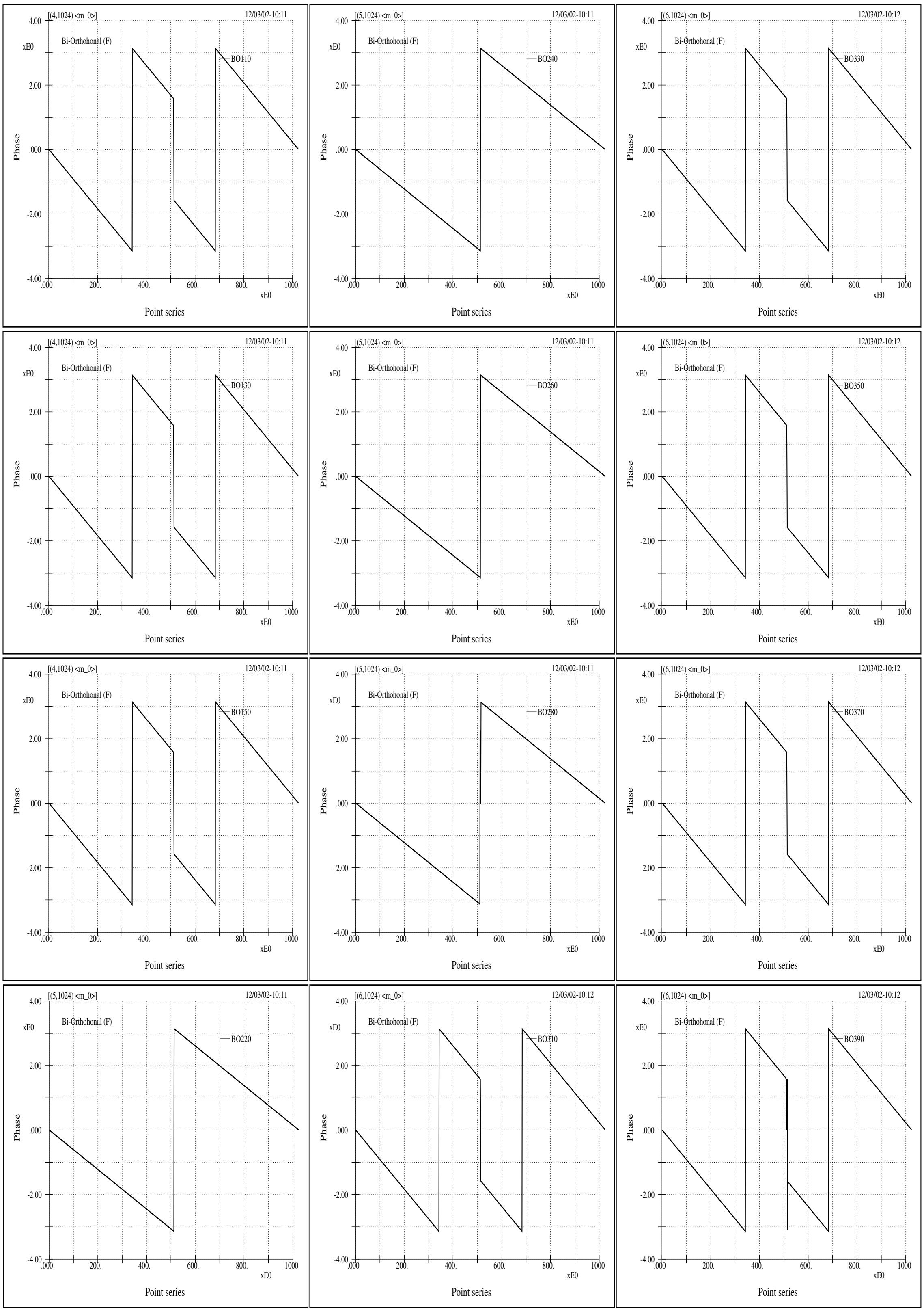

Figure 4.7: The phase distributions of the m_0 functions of the bi-orthogonal wavelets.

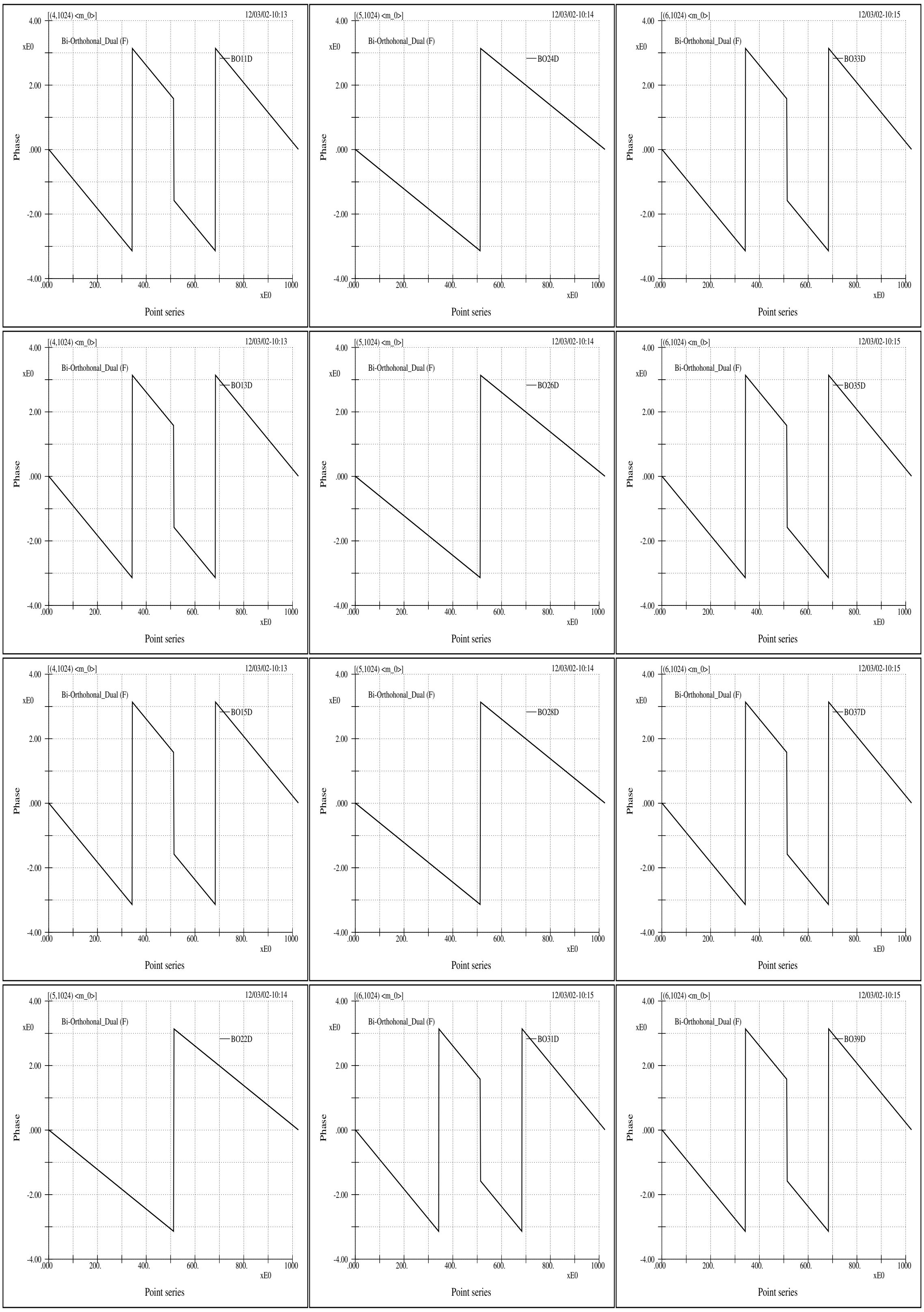

Figure 4.8: The phase distributions of the m_0 functions of the bi-orthogonal wavelets.

Chapter 5

Continuous Wavelet Counterpart of the Identified Optimum Basis

5.1 Discrete wavelet transforms versus continuous transforms

In the introductory chapter we listed a few properties related to a few time-frequency analysis methodologies, such as Fourier transform, short time Fourier transform (STFT), discrete wavelet transform (DWT), as well as continuous wavelet transform (CWT). And in a related previous research the Hilbert transform and the analytical signal approach were also studied and their advantages and disadvantages were highlighted ([13]). In fact one of the main themes for all of these discussions centers on the spirit of the present chapter regarding the minimization of uncertainty effects.

In this chapter, inheriting the identified discrete optimum basis, we mainly focus on the different usages of DWT and CWT concerning their practical applications to water waves related signals. That is to say, what is the continuous wavelet counterpart of the semi-orthogonal cardinal spline wavelet? And why is there the need of a continuous one.

Herein we emphasize that DWT and CWT should be treated as two different entities — since, unlike the discrete and continuous Fourier transforms where they are dealing with the same basis as well as deploying basically the same formulations, DWT and CWT generally refer to two quite different methodologies which focus on their individual function bases as well as different data treatment schemes. Most profoundly we press on the concerns of the following points:

- In general, the dilation lattice is in logarithmic measure for discrete wavelet transform (e.g., the ${a_0}^j$ in the stability condition to be mentioned) and in linear measure for discrete short time Fourier transform (e.g., the $e^{-i2\pi mt}$ in the above mentioned Gabor type frame). Continuous transforms do not involve lattice. The concept of lattice is associated with the concept of time-frequency density, which is defined as the inverse of the product of dilation and translation steps [9]. For short time Fourier transform frames, due to Shannon sampling theorem, the time-frequency density must not go beyond the value of generalized Nyquist density, $(2\pi)^{-1}$. For wavelet transform, however, there is no such a clear-cut limit of time-frequency density. Moreover, Balian-Low theorem depicts that there is no good time-frequency localization for a short time Fourier transform frame if constructed under a strict time-frequency lattice; on the contrary, numerous wavelet bases with good time-frequency localization have been given [4, 9, 20]. These physically imply that wavelet transform may provide better zoom-in.

- The existence of a lattice structure can be either practical or impractical. For water waves, if we don't anticipate any significant gaps in the scale contents, that is to say, the physical process involves time and spatial scales that are "changing" or "evolving" in a relatively continuous sense, we generally do not appreciate the use of frames. Here a continuous transform may provide better chance of success.

- Both continuous and discrete wavelet transforms implement a process of integral wavelet transform over the real line $\mathbf{R}$ in a continuous sense but they analytically emphasize the use of different integration symbols: $\sum$ and $\int$. Digitally sampled signals are certainly discrete, but this is irrelevant to the methodology of continuous wavelet transform or discrete wavelet transform. The main difference, from the application point of view, is that there is no practical interest of reconstruction (or inverse transform) for continuous wavelet transform due to the redundant or non-orthogonal nature of its wavelet coefficients. Both methods are capable of decomposing either functions defined over the real line or signals sampled discretely. In reality, applying continuous wavelet transform to sampled data is implemented in a discrete manner; vis-à-vis, doing discrete wavelet transform for an unlimited ladder, such as that of the standard multiresolution analysis of [17], can describe any function in infinite detail, i.e., over the whole real line. The concept of unlimited ladder of discrete wavelet transform is illustrated by two examples shown in Figures 2.21 through 2.28 where the blow-ups of individual segments of wavelet curves are shown. The figure also illustrates possible bizarre behaviors of certain wavelets and indicates that mother wavelets with short support lengths might not be of ideal choices. In addition, a few discrete wavelet transform formulas when generalized in the limit sense are quite helpful in explaining a few continuous wavelet transform characters.

- All of the Riesz wavelets studied in the previous chapter handle bases with frame bounds that are either tight or relatively tight; whereas the continuous wavelet does not involve frame bounds and might not have frame bounds at all when it is analyzed in the sense of discrete wavelet transform, i.e., not even qualified as a Riesz wavelet. However, we will see that there is a very natural transition from the discrete wavelet to its continuous counterpart.

- Apart form the specific features listed in the above items, there is a practical interest in what can be done to improve the physical relevance between the basis functions and the wave constituents of our signals. For example: does the decaying features of basis functions akin to the physics of component waves? And this is the topic to be discussed in the next chapter.

5.2 The wavelet perspective of an optimum basis

The name of “Wave”-“let” hints a core concept of wavelet analysis: the decaying properties of the basis functions both in time or frequency domains are at the heart of all sorts of function bases, and different intricate analytical properties of wavelets are just manifesting to these decaying features – to be further clarified in the next section. And since two decay properties that are analytically quite differentiable may only have very minor visual differences in their wave forms such as those shown in Figures 2.13 and 2.14, one generally feels that the bearing of wavelets’ physical implications is not proportional to their analytic interests. Nevertheless, we still can benefit from the wavelet approach due to its flexibility in devising the analyzing wavelets as well as its adaptability in forging the algorithms. But versatility does not come without the price of ambiguity. For example, the power spectra of a function are shift-invariant; whereas, wavelet spectra are highly shift-variant [18]. Figure 5.1 shows such a property and it gives us the idea of how significant the phase effects may be. And this figure should be regarded as the counterpart figure in the wavelet analysis to those in the Fourier analysis given in a previous study on the analytic signal approach by the author [16]. Note that all these figures indicate the possible usefulness associated with the uses of non-orthonormal or redundant function bases, as well as the drawbacks of bases with tight frame bounds.

5.3 Implications of wavelet frame bounds

If a function $\psi(t)$ is to be qualified as a wavelet of CWT, then the only requirement is that $\psi(t)$ meets the “admissability condition,”

$$2\pi \int_{-\infty}^{\infty} \frac{|\widehat{\psi}(\omega)|^2}{|\omega|} d\omega = C_\psi, \tag{5.1}$$

where C_ψ is a constant specific to individual ψ, and $\widehat{\psi}(\omega)$ is the Fourier transform of $\psi(t)$. Here, among several definitions of the Fourier transform forward and inverse pair,

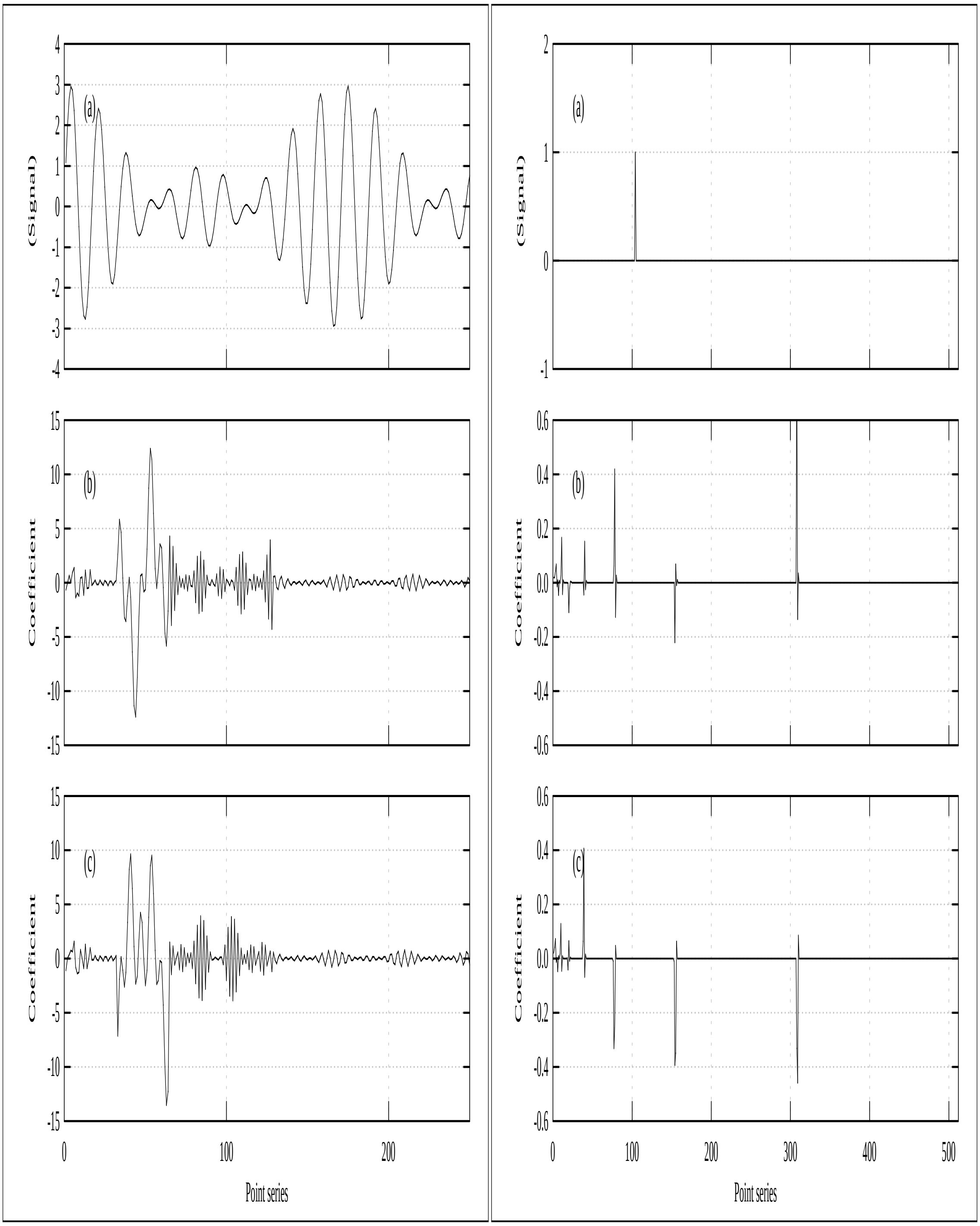

Figure 5.1: The shift non-invariant property of wavelet transforms. Top figure in each column shows individual signal. The middle one shows the wavelet coefficients. The bottom one shows the wavelet coefficients for the shifted signal (right column: 20 points to the left (using BO22D); left column: 3 points to the left (using ON33A)). Note that even though Fourier power spectrum is shift-invariant, Fourier spectral coefficients (without the second power) is still shift-variant. This property is linked to the poor performances of coherences associated with orthonormal bases to be explained in a later chapter.

the adopted one is:

$$\widehat{\psi}(\omega) = \frac{1}{\sqrt{2\pi}} \int_{-\infty}^{\infty} \psi(t) e^{-i\omega t} dt \tag{5.2}$$

and

$$\psi(t) = \frac{1}{\sqrt{2\pi}} \int_{-\infty}^{\infty} \widehat{\psi}(\omega) e^{i\omega t} d\omega. \tag{5.3}$$

The admissability condition is the integration of power spectrum weighted by the inverse of the absolute value of frequency; therefore, it implies that the wavelet should have little power at low frequency and is total nil at zero frequency, i.e., the area between the wavelet curve and the abscissa integrates to zero. This feature of reasonable decay and finite support length is the outright instinct of wavelet. The dilated and translated versions of this wavelet are $\psi_{a,b}(t) = \frac{1}{\sqrt{a}}\psi(\frac{t-b}{a})$, where $a > 0$ and $a \in \mathbf{R}$ and $b \in \mathbf{R}$ are the dilation and translation parameters, respectively; and $\frac{1}{\sqrt{a}}$ is the normalization factor for L^2-norm. The $\psi_{a,b}$ satisfies admissability condition too.

The admissability condition is a very loose constrain; it does not provide a clear concept of redundancy concerning applying CWT to discretely sampled signals. To illustrate this redundancy, let us use the discrete wavelet frame (since the frame wavelet certainly qualifies as a wavelet for CWT): $\psi_{a_0,b_0;j,k}(t) = {a_0}^{-j/2}\psi(a_0^{-j}t - kb_0)$, where a belongs to the set of discrete dilations a_0^j and b to the set of discrete translations $a_0^j kb_0$; $j, k \in \mathbf{Z}$; and $a_0 \neq 1$ and $b_0 > 0$ are fixed positive constants. For such a discrete wavelet frame we need to impose a more restrictive condition on $\psi(t)$ for its admittance, i.e., the stability condition,

$$b_0 A \leq 2\pi \sum_{j\in\mathbf{Z}} |\widehat{\psi}({a_0}^j\omega)|^2 \leq b_0 B, \tag{5.4}$$

where A and B are positive constants and $0 < A \leq B < \infty$. The fixed constants b_0 and 2π are intentionally kept since they are related to normalized wavelet basis and since the magnitudes of A and B are related to the redundancy of the basis.

The stability condition may look abstract, but we give its physical implication as: to be able to let a function be reconstructed from its wavelet coefficients, i.e., the operation is reversible, we need a process which is convergent when summing all its scales or frequency components. It is therefore necessary that the sum of the power of all the constituent elements can neither be nil or infinity. If the sum is zero, then the elements are all of zero measure — nothing exists. If the sum is infinity, then the elements are significantly overlapping in time and frequency — there is either too much dependence or too much ambiguity and tangling (just like two vectors paralleling to each other do not constitute a good vector basis for two dimensional vector space).

Speaking of the reconstruction of a function from its wavelet coefficients one always involves a dual wavelet except for orthonormal basis where the wavelet itself is its own dual — self-dual. And since the roles of a wavelet and its dual can always be interchanged in both decomposition and reconstruction, the above statements apply equally well for dual wavelet; but their frame bounds will generally be different since the sets of convolution coefficients are different as hinted by the different entropy values given in the previous chapter.

If the basis functions are normalized and the inequality of the stability condition are optimized for both the greatest lower bound and the lowest upper bound, i.e., when A and B are defined as

$$A = \inf\left[\frac{2\pi}{b_0}\sum_{j\in\mathbf{Z}}|\widehat{\psi}({a_0}^j\omega)|^2\right], \tag{5.5}$$

$$B = \sup\left[\frac{2\pi}{b_0}\sum_{j\in\mathbf{Z}}|\widehat{\psi}({a_0}^j\omega)|^2\right], \tag{5.6}$$

then an indication of the redundancy is the average value of A and B, $\frac{A+B}{2}$, supposed that A and B are close to each other (almost tight). We elucidate the possible extreme redundancy of CWT as follows. If the dilated and translated versions of a function originating from a certain set of discrete steps (a_0, b_0) constitute a frame with frame bounds A and B, then the frame bounds of a basis using the same function but with finer discrete steps, say

$a_0/2$ and $b_0/2$, will contain the bounds of coarser discrete steps; therefore, the new lower and upper bounds both grow together. This nested relation can be extended infinitely and in the limit sense it is included in the algorithm of CWT. This is the reason why there is no practical value of numerical reconstruction in CWT, although CWT is reversible analytically. Another intuitive explanation is even easier to comprehend: when apply CWT to discretely sampled signal, since for each scale the number of wavelet coefficients is the same as the number of data points and since we can specify scales in whatever resolution we like, we virtually have an unlimited number of wavelet coefficients. The sum of the powers of these coefficients can be unimaginatively huge, or even unbounded; On the other hand, the sum of signal energy is fixed. If we generalize the redundancy concept of DWT, i.e., the ratio between the two sums indicates the degree of redundancy, then for discretely sampled signal a continuous wavelet transform can possibly yield immense redundancy. Though extreme redundancy may exist, we argue that the information content or usefulness associated with the redundancy may behave like a cumulative pdf curve of a Gauss function which may saturate at a later stage, and in reality our numerical results from studies of coherent behaviors of wind-, wave- and current-related signals undoubtedly vindicate this point [14].

5.4 Beneficial scenarios relevant to the redundancy

Redundancy may be a nuisance in certain applications such as those that focus on the perfect reconstruction of signal or on the efficiency of coding and decoding; however it has also shown its promising aspects in several applications. Three prominent points are the results of established cases: (1) Redundancy does not mean that a whole bunch of coefficients are needed to give a good replicate of the original signal, that is to say, significant signal contents can still be retrieved from only a comparatively small amount of coefficients with respect to that of tight or almost tight wavelet frames. (2) Redundancy means that effects of noise either embedding in the sampled signal or arising from the nature of numerical processes (such as frequency leakage) can be reduced by taking advantage of the vast sample space of transform coefficients. (3) If additional features, such as "total positivity" and " complete oscillation" of wavelet are incorporated, the effects on noise reduction or ambiguity removal may be greatly enhanced; together with the redundancy effects they facilitate the design of a very beneficial analyzing scheme. An example of the first point is Mallat and Zhong's [18] (see also Froment and Mallat [10]) signal reconstruction from local maxima using a quadratic spline wavelet. In fact, the mother wavelet they used is basically a loose wavelet (i.e., a wavelet with analytical aspects not being well defined and therefore not really to be qualified as a wavelet), but they were able to recover images quite well using only local peak values of wavelet coefficients that are associated with only dyadic scales. For the second and third points, our studies on the coherent features in the wind, wave, and rain coupling system serve as an example [14].

One last point to note is to compare the admissability condition of CWT with the stability condition of DWT. Here one can easily perceive the great difference in flexibility between the two. In addition, the stability condition is a necessary condition, and not all choices for ψ, a_0, and b_0 lead to wavelet frames. Moreover, stability may not guarantee a good numerical behavior. Figure 6.1 shows the results of a few numerical experiments, where the problems of numerical convergence are illustrated using the blow-ups of wavelet curves. In the figure two bi-orthogonal wavelets are blown up around their individual points using refinement cascade, and the blow-up curves show the possible intrinsic absurdity arising from peculiar analytical properties associated with these wavelets. Here, the two bi-orthogonal wavelets are, respectively, with four and twenty filter weights and both are constructed from quadratic spline scaling function [9]. The top sub-figure indicates a case where the DWT fails numerically to characterize the mother wavelet (not converging) even though the associated wavelet frame qualifies theoretically as a Riesz basis. The bottom sub-figure shows strange alternating inclinations of wavelet curves with a poor convergence. The figure also illustrates the point that, for studying water-wave related signals and their physics, most of the fancy wavelets with bizarre wave forms are not of our choice, as are also indicated by their high entropy values given in the previous chapter.

5.5 The continuous counterparts or the optimum basis

Let the Gaussian function be

$$g_\alpha(t) = \frac{1}{2\sqrt{\pi\alpha}} e^{-\frac{t^2}{4\alpha}}, \tag{5.7}$$

where α is a representative value of the second moment of the Gaussian function and the constants is for the purpose of normalization, the modulated Gaussian is

$$G^\alpha_{b,\omega}(t) = e^{i\omega t} g_\alpha(t-b). \tag{5.8}$$

And the Gabor transform of a function f is

$$\left(\mathcal{G}^\alpha_b f\right)(\omega) = \langle f, G^\alpha_{b,\omega}\rangle = \int_{-\infty}^{\infty} f(t) e^{-i\omega t} g_\alpha(t-b) \mathrm{d}t. \tag{5.9}$$

As is stated by Daubechies ([9]) that the Morlet wavelet is almost identical to a modulated Gaussian, and as is given by Chui ([4]) a modulated Gaussian matches almost exactly with cardinal B-spline wavelet of order greater than or equal to three, i.e., for $m \geq 3$, the even order ψ_m's (such as the cubic spline wavelet ψ_4) match almost exactly with

$$\mathrm{Re} G^\alpha_{b,\omega}(t) = (\cos\omega t) g_\alpha(t-b) \tag{5.10}$$

and the odd order ones with

$$\mathrm{Im} G^\alpha_{b,\omega}(t) = (\sin\omega t) g_\alpha(t-b) \tag{5.11}$$

for a certain set of values α, b, ω.

In accord with these observances we therefore have an extremely natural transition from the identified best basis wavelet based on DWT to the following Morlet wavelet based on CWT,

$$\psi(t) = \pi^{-1/4}(e^{-i\omega_0 t} - e^{-\omega_0^2/2})e^{-t^2/2}. \tag{5.12}$$

Centering on the enhancements of physical modeling of water wave signals, in the following chapter we will further work on the optimization of the CWT processes based on findings of the present chapter. ❖

Chapter 6

The Continuous Wavelet Transform Using Adapted Time-Frequency Windows

6.1 The demand of better physics

In addition to the various concerns about the peculiar properties specific to discrete and continuous wavelet transforms as are stated in the previous chapter, herein we focus on the practical interest in what can be done to improve the physical relevance between the basis functions and the wave constituents of our signals. For example: does the decaying features of basis functions akin to the physics of component waves? In fact, this simple question outlines another fundamental theme of this chapter: if time-frequency windows of fixed shape and size (the case of STFT) is less suitable than time-frequency windows of fixed size but with flexible shape (the cases of DWT and CWT) in characterizing multi-scale transient signals, then time-frequency windows which are flexible in both shape and size should provide even better adaptations. The theme is intuitive right, the background is not without commitments.

Based on this perception, further concerns evolving from the previous chapter can be put forward quite simply: (1) Can we utilize this redundancy to improve the relationship between wavelet's analytical form and its physical interpretability? (2) If redundancy leads to adaptation, does the adaptation still preserve the complete information content of the signal studied? (3) Is the scheme of adaptation efficient and easy to implement?

Question one is related to the distribution or the degrees of freedom of time-frequency windows in the phase plane and will be dealt with in the next chapter. Question two will be answered through the verification for the existence of a condition of "resolution of identity" using a special case of Morlet wavelet, as is also to be given in the next chapter; for now, a short explanation is that, if one just applies the adaptation to finite range(s) of scale, then what is lost or unaccounted for in the adaptation process can still be recovered from some dilated and translated versions of some finer scale wavelets originating from the same $\psi(t)$ in the CWT. The success of Mallat and Zhong's case also indicates such a possibility. Question three depends on the adaptation scheme. But, based on the somewhat intuitive adaptation used here, it is stated that nothing complicate is introduced.

One practical aspect for all the three points is: when analyzing signal we are almost always interested in only finite scale range(s), so what is really needed is to implement the adaptation locally. Hence it may be beneficial not to stick with stubborn time-frequency windows and to adopt a scheme that is numerically with the same easiness and physically more sound.

6.2 Degrees of freedom and the uncertainty relation

The flexibility of constructing wavelet function basis, i.e., the possibility of the adaptation, is associated with the number of degrees of freedom of the time-frequency windows within a phase plane. The number of degrees of freedom for an orthogonal basis is generally defined as the total area of the phase plane divided by the area of the time-frequency window corresponding to that determined by the mother wavelet. For any time-frequency kernel the maximum number of degrees of freedom is determined by the Heisenberg uncertainty relation or Heisenberg's inequality [3]. It is illustrated here that, even though it is impossible to increase the limiting degrees of freedom, there is no further limitation imposed upon the present adaptation. Besides, this section also serves two purposes: (1) illustrate the basic functionality of the modulation mechanism for STFT, which in turn is conceptually the same as the dilation mechanism for WT; (2) outline the relation between redundancy and the Heisenberg uncertainty using possible distribution of time-frequency windows within a phase plane.

The uncertainty relation states that the product of bandwidth Δ_ω and duration Δ_t of a signal cannot be less than a minimum value of $\frac{1}{2}$ when the Δ_t and $\Delta\omega$ are defined as the standard deviations of packet energy $|f(t)|^2$ and power spectrum $|\widehat{f}(\omega)|^2$ with respect to their centroids, respectively:

$$\Delta_t{}^2 = \frac{\int_{-\infty}^{\infty}(t-\bar{t})^2|f(t)|^2 dt}{\|f(t)\|^2}, \tag{6.1}$$

$$\Delta_\omega{}^2 = \frac{\int_{-\infty}^{\infty}(\omega-\overline{\omega})^2|\widehat{f}(\omega)|^2 d\omega}{\|\widehat{f}(\omega)\|^2}, \tag{6.2}$$

where $\bar{t} = \int_{-\infty}^{\infty} t|f(t)|^2 dt/\|f(t)\|$ and $\overline{\omega} = \int_{-\infty}^{\infty} \omega|\widehat{f}(\omega)|^2 d\omega/\|\widehat{f}(\omega)\|$. As is also illustrated in Chui's treatise textbook [4], the time-frequency window, $\Delta_t\dot{\Delta}_\omega$, of the semi-orthogonal wavelet is nearly equal to the minimum value of the Heisenberg uncertainly principal, and this very optimistically provides the opportunity for applying the adaptations. That is to say, there is an easy to way get round of the uncertainty relation by going through a modulation process (i.e., multiplying a basis function with a complex exponential). Since in Fourier analysis a modulation in one domain corresponds to a shift in the other domain, such a process causes the new variance Δ_ω to increase dramatically. Figure 6.2 shows such a mechanism. It is seen that the new $\Delta_t\Delta_\omega$ is significantly larger than $\Delta_t D_\omega$, i.e., even larger than the limiting value for Heisenberg uncertainty relation; therefore, there is quite a lot of flexibility to devise the time-frequency windows. In view of the similarity between the modulation mechanism for STFT and the dilation mechanism for WT, especially for the case of Morlet wavelet, we anticipate that there is an ample space for adapting the time-frequency windows. Furthermore, as pointed out by Bracewell [3], there exists no theorem depicting the lower limit of $\Delta_t D_\omega$, i.e., no new restriction for D_ω; therefore no further limitation on the number of the degrees of freedom is induced. Overall, it is quite flexible to draw time-frequency windows which generally do not violate the uncertainty relation when we express a signal in its two dimensional phase plane.

6.3 Time-frequency windows of flexible size and the physics

The algorithm and the physics associated with the adaptation of time-frequency windows can be illustrated easily by going through practical examples. Though the adaptation does not need to be confined to any specific type of wavelet, the Morlet wavelet readily serves for such a purpose. As was stated in the previous chapter that the Morlet wavelet is almost identical to a modulated Gaussian, and a modulated Gaussian matches almost exactly with cardinal B-spline wavelet of order greater than or equal to three, which is exactly the identified best basis wavelet. Overall we therefore, on the one hand, benefit from an extremely natural transition from DWT to CWT, on the other hand, gain the practical merit of the adaptation.

Before we go into the adaptation, let us recount more explicitly two very important features that distinguish the identified optimum basis from the other bases and that definitely contribute to the causes of the optimum basis' successful applications: (1) The best basis' cardinal spline scaling function and its associated wavelets possess, respectively, the nice properties of "total positivity" and "complete oscillation". We note that these two properties physically imply that its wave form is relatively smooth and without ad hoc variations when compared with some fancy wavelets with finite support lengths. (2) The cardinal B-spline wavelet is either symmetric or anti-symmetric. Therefore, it benefits from the linear-phase filtering. The physical implication of this is: slight differences in wavelet coefficients will not cause significant differences in their reconstructed wave forms, or alternatively, the modulations of the wave forms are comparatively less abrupt. With more natural transitions for both forward and inverse transforms under various circumstances, the impacts to our perception or visualization of an interaction process due to varying input conditions are leaning toward relatively evolutionary tendencies rather

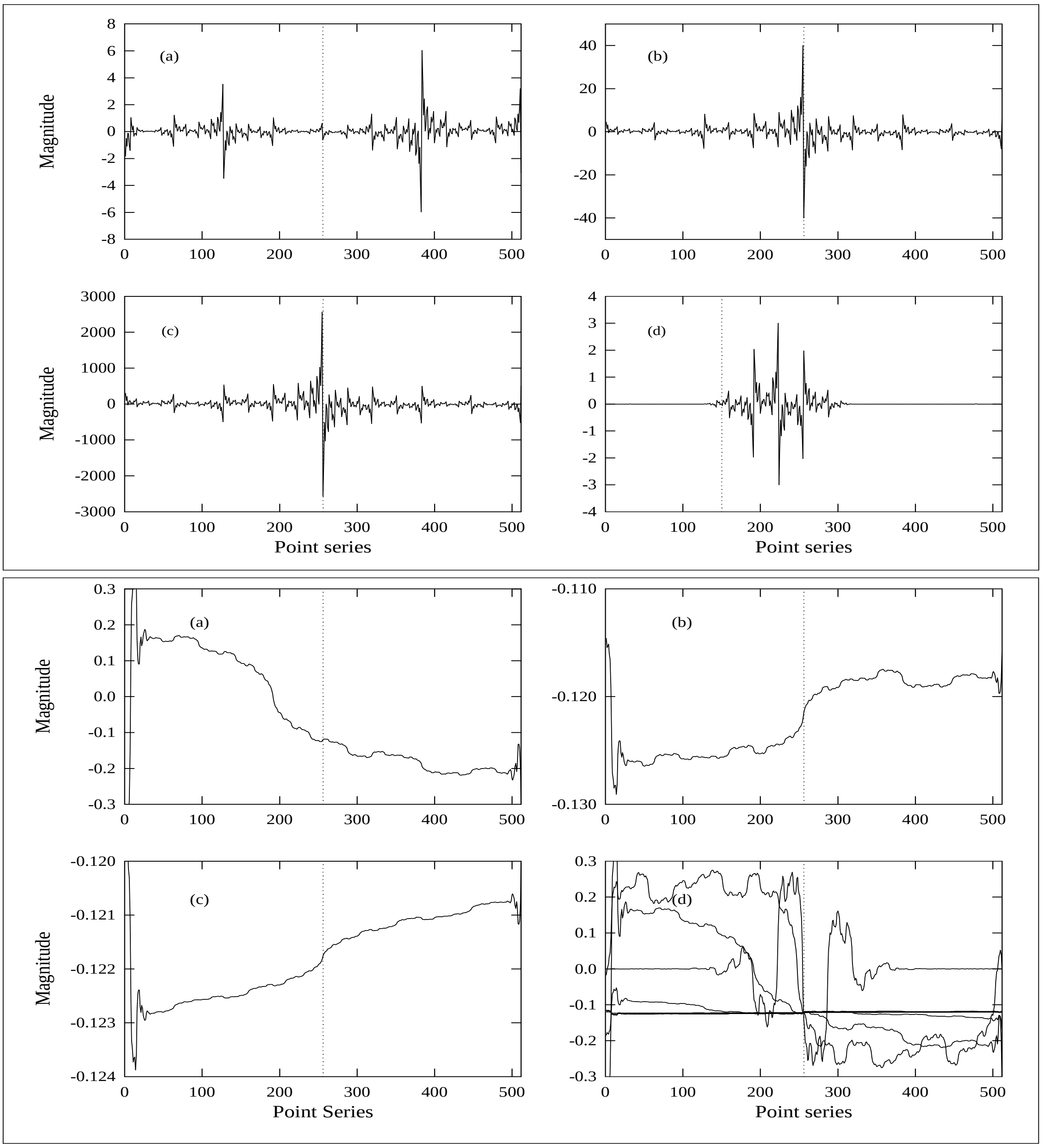

Figure 6.1: Wavelets with fancy analytical properties are often of peculiar wave forms and are not of our choice for studying water-wave related physics — Either judging from their entropy values given in the previous chapter or form their stability conditions shown here. Here the blow-ups of bi-orthogonal wavelets BO31O and BO35O are shown, respectively, in top and bottom halves of the figure. Related data for BO31O is: {Blow-up point: 150 (located at the dotted line in figure (d)); Origin: level 2, position 12 (i.e., U_2^{12} in Figure 2.20); Length: 512 (the curve in figure (d)). Figures (a), (b), and (c) show successive blow-up scale of 2^6. The blow-ups diverge rapidly, i.e., the wavelet fails to identify itself numerically in the refinement cascade.} Related data for BO35O is: {Blow-up point: 256 (located at the dotted line in figure (d)); Origin: U_2^{12}; Length: 512 (one of the curve in figure (d) with parts of the curve coincide with parts of the abscissa). Figures (a), (b), and (c) show successive blow-up scale of 2^6. The blow-ups poorly converge but with peculiar inclinations.}

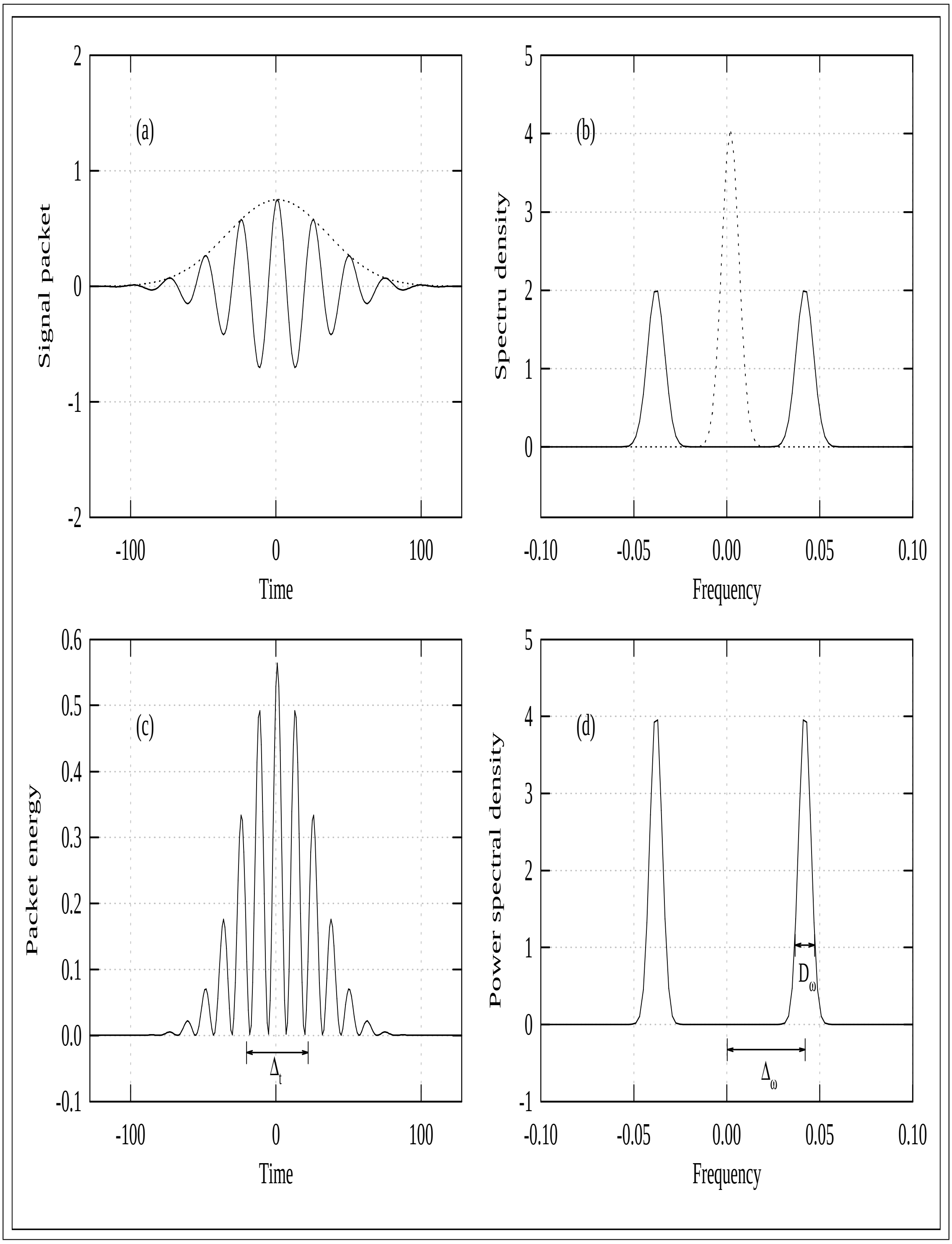

Figure 6.2: The uncertainty relation and the modulation versus shift property (adapted from Bracewell 1986). It is seen that a modulation process renders $\Delta_t \Delta_\omega \gg \Delta_t D_\omega$. This property makes possible that the new value of $\Delta_t \Delta_\omega$ can be significantly larger than the limiting value of Heisenberg uncertainty relation, and therefore provides a great flexibility in devising the time-frequency windows. The implication of this to wavelet's counterpart is explained in the text.

than drastic turnovers. Still, one additional implication of practical significance is: distortions are far less severe when noise and uncertainty are poignant. The phase plane in Figure 6.3 and the various blow-up curves in Figures 6.1, 2.27 and 2.28, as well as figure 5.1 manifest the problems and possible difficulties associated with wavelet bases that do not posses these properties.

Up to this point we have illustrated many specific properties, associated either with DWT or with CWT, that bestow upon our desires when analyzing our water wave related signals; even though their outstanding effects might only be appreciated when we get to the reality of analyzing experimental data. But here let us embark the further work on an improvement — enhancing wavelet's physical implication based on the affinity between the identified best basis and the Morlet wavelet.

The Morlet wavelet is the following complex function:

$$\psi(t) = \pi^{-1/4}(e^{-i\omega_0 t} - e^{-\omega_0^2/2})e^{-t^2/2}, \tag{6.3}$$

in which ω_0 is a constant related to the carrier frequency and the term $e^{-\omega_0^2/2}$ justifies the admissability condition. Its Fourier transform is almost a shifted Gaussian and is given by

$$\widehat{\psi}(\omega) = \pi^{-1/4}[e^{-(\omega-\omega_0)^2/2} - e^{-\omega^2/2}e^{-\omega_0^2/2}]. \tag{6.4}$$

In addition to the general meaning of the modulation frequency, the ω_0 has the physical implication of the amplitude ratio r — the ratio between the second highest peak and the first highest peak of $\psi(t)$ — i.e.,

$$r = \psi(t_2)/\psi(0), \tag{6.5}$$

in which t_2 is the abscissa of the second highest peak. The exact value of t_2 can be obtained by solving numerically the transcendental equation derived from the derivative of the ψ function, but a fairly good estimate is obtained by simply dropping the second term of the above complex function since the second term is generally five order of magnitude less than the maximum value of the first term, i.e.,

$$\omega_0 \approx \frac{2\pi}{t_2} \approx \pi \left(-\frac{2}{\ln r} \right)^{1/2}. \tag{6.6}$$

The higher the ω_0 is, the smaller the ratio r becomes. If ω_0 is constant, then the ratio r for different wavelet dilations or scales keeps constant too. Here comes the core question: whether constituent wave components of different scales and time spans all possess this fixed decay feature? To show that this is not true, let us examine the composite water wave system that is with viscous damping.

For deep water waves with a clean surface the energy losses due to viscous dissipation arise almost entirely from the straining of the irrotational motion in the water column, and the part of contribution from viscous stresses in the surface layer is negligible. It was shown [11, 21] that the time rate of change of the energy density is

$$\dot{E} = -2\mu\sigma^2 {a_w}^2 k, \tag{6.7}$$

where μ, σ, a_w, and k are the dynamic viscosity of the water, the wave frequency, wave amplitude, and wave number, respectively. Since in deep water $E = (2k)^{-1}\rho\sigma^2 {a_w}^2$, where ρ is the water density, the attenuation coefficient

$$\gamma_\nu = -\frac{\dot{E}}{2E} = 2\nu k^2, \tag{6.8}$$

where ν is the kinematic viscosity of the water. Therefore the energy density of the wave evolves as

$$E = C_1 e^{-2\gamma_\nu t}, \tag{6.9}$$

where C_1 is a constant, and the amplitude decreases with time in accordance with

$$a_w = \sqrt{\frac{C_1 2k}{\rho\sigma^2}} e^{-\gamma_\nu t} = C_2 e^{-2\nu k^2 t}, \tag{6.10}$$

where C_2 is a constant if σ does not vary. Comparing the decay of wave amplitude of Morlet wavelet with the decay of the physical model, one sees both similarity and dissimilarity. The similarity is that the attenuation coefficients in both models have inverse square dependence on scales — the former in $(1/a)^2$ and the latter in k^2. The dissimilarity is in the time dependence of the exponent in the exponential — in Morlet wavelet it is in t^2 dependence, while in the physical model it is in linear dependence. It is therefore anticipated that Morlet wavelets based on a fixed modulation shape are not good representations of water waves of different scales. Or stated otherwise, basis functions originating form a single mother Morlet wavelet do not form a good basis.

Now the situation is clear: the constant ω_0 either overestimates the viscous decay of water waves at the low-frequency end or, otherwise, under-estimates those at the high-frequency end. Form a practical judgement of the modulation curves, it is quite reasonable to argue that the deviation is probably more significant for waves with a longer life span when a standard r value of Morlet wavelet, i.e., $r = 0.5$, is assumed. The perceptions here provide the footing for the present adaptation — with different values of amplitude ratio r for different wave scales we are really attemptimg to simulate the evolution process with a more realistic condition. The expansion or contraction of wavelet support length for a specific scale just reflects the devising of flexible constructions of time-frequency windows, and adjusting r is in turn using a variable ω_0. The general guideline is to use a comparatively larger ω_0 (associated with a narrower frequency band) for waves of a longer time support; and vice versa, a comparatively smaller ω_0 (a wider frequency band) for a shorter life span. Here it naturally comes to assume the ω_0 to be a function of scale, i.e., $\omega_0 = \omega_0(a)$. And the varying shapes and sizes of the time-frequency windows are now determined by

$$\psi_a\left(\frac{t-b}{a}\right) = \pi^{-1/4}\left[e^{-i\frac{\omega_0(a)}{a}(t-b)} - e^{-\omega_0(a)^2/2}\right]e^{-\frac{(t-b)^2}{2a^2}}. \tag{6.11}$$

6.4 The physical perception of the sizes and shapes of scales and the adaptations

Earlier we have stated a few nice features of the identified best basis. There is one additional feature that is practically significant because of its relevance to the Morlet wavelet — the physical perception of the sizes and shapes of "scales". Without such a property everything will look obscure. In fact, we have seen a lot of ambiguities or abstractions in many studies where they only involve presentations using non-dimensional scales rather than using the more appropriate physical quantities of carrier frequency even though they are working on modulated Gaussian or Morlet wavelets. We note that the wavelet coefficient generally refers to "scale" not to "frequency". Scale has no dimension, but carrier frequency has a physical unit and is associated with a Gaussian bell modulator. Furthermore, scale generally corresponds to complicate combination of several frequency bands such as what implied by the compactly supported orthogonal wavelets shown in Figure 6.3. Therefore, in order to have a clear picture of a "scale" one needs to consider: What does the basic wavelet look like? What is the actual support length? And, what is the physical sampling interval? All these severely tangle our thought, and we get lost easily. Take as an example: the numerical processes for both discrete Fourier transform and DWT care nothing about the physical units and only the index is important; however, there is an easy conversion from index to frequency for Fourier coefficient, but not for wavelet transforms except the ones associated with the Morlet wavelet. It is totally impossible to visualize the corresponding object just from the index of a wavelet coefficient. For the best basis and the related adaptation the difficulty is avoided, since the precise and physical "carrier frequency" is easily seen to be $\omega = \omega_0(a)/a$, supposed that $\omega_0(a)$

is large enough, say above 5. Again, the point to caution is: illustrations using scale parameter a can be confusing and misleading since the same a may correspond to different actual scales or frequencies when different adaptations or different wavelets are used.

As was stated in the previous section that the present adaptation can always be applied to finite scale range(s) and that the transform only needs to be implemented for scale range(s) that we are interested in. Still, we give an additional description of the flexibility concerning this. Since one can always regard that the set of sampled data points is derived from a certain specific function, but there are basically infinitely many functions which can pass all these sampling points. And since the functions passing through these points may be either band-limited or -unlimited but the sampled signal is always band-limited (since numerical analysis is always associated with finite scale range); therefore, the situation indicates that there exists freedom to make adaptation for ω_0 and also implies the possible redundancy when CWT is applied to the sampled signals. The remaining problem is how to define a suitable decay parameter ω_0. Nevertheless, based on the above mentioned practical concern of wave decay and the somewhat intuitive adjustment, we show the possible improvements in time-frequency resolutions when the adaptation is applied to experimental data. But let us first give a numerical simulation.

For the simulated data we use a parabolic chirp where the frequency range of interest covers the whole band width of the signal, i.e., from almost zero frequency to that corresponding to Nyquist sampling rate. And a linear variation of $\omega_0(a)$ from 10 (for large scale end) to 7 (for small scale end), as opposed to the commonly adopted fixed value of 5.3 (corresponding to $r \approx 0.5$), is assumed. As is seen from Figure 6.3, the adapted one gives better frequency localization for almost all frequencies except the lowest two carrier frequencies (in fact the adaptation can be further adjusted for this part, and to have better resolutions for these two carrier frequencies the values of their $\omega_0(a)$ should be less than 5.3, but the concern here is mainly on the serious edge effects). A phase map for the complex wavelet coefficients derived from a refined ridge extraction scheme is also shown as the top right sub-figure. Here it provides a much better identification of scales of main power contents than what can be provided by Morlet wavelet.

For the experimental data water waves measured in the wind blowing oval tank are used, in which reasonable frequencies should lie between 1.5 and 10 Hz. Earlier we mentioned that the Morlet wavelet is likely to overestimate the decay of longer waves in the long run; therefore, relative to higher frequency waves, we should reduce the decay parameter ω_0 for low frequency ones. Based on this understanding we heuristically assume

$$\mathrm{Erfc}\left[\frac{4}{10}\left(\frac{\omega_0}{a}+2.5\right)-2\right]3+5=a\omega \tag{6.12}$$

where Erfc is the complimentary error function and ω is the carrier frequency. This equation may be modified according to the type of signal studied or according to the frequency range of one's interest. Figure 6.4 shows the curve of the function. The logic for the choice of its constants is self explained in the attached program piece. Figure 6.5 shows results without and with the adaptation. Here, the varying $\omega_0(a)$ is from 9.16 (for the large scale end) to 5.26 (for the small scale end), as opposed to the fixed value of 5.3. Again there are less smearing effects at the lower portion of the time-frequency plane since we mainly adjust decay parameters for the low-frequency end.

A few additional points are: (1) The dominant carrier frequency is about 2.4 Hz in this case; (2) Waves of all frequencies keep constantly evolving, since light and dark regions constantly interlace; (3) There are grouping effects. Waves with significant energy contents are more enduring and the durations of darker bands are much longer than those of higher frequencies. This indicates that our adjustment for decay parameters is based on a reasonable ground; (4) There is an obvious bifurcation among scales, especially for the intermediate frequency range of about 3 to 4.5 Hz; it suggests that the phenomenon of energy cascade from where energy concentrates to neighboring areas. Judging from these characters it seems that the energy phenomenon in a multi-scale wave field is somewhat similar to that in a turbulent flow field (see Tennekes and Lumley [23]).

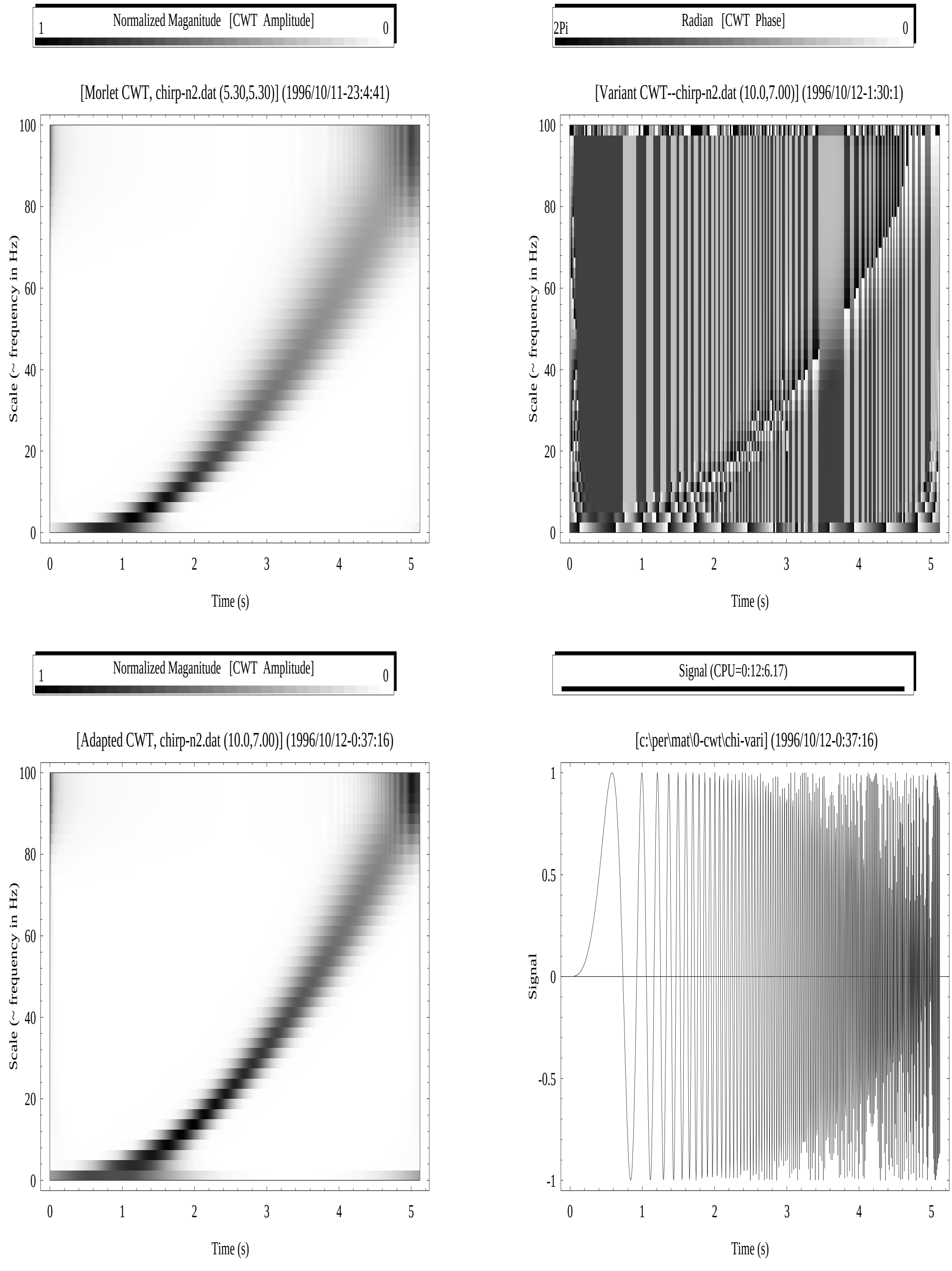

Figure 6.3: Phase plane characters for a parabolic chirp `(bottom right)` with `(top left)` and without `(bottom left)` adapting time-frequency windows. Top right shows a map of the phase that is obtained from using a newly devised wavelet variant by Lee and Wu [15]. The wavelet variant has properties quite in contrast to those of Morlet wavelet and has refined ridge extraction capability.

```
obeg=11.;  oend=5.;
fcenter=2.5;  fdilation=10/4;   fshift=2. ;

perfc=Plot[ Erfc[(1/fdilation)* (freq +fcenter)-fshift]*
                           (obeg-oend)/2+ oend, {freq, -2.5, 8.5} ]
```

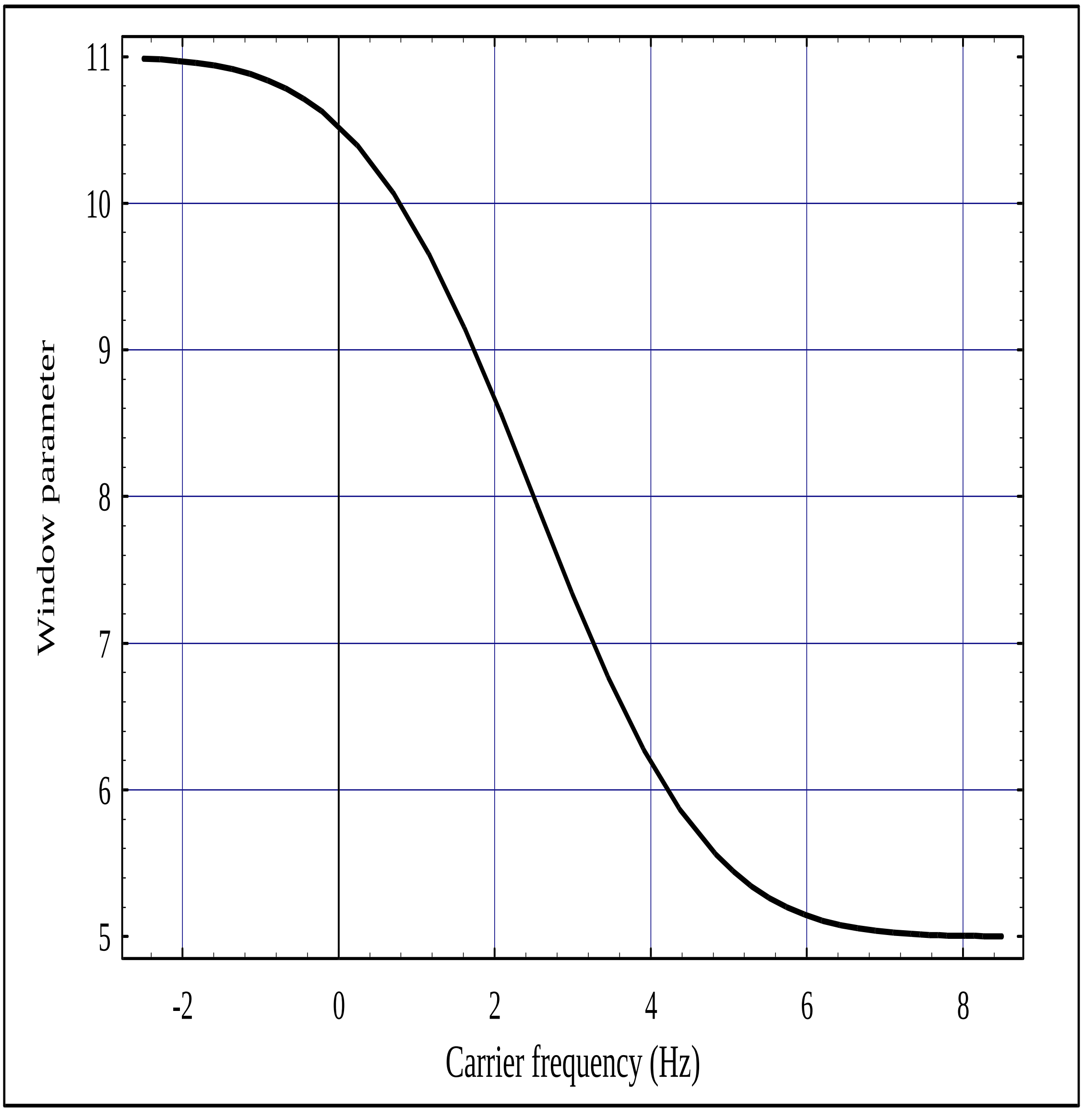

Figure 6.4: The assumed wave decay parameter ω_0 as a function of carrier frequency. The curve can be adjusted according to several parameters: approximate peak frequency, significant range of frequency, range of decay parameter, as well as a shift adjustment parameter; as are indicated in the attached program piece.

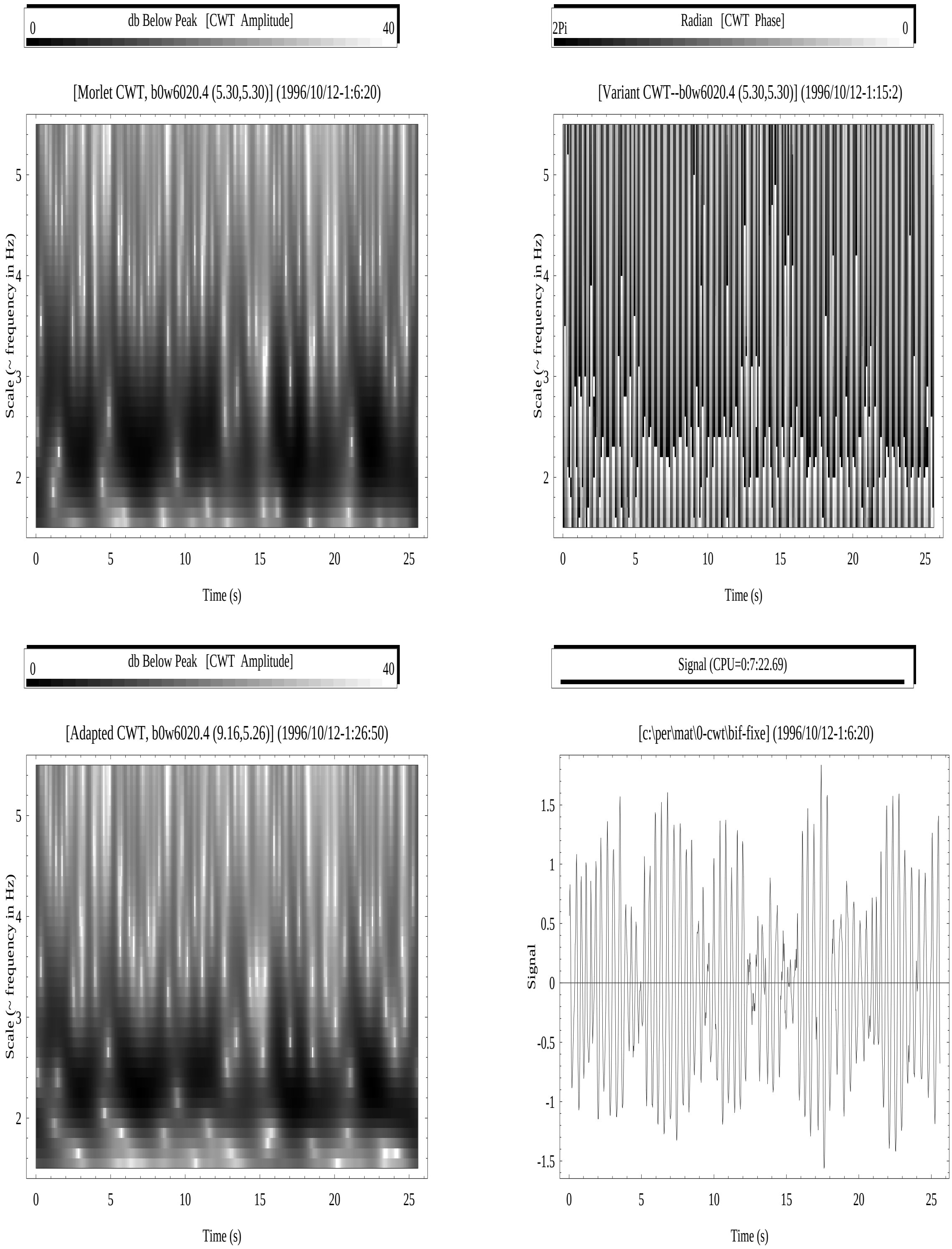

Figure 6.5: Phase planes of a water-wave signal measured in a wind blowing oval tank (top left: without adaptation; bottom left: with adaptation; top right: phase plot; bottom right: wind-wave signal.) Since the assumed adaptation mainly adjusts the decay coefficients for low-frequency part, there is less smearing there. Again, the phase plot using the same wavelet variant as of Figure 6.3 provides a clearer identification of ridges of the main power, which is not possible for the Morlet wavelet.

6.5 Existence of admissability condition

Earlier we gave a somewhat physical description on how the present adaptation manages to provide an almost “lossless” operation. Lossless means that the full information of a function is preserved during the transform and that we can recover the function from its wavelet coefficients, i.e., there exists a reverse operation. In the following we provide a more formal description through validating the existence of the identity resolution, which is basically just to show the existence of an admissability condition.

In an earlier illustration of the adaptation, a modified basis of wavelets was formed by adjusting the support length of dilated versions of $\psi(t)$ using different values of ω_0 which is further assumed to be a function of a. Furthermore, as explained in the previous section, a simple adaptation is the modification of carrier frequency according to $\omega = \omega_0/a$, i.e., $\omega_0 = a\omega$, we therefore further assume that ω_0 is a generalized function of $a\omega$ and the wavelet is

$$\psi_{\omega_0}(t) = \psi(t\ ;\omega_0(a\omega)). \tag{6.13}$$

Its dilated and translated versions are given by

$$\psi_{a,b;\omega_0}(t) = \frac{1}{\sqrt{|a|}}\psi\left(\frac{t-b}{a};\omega_0(a\omega)\right). \tag{6.14}$$

And the wavelet coefficients of a function $f(t)$ are given by

$$\begin{aligned} \mathrm{W}f_{\omega_0}(a,b) &= \langle f, \psi_{a,b;\omega_0}\rangle \\ &= \int_{-\infty}^{\infty} \frac{1}{\sqrt{|a|}} f(t)\overline{\psi_{\omega_0}\left(\frac{t-b}{a}\right)}dt \\ &= \int_{-\infty}^{\infty} \sqrt{|a|}\,\widehat{f}(\omega)\overline{\widehat{\psi}_{\omega_0}(a\omega)}e^{-ib\omega}d\omega, \end{aligned} \tag{6.15}$$

in which $\widehat{\psi_{\omega_0}}(\omega) = \widehat{\psi}(\omega;\omega_0(a\omega))$. We follow the formalism to check that the inner product of two functions f and g, $\langle f, g\rangle$, can be recovered from the integration of the projection of $\mathrm{W}f(a, b; \omega_0)$ into $\mathrm{W}g(a, b; \omega_0)$ along both real lines of dilation and translation variables. That is, whether the following equation exists:

$$\int_{-\infty}^{\infty}\int_{-\infty}^{\infty}\frac{1}{a^2}\mathrm{W}f(a, b; \omega_0(a\omega))\overline{\mathrm{W}g(a, b; \omega_0(a\omega))}dadb = C_{\psi_{\omega_0}}\langle f, g\rangle, \qquad (6.16)$$

where $C_{\psi_{\omega_0}}$ is a constant. If it exists, then when g is taken as the Gaussian function with its variance approaching zero (i.e., g is practically the delta function $\delta(t)$), the inner product $\langle f(t'), g(t'-t)\rangle = \langle f(t'), \delta(t'-t)\rangle$ will recover $f(t)$ and the condition of the identity resolution is guaranteed.

The right hand side of the above equation equals to

$$\int_{-\infty}^{\infty}\int_{-\infty}^{\infty}\frac{1}{a^2}\left[\int_{-\infty}^{\infty}\sqrt{|a|}\,\widehat{f}(\omega)e^{-ib\omega}\overline{\widehat{\psi}(a\omega; \omega_0(a\omega))}d\omega\right]\times$$

$$\left[\int_{-\infty}^{\infty}\sqrt{|a|}\,\overline{\widehat{g}(\omega')}e^{ib\omega'}\widehat{\psi}(a\omega'; \omega_0(a\omega'))d\omega'\right]dadb. \qquad (6.17)$$

With the following two identity equations

$$\begin{aligned}
&\widehat{F_a}(t, \omega_0(a\omega))\\
&\quad= \frac{1}{\sqrt{2\pi}}\int_{-\infty}^{\infty}e^{-it\omega}\sqrt{|a|}\,\widehat{f}(\omega)\overline{\widehat{\psi}(a\omega; \omega_0(a\omega))}d\omega\\
&\quad= \frac{1}{\sqrt{2\pi}}\int_{-\infty}^{\infty}e^{-it\omega}F_a(\omega; \omega_0(a\omega))d\omega, \qquad (6.18)
\end{aligned}$$

$$\overline{\widehat{G_a}(t, \omega_0(a\omega))}$$

$$= \frac{1}{\sqrt{2\pi}}\int_{-\infty}^{\infty}e^{it\omega}\sqrt{|a|}\,\overline{\widehat{g}(\omega)}\widehat{\psi}(a\omega; \omega_0(a\omega))d\omega$$

$$= \frac{1}{\sqrt{2\pi}} \int_{-\infty}^{\infty} e^{it\omega} \overline{G_a(\omega; \omega_0(a\omega))} d\omega, \tag{6.19}$$

one has

$$\int_{-\infty}^{\infty} \int_{-\infty}^{\infty} \frac{2\pi}{a^2} \widehat{F_a}(t; \omega_0(a\omega)) \overline{\widehat{G_a}(t; \omega_0(a\omega))} dadt$$

$$= \int_{-\infty}^{\infty} \int_{-\infty}^{\infty} \frac{2\pi}{a^2} F_a(\omega; \omega_0(a\omega)) \overline{G_a(\omega; \omega_0(a\omega))} dad\omega$$

$$= \int_{-\infty}^{\infty} \int_{-\infty}^{\infty} \frac{2\pi}{|a|} \widehat{f}(\omega) \overline{\widehat{g}(\omega)} |\widehat{\psi}(a\omega; \omega_0(a\omega))|^2 dad\omega$$

$$= 2\pi \int_{-\infty}^{\infty} f(t) \overline{g(t)} dt \int_{\infty}^{\infty} \frac{|\widehat{\psi}(a\omega; \omega_0(a\omega))|^2}{|a|} da$$

$$= 2\pi \langle f, g \rangle C_{\psi_{\omega_0}}. \tag{6.20}$$

Now the resolution of identity is fulfilled if the following admissability condition is satisfied,

$$\int_{-\infty}^{\infty} \frac{|\widehat{\psi}(a\omega; \omega_0(a\omega))|^2}{|a|} da = C_{\psi_{\omega_0}}. \tag{6.21}$$

This condition is more restrictive than Equation 5.1 in that $\widehat{\psi}(0, \omega_0(u)) = 0$ for all $u \in \mathbf{R}$. Otherwise, there is no other restriction since what is changed in the integration is limited to finite range and is anticipated to be finite. The case using Morlet wavelet complies with such a validation and therefore satisfies this condition. ❖

Chapter 7

Conclusions

Comprehensive sets of various discrete wavelet categories are studied for the interests of the water wave related applications, and their relevant characterizations and various intrinsic properties are illustrated. The numerical analyses and the associated data processing are developed from the ground up using the Asyst programming language, as well as several add-in components. These tools make possible the extensive depictions of the wavelet natures, such as their mother and farther wavelets, the translations and dilations concepts, the zoom-ins or blowups of any individual wavelet, concept of time-frequency windows, uncertainty relationship, and the linear phase filtering features — more importantly, if possible, their physical implications, practical usefulness, and the advantages or disadvantages in water wave applications.

Using signals obtained from wave-tank experiments and under various entropy criteria, the entropy statics for the whole set of wavelets, as well as the Fourier basis, are analyzed. To the greatest extent the results show that the sole optimal discrete wavelet basis is the dual semi-orthogonal cardinal spline wavelet.

The entropy results are of statistical approach; they provide no clue as to which analytical factor that gives rise to their performances for our water wave signals. In this regard, we examine the phase distributions of a wavelet characterizing function for all the wavelets. It is also fully identified that there are extremely well correspondences between the various behaviors of phase distribution features and those of the entropy statistics. It is therefore concluded that a wavelet function basis's phase distribution feature determines its usefulness in water wave physics and that the linear phase feature is a requirement of an optimum basis.

Moreover, based on the identified minimum entropy Riesz wavelet, i.e., the cardinal semi-orthogonal cubic spline wavelet, we explore its continuous wavelet counterpart for the purpose of incorporating additional specific advantages that are key to its usefulness in our applications. These mainly concern the manipulation of wavelet redundant or non-orthogonal features for the purpose of uncertainty reduction.

In addition to the above two optimizations, a third one is applied to the continuous wavelet counterpart. For this we propose a mechanism of flexible constructions of wavelet time-frequency windows and the method of such an adaptation.

The decaying properties of water waves of different scales were used to justify the concept of the present adaptation. Both numerical simulation using chirp signals and experimental data acquired from the wave tank were used to show overall improvements of time-frequency resolutions in their phase plane representations. In a more formal way, the resolution of identity was also validated for a particular construction using a modulated Gaussian wavelet. In fact, this illustrates one additional flexibility of wavelet analysis, and, together with the similar flexibility in wavelet packet decompositions outlined in the previous chapter (i.e., the almost unlimited constructions of tree-like decompositions) and the concepts of time-frequency windows related to multi-voice or multi-wavelet algorithms [9], the intuition of making flexible constructions of time-frequency windows for wavelets other than the Morlet wavelet is not unjustified.

Though the present adaptation is in some sense intuitive, it is physically sound and fits into the instability nature of water waves. More importantly, being based on an optimum basis in DWT and further combined with the several specific features related to CWT, the present approach is anticipated to be a more suitable methodology for the analyses for water wave related signals — especially when considering the extractions of micro phenomena, such as the possibly feeble energy features evolving under limited or restricted conditions of model experiments.

Finally, one last point to note is the following statement — the author firmly believes that if you ever find an individual wavelet you have great chance to assign it into one of the categories covered here; and if not, you have great reason to conceive that its properties must fall within (or between) the covered characterizations; and thus, in water wave applications, its fate or possible usefulness is decreed accordingly — overall, it is really hard to beat the optimum basis and the methodology as are identified in this study. ❖

APPENDIX A

中 文 概 述

第一章　　引言

不同的訊號分析法有其不同的專善與優缺點。從典型而用途廣泛亦且成果豐碩的傳統波譜分析法以迄較近之仔波分析，我們有傅立葉分析、加窗富立葉分析、蓋博解析訊號分析法或希伯轉換、各種基於不同設計基核分佈函數的時頻分析法、離散仔波分析、暨與離散仔波法可說不相同的連續仔波轉換分析法。

在這一章中首先我們說明了各種分析法的大致特性與區別或長短處，主要並闡述非穩態下物理與解析之相應表徵。事實上，所有的時頻分析法都可以歸之爲加了罩窗的轉換，只是不同分析法對如何加窗是有極其不同的設計。此處我們以仔波轉換與加窗的富立葉轉換例舉他們的加窗特質，並引出何以仔波分析對非穩態與穩態的適用性都有其可能用途。

整體而言，本研究內容主要可分爲五大主題部分。而其工作方向則在於水波相關訊號分析上的三項分析優化工程。

第一部分之重點在於研究相當廣泛而完整的離散仔波類屬暨其衍生類屬。探討其各項解析與數値行爲，包括母仔波、父仔波、移位與展縮現象、爆展特性、仔波包延伸行爲，等，並將可能之物理表徵與使用性加以說明。

第二部分之重點在於取得水波分析應用之最適化離散仔波轉換函基。所取得之最適函基是基於廣泛之仔波類屬，另及富立葉函基，並以多種熵値標準鑑取。此爲第一項優化工作。

第三部分則在探討何種數理要素造成了第二部分之統計熵値結果。也就是說在於探尋仔波函基的何種數學因子對水波訊號之模擬表現具有操控的關鍵。此部分

我們驗証了仔波特性函數之相位分佈情形爲操控因子。

第四部分則在於仔波分析於水波之應用之雙優化。所謂的雙優化是在最佳離散仔波的基礎上加入一些連續轉換所特有的特性與優點。

第五部分則在於分析的參優化，亦即探討如何增進函基與水波之實際關聯性，此項優化是調適時頻窗使之能更符合水波實際物理現象。

第二章　　各類屬離散仔波函基特性研究

在幾乎所有的試驗模擬中，無可避免的是，其模擬因子無法全面兼容，而其模擬尺度有其拘限。特別是在面對一個牽涉多尺度、多維向的複雜問題時，往往最重要的就是要能表徵它的非穩態性或突變性行為，若我們的數據分析鑑取方法無法比較全面性的掌握當中的尺度，那一些互作用現象即無法顯現或正確描述，因此，尋找一個適用於多尺度、並具備最佳化的模擬函基是為必然的訴求。針對這一訴求，在這一章中，我們選取了類屬含蓋廣泛而完整的離散仔波函基加以比較研究，探討其各項解析與數理行為與實際意涵。

我們由基本起、原始性地開發一完整、亦且相當彈性化的數值分析程式，並加入一些輔助功能與程式套件，期使得以深入瞭解仔波暨相關分析。數值模擬之內容包括母仔波與父仔波、仔波包、仔波相關涵數之相位與線性濾波特性、各種仔波相關函數局部展開行為等。也經由這些最根本的瞭解，庶幾在各章節中得以說明一些應用分析的表徵，也就是說將解析特質與其於水波數值分析之表現關聯在一起，並藉此判定不同仔波類屬的相對有用性。

第三章　　熵值與最適函基之鑑取

在仔波的應用上，有一些研究是可以不牽涉仔波的物理義涵，例如在電子學訊號傳輸、影音壓縮、圖像邊界鑑選等，它們可以只强調效能最佳、速率最快、誤差最小；可是我們水波研究則主要著眼在物理上，而不在數值效能與速度。在前者應用研究中，爲達到所要目的，則其函基之不同尺度仔波與訊號成分波必需相近。不夠，話說回來，針對我們水波用途，如果我們所選取的函數分佈形狀與我們訊號構成成分之形狀差異甚多，那我們如何可以安心地認爲它可以模擬我們所要的物理。也如是乎，殊途同歸，速度與效能自然地成爲我們的鑑取規範。這一規範也就是所謂的最小熵值。

熵值基本上是爲一統計物理量，一般物理上它的最簡單（或普遍）的義涵是爲無用之能量，也常代表一種亂度。在此處，它最簡明的意義可以表示爲一種距離，也就是說，我們是要求取一個無用資訊最少、而與原始訊號距離最短的函基。而更具體的說，我們是從各個仔波轉換（包括仔波包轉換）所取得的係數中，判定那個轉換可以用最少的係數，以反轉換取得與原來訊號最近似之結果。

此處我們應用各種熵值統計規範於水槽風生水波訊號，從而一致判定最適離散仔波是爲半正交樞點順適仔波。其它相關說明項目有：不同熵值定義與實際數值處理手法；訊號重建概念；各類屬仔波於內於外的表現趨勢；誤差比較；暨這些表現與仔波解析之對應因子等。

第四章　最適函基與特性函數之相位分佈關聯

在前面的章節裡，我們一方面例示了各類屬離散仔波之各種行爲特性，一方面用統計手法，在各種熵值標準下一致取得最佳離散仔波爲半正交樞點順適仔波。在這些探析中我們只看到了它們的行爲表現，卻未究取其造成解析因子或根基源頭，這一章的目的即在於這項的工作，也就是取得相應於統計熵值表現的數學要素，亦即函基的何種解析因子是水波相關訊號分析其表現的關鍵。

毫無疑問地，此處我們所研究之仔波特性函數之相位分佈情形可以充分，甚或完全，掌握此章所要的目的。這是因爲我們所歸納得的各類屬離散仔波之特性函數相位分佈狀況、行爲表現、演化趨勢等，在在都可以找到相對應的熵值表現行爲與分佈演化趨勢。而整體的結論是：特性函數之線性相位分佈是適切模擬水波訊號所必需之條件。

第五章　最適離散仔波函基之相應連續仔波

在前面的章節裡，各項討論內容暨鑑取得之最佳半正交樞點順適仔波是建構於離散仔波之多解析度分析。在這一章中我們說明了何以需要一個相應的連續仔波暨轉換，這主要的癥結在於降低分析之不定性，也就是比較離散與連續仔波轉換之優缺點及特性，從而在最適函基之優點上再加入連續仔波所特有之性質，因而將分析雙優化。基於這一改良，我們亦指出最佳離散仔波其相對應的連續仔波爲何。此處我們首先必需强調連續仔波轉換是不同於離散仔波轉換的，因爲不似富立葉轉換，其連續與離散轉換不但在基本上應用的函基是一致的，其分析建構手法基本上亦是相同的；然而連續與離散仔波轉換不但其函基可以完全不同，其分析建構方法更可大異其趣。至於本章相關內容則另有下列諸要項：

- 連續與離散仔波轉換展縮級距之差異暨其與水波衍轉與演化之相配性要求；
- 時頻窗密度之具體觀念及時頻窗局部性之限制與適切性；
- 連續與離散仔波轉換在分解與重建一個函數之實質差異；
- 母仔波自變數分佈範圍對實際水波分析結果之效應；
- 函基框架束限值在連續與離散仔波轉換之含義及其數學與肇生物理現象；
- 連續仔波轉換其贅餘性在水波訊號分析之可用性；
- 仔波函數其衰減特性之含義；

- 指出下列諸函數之關聯性與自然對應性，如高斯函數、載波高斯函數、蓋伯轉換、半正交樞點順適仔波、與莫利連續仔波函數，因而由最佳離散函基而尋得相應之最適連續仔波函基。

第六章　　基於調適化時頻窗之連續仔波分析

在前面幾章中我們從事了兩項針對水波訊號分析的優化工程，在這一章中實際可說是要再加以一個分析優化工作，因而形成一套參優化水波分析。具體而言，就是將上一章取得之最適連續仔波轉換的時頻窗加以改良，使其更能眞確模擬水波相關訊號。

我們的立論實際上很簡單：針對多尺度水波相關訊號研究而言，如果所使用函基其時頻窗之大小與形狀俱爲固定（如短時富立葉分析），則其結果將不如使用那些函基其時頻窗之大小爲固定但形狀是變異不同的（如各離散與連續仔波轉換）；那麼時頻窗之大小與形狀俱都可彈性變化的函基，不就更能符合多尺度、多互作用之複雜水波現象，因而提供一種更適切模擬分析。基此，本章主要涵蓋內容有：

- 應用贅餘性增進仔波解析與實際物理可解說性之關聯；
- 說明海參堡不定性關係式與時頻窗自由度之關聯。而這一自由度之特性正是時頻窗調適化之根據；
- 以二次方漸高頻數值模擬訊號圖示說明時頻窗調適化之效應；
- 解說可調適時頻窗之仔波與實際水波物理相應性，此處我們以水波之黏滯性衰減行爲相較於連續仔波函數分佈情形，從而亦說明如何調適仔波之時頻窗；
- 敘述所取仔波其「全正性」與「全振性」所造成之實際效應，如仔波形狀不

突兀，則波形相近之水波訊號其仔波轉換結果之係數分佈差異將較自然而不駭愕；

- 說明線性濾波特性之效應，在此一情況下，若轉換係數有些微差異，其反轉換之結果或重建之訊號形狀將不會有巨大差異，這點的重要意涵則在於說明波形之演化爲漸進式的，綜合上一點，也因爲正、反轉換都爲衍化式而非突變式，因而試驗訊號分析之研判與歸納不但較易掌握，互作用因子亦較易顯現；
- 指出許多研究只用無因次的尺度來說明實際具有因次的物理現象，因而造成具體形象認知之重大障礙。針對這點，本研究明確地說明所用載波頻率之優點；
- 以補償誤差函數模擬依尺度或載波頻而變動的時頻窗；
- 進一步數學驗証我們所使用之調適化時頻窗連續轉換函基符合連續仔波之入門允當資格，亦即其轉換係數保有訊號之完整性。

第七章　結論

爲了鑑取得一個水波相關訊號分析應用上最適化的仔波分析技法，我們由源頭、最根本起，開發了一個相當徹底的仔波分析程式，程式主要以Asyst 語言撰寫，另亦發展其相關套件。

所研究內容包含相當廣泛而完整的離散仔波類屬及其衍生類屬。首先吾人探討其各項解析與數值行爲，並將其可能之對應物理表徵與可能之使用性加以說明。

而爲了要在廣泛離散之仔波類屬中鑑取最佳的函基，我們以各種標準下的熵值表現一致判定最佳離散仔波是爲半正交樞點順適仔波。

所謂的熵值鑑定是一統計手法，它無法看出何種解析因子造成函基之不同表現。針對這一訴求，我們研究各仔波其特性函數之相位分佈情形，將其結果之衍化與相關趨勢行爲對比於熵值之表現行爲，從而斷定線性相位分佈是爲最適化數理根由，亦是必備條件。

對一複雜的水波訊號系統而言，前面所取之最適化離散仔波可說是分析優化的第一項工作，其分析仍有一重大考量是爲分析不定性之增進。針對這一基本訴求，此處我們說明引入連續仔波轉換之原因與需求，亦即第二項優化工程。此外亦闡明各種數理要義暨相應物理表徵。

在前述雙重優化下，我們又針對最佳仔波與所模擬水波實際物理現象之差異加以探討說明，從而再加引入時頻窗調適之機制。蓋因不同尺度之水波其演化衰減趨勢與仔波轉換其時頻窗之大小爲固定所呈現的趨勢並不相符。此外，此處亦驗証這一調適符合連續仔波之資格允當性。

最後作者謹表示：或許你會看到一些零散而有點默生的離散仔波，但吾人深信，大部分情形下，它將可以被含蓋在這篇文章所探討的類屬中；如果不是，則吾人亦深信，你也大概可以把它的屬性歸納於介於我們所探討的仔波類屬之間，也如是乎，它於水波物理上的應用性、或是可使用性將不超乎本文之認定。

APPENDIX B — Wavelet 該如何中文稱之？

【摘自本所「研究計畫簡訊第一季」】

值此計畫之伊始，就讓我們來討論一個比較有趣、也是最根本的話題，那就是英文的wavelet 該如何中文稱之？也藉此順便涉略wavelet 的一些相關概念。

Wavelet 如今似乎最常見的翻譯是「小波」，而本人則習慣叫它爲「子波」，然而個人認爲最貼切的譯法應該是「仔波」。話說當年，約莫是1993 年初，是我在國外初次接觸wavelet ，而比較大規模的自我研習則大概又在一年之後。因爲先前在國內並無接觸，自然對它的中文譯法也無從得知。另一方面也因wavelet 的主要理論與應用學門並不在海洋科技領域，就我所知，學校內並無wavelet 的課程（包含當時數學系及各研究所所開課程），所認識之老中也無人從事這一課題，所以也無人相詢。如是「子波」的稱呼就建立在我的習慣上了。如果當時有如現在這樣發達且簡易而方便的Internet ，或許也就可以查到它的叫法，從而附會主流。

言歸正傳，也讓我們來說說爲何仔波的譯法最爲貼切。從英文字義講-let 是一個名詞附尾，比如我們所常聽到droplet 、piglet 。這個附尾代表小、年輕、局部，而有活蹦亂跳的含義。但把英文的wavelet 稱之爲「小波」，我認爲最大的致命傷就是中文的「小」跟「波」形成一種非常泛濫的概念，容易讓人聯想它是小小的波（small wave ），也不免讓人想起是否有個相對應的大波？它缺乏一种像英文wavelet 那樣的專有名詞的氣度：另一方面，從數學內涵而論，wavelet 的精神絕對不是在大小方面，它主要的觀念是在强調一種局部性分佈的波，你要它多大就可多大，要多小就多小。此外小波的叫法也缺乏wavelet 的一些內涵，如多元性（無窮多種）、變異性（各形各色）、勁暴性（奇奇怪怪）。再者，小波的叫

法也很難讓人把它與函基（function basis ）構成函數作一些關聯連想，而wavelet 的重要用途無不肇始於它所衍化形成的函基。另外値得一提的是，實際上，數學的分析可以完全不涉單位，而沒有單位，也就無所謂的絕對大小；而在實用上，一般離散數値解析的整個處理流程可說也可完全不涉單位（只涉及序列），只需於最後的結果適當的考慮加入單位即可。如是，這種大小的區別比較就非核心問題所在。

至於第二種稱法「子波」，個人認爲，相對於小波，它比較有專有名詞的氣度，不會像小波有著那樣泛濫的意義。事實上子本身就有小的含義，再者它影射仔的年輕與動力，而它似乎亦表示可成長、演化。不過有個缺點，那就是，wavelet 的學門無不在訴說mother wavelet ，可是這mother wavelet 的中譯法「母子波」，可能給門外漢一種「霧煞煞」的感覺，或者會讓人聯想到跟「子」有相對應的意涵（同樣的，father wavelet 「父子波」也容易有所混搖），事實上此處的「母子」並非比照倫理上或家庭上的的長幼關係，這裡「母」跟「子」必需完全分離，「母」在此處的主要意涵是源頭，也就是說母子波最貼切的說法是源頭子波（用以製造或生成其它子波以便形成一個函基）。

有了上面的論述，似乎「仔波」叫法的優點也已不述自明了。「仔」者小也、子也，但卻毫無小或子的泛泛，「仔波」很自然地形成一個專有的名稱。再者仔也，桀驁不馴、有活力、也可能不按牌理出牌- 這顯示它的多元性、變異性、奇特性。而仔也有一種容易呼朋引友，自我膨脹，形成一種特立獨行的群體- 這顯示它與函基的意涵有如是密切的關聯。至於「母仔波」、「父仔波」，與「母子波」、「父子波」的差異，我想大概也是不說而自可分明。

BIBLIOGRAPHY

[1] Auscher, P. Wavelet bases for $L^2(\mathrm{R})$ with rational dilation factor. In M. B. Ruskai, G. Beylkin, R. Coifman, I. Daubechies, S. Mallat, Y. Meyer, and L. Raphael, editor, *Wavelets and Their Applications*, pages 439–452. Jones and Bartlett Publishers, Boston, New York, USA, 1992. 6

[2] Battle, G. Cardinal spline interpolation and the block spin construction of wavelets. In C.K. Chui, editor, *Wavelets: A tutorial in Theory and Applications*, pages 73–90. Academic Press, Inc., San Diego, California, USA, 1992. 23

[3] Bracewell, B. *The Fourier Transform And Its Applications*. McGraw-Hill Book Company, Singapore, second edition, 1986. 90, 91

[4] Chui, C. K. *An Introduction to Wavelets*. Academic Press, Inc., San Diego, California, USA, 1992. 23, 25, 36, 52, 57, 78, 86, 91

[5] Chui, C.K. On cardinal spline-wavelets. In M. B. Ruskai, G. Beylkin, R. Coifman, I. Daubechies, S. Mallat, Y. Meyer, and L. Raphael, editor, *Wavelets and Their Applications*, pages 439–452. Jones and Bartlett Publishers, Boston, New York, USA, 1992. 23, 36

[6] Cohen, L. *Time-Frequency Analysis*. Prentice Hall PTR, Englewood Cliffs, New Jersey, USA, 1995. 1

[7] Coifman, R., Y. Meyer, and M.V. Wickerhauser. Size properties of wavelet packets. In M. B. Ruskai, G. Beylkin, R. Coifman, I. Daubechies, S. Mallat, Y. Meyer, and L. Raphael, editor, *Wavelets and Their Applications*, pages 453–470. Jones and Bartlett Publishers, Boston, New York, USA, 1992. 6, 22

[8] Coifman, R., Y. Meyer, and M.V. Wickerhauser. Wavelet analysis and signal processing. In M. B. Ruskai, G. Beylkin, R. Coifman, I. Daubechies, S. Mallat, Y. Meyer, and L. Raphael, editor, *Wavelets and Their Applications*, pages 153–178. Jones and Bartlett Publishers, Boston, New York, USA, 1992. 6

[9] Daubechies, I. *Ten Lectures on Wavelets*. SIAM, Philadelphia, USA, 1992. 6, 9, 14, 21, 52, 56, 57, 65, 78, 85, 86, 108

[10] Froment, J. and, S. Mallat. Second generation compact image coding with wavelets. In C.K. Chui, editor, *Wavelets: A tutorial in Theory and Applications*, pages 655–678. Academic Press, Inc., San Diego, California, USA, 1992. 85

[11] Lamb, H. *Hydrodynamics*. Cambridge University Press, Cambridge, England, sixth edition, 1932. 96

[12] Lee, Y.R. *Interaction Scales in a Wind, Wave, and Rain Coupling System*. Ph.D. Dissertation, University of Delaware, Newark, Delaware, Nov. 1999. 6

[13] Lee, Y.R. Signal analysis from wave modulation perspective. Technical report, No.2001–09, Institute of Harbor and Marine Technology, Taichung, Taiwan, 2001. 2, 77

[14] Lee, Y.R., and J. Wu. Wavelet coherences based on an optimum analyzing function basis. In *Proc. 20th Conf. On Ocean Engineering in Taiwan*, pages 109–116, 1998. 84, 85

[15] Lee, Y.R., and J. Wu. A quasi-wavelet function bases for improved time-frequency characterizations. *Proc. 21th Conf. on Ocean Engineering in Taiwan*, pages 101–108, 1999. 101

[16] Lee, Y.R., and J. Wu. Wave characterizations based on Gabor's analytic signal procedure. *Proc. 22th Conf. on Ocean Engineering in Taiwan*, pages 208–215, 2001. 80

[17] Mallat, S. Multiresolution approximation and wavelets. *Trans. Amer. Math. Soc.*, 315:69–88, 1989. 14, 79

[18] Mallat, S., and S. Zhong. Wavelet transform maxima and multiscale edges. In M. B. Ruskai, G. Beylkin, R. Coifman, I. Daubechies, S. Mallat, Y. Meyer, and L. Raphael, editor, *Wavelets and Their Applications*, pages 67–104. Jones and Bartlett Publishers, Boston, New York, USA, 1992. 80, 85

[19] Massopust, P.R. *Fractal Runctions, Fractal Surfaces, and Wavelets*. Academic Press, Inc., San Diego, California, USA, 1994. 52

[20] Meyer, Y. *Wavelets and operators*. Cambridge University Press, New York, USA, 1992. 9, 52, 78

[21] Phillips, O.M. *The Dynamics of the Upper Ocean*. Cambridge University Press, New York, USA, second edition, 1977. 96

[22] Press, W. H., S. A. Teukolsky, W. T. Vetterling and B. P. Flennery. *Numerical Recipes in Fortran*. Cambridge University Press, New York, USA, second edition, 1992. 14, 52

[23] Tennekes, H., and J.L. Lumley. *A First Course in Turbulence*. The MIT Press, Cambridge, Massachusetts, USA, 1972. 100

[24] Wickerhauser, M.V. Acoustic signal compression with wavelet packets. In C.K. Chui, editor, *Wavelets: A tutorial in Theory and Applications*, pages 679–700. Academic Press, Inc., San Diego, California, USA, 1992. 6

[25] Wickerhauser, M.V. Comparison of picture compression methords: wavelet, wavelet packet, and local cosine. In C. K. Chui, editor, *Wavelets: Theory, Algorithms, and Applications*, pages 585–621. Academic Press, Inc., San Diego, California, USA, 1994. 22, 53, 54